Scintillateurs et autres détecteurs optiques de particules

Rémi Chipaux

▶ **To cite this version:**

Rémi Chipaux. Scintillateurs et autres détecteurs optiques de particules. Physique [physics]. Université Pierre et Marie Curie - Paris VI, 2011. ⟨tel-00573492⟩

HAL Id: tel-00573492

https://theses.hal.science/tel-00573492

Submitted on 4 Mar 2011

Université Pierre et Marie Curie, Paris VI
Spécialité : Sciences Physiques

Scintillateurs
et autres détecteurs optiques de particules

Mémoire présenté en vue d'obtenir l'habilitation à diriger des recherches

Rémi Chipaux
CEA/DSM/IRFU/SÉDI

Soutenu le 6 janvier 2011 devant le jury composé de :

Pierre Bareyre
José Busto   rapporteur
Thomas Patzak
Joël Pouthas   rapporteur
Stefaan Tavernier   rapporteur
Pascal Vincent

À mon père,
Claude Chipaux,
qui nous a quittés le 17 avril 2010.

Ce travail n'existerait pas sans la participation de nombreuses personnes, qui a des titres divers m'ont accompagné tout au long de ces années.

Table des matières

Introduction

Au moment de commencer ce mémoire se posait à moi la question de dégager une cohérence dans mes travaux de recherche et dans mon chemin professionnel. Question à laquelle je n'avais pas de réponse claire à l'époque. Pas facile en effet, avec un tel parcours, de la physique des solides à la simulation des détecteurs pour l'astrophysique, en passant par la chimie inorganique, un peu, l'optique et la spectroscopie, beaucoup plus, le vieillissement des matériaux sous rayonnement, la photodétection, etc.

Quelques aspects récurrents dans ce parcours se dégagent cependant. Tout d'abord l'intérêt pour les matériaux solides, réminiscence de ma formation initiale, étudiés au fil des ans d'abord pour leur propriétés magnétiques, puis optiques, spectroscopiques et scintillantes en vue de la détection de rayonnements.

Les rayonnements, justement, en constituent un autre. Présents dès mon stage de DEA, comme moyen, puis danger, préoccupation, et finalement contrainte en même temps que sujet d'étude, ils sont le véritable fil rouge de ces travaux.

Un troisième aspect est sans doute la volonté de comprendre les problèmes et les observations, en essayant de les généraliser pour en dégager les paramètres importants, par des modèles s'appuyant avant tout sur la physique. L'importance également de ne jamais avoir une confiance absolue dans les programmes d'analyse ou de simulations tout faits, même les plus simples (voir [1]…), d'en connaître les limites, d'apprendre à en reconnaître les bugs, et donc de ne pas hésiter à se plonger dans la programmation, quitte à y perdre, outre son Fortran, un peu de temps…

Si mes premiers travaux (thèse et post-doc) étaient assez solitaires, les suivants ont été tous été faits au sein de collaborations internationales, et pour la plupart pluridisciplinaires, source d'enrichissement et d'efficacité.

J'émettrais peut-être le regret de ne pas avoir eu l'occasion d'encadrer plus de thèses, pour justifier encore mieux ce mémoire, soit pour raison de conjoncture, soit en raison du caractère risqué des sujets de recherche. Le domaine de l'instrumentation n'est pas facile pour cela, les sujets intéressants se présentant le plus souvent lorsque la pérennité du projet n'est pas assurée, et soumise à des aléas qui ne sont pas tous du domaine scientifique. Ce regret est largement tempéré par la qualité des travaux des doctorants que j'ai pu encadrer.

Exposé des travaux de recherche

1. Thèse de doctorat

Ma thèse a porté sur l'étude des réactions de synthèse de certains borures d'uranium, de neptunium et de plutonium à partir des métaux purs ou de leurs oxydes et des propriétés magnétiques des composés ainsi synthétisés, par mesure de susceptibilité magnétique et spectroscopie Mössbauer. L'élaboration et la caractérisation par diffraction X des échantillons se sont déroulées au sein du Laboratoire d'Étude et de Fabrication des Combustibles Avancées au CEA de Cadarache, les mesures magnétiques au sein du Département de Recherche Fondamentale du CEA de Grenoble.

Le dioxyde d'uranium UO_2 réagit avec le bore ou le carbure de bore B_4C pour former le tétraborure UB_4. Les propriétés de UB_4 restent peu claires, et semble-t-il dépendantes de la stœchiométrie des échantillons. Une substitution du bore par le carbone peut également être invoquée.
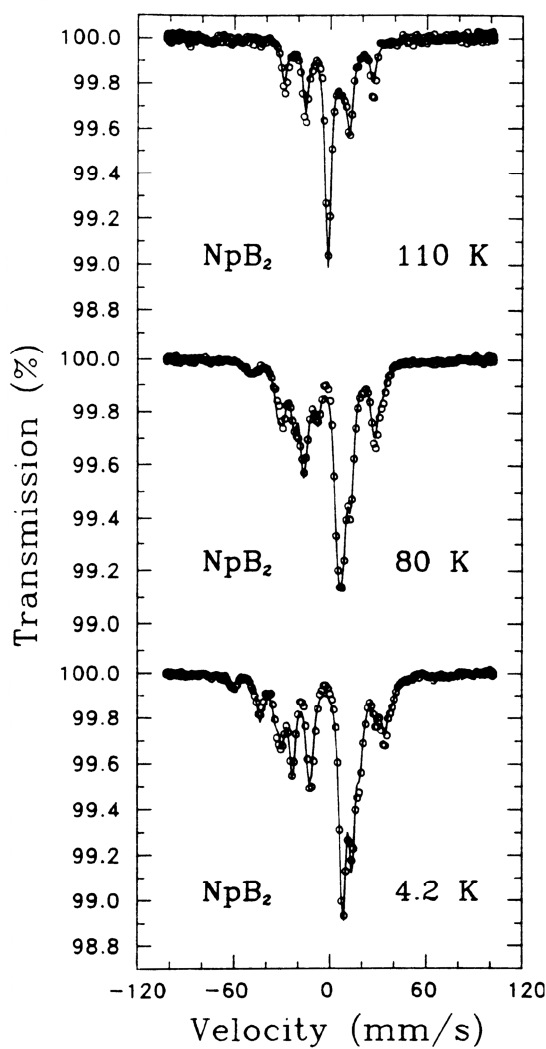
Figure 1-1 :
Spectres Mössbauer et ajustements pour
NpB₂

Le neptunium et le plutonium sous forme métallique réagissent avec le bore à 1170 K pour former les diborures. Les solutions solides $Np_{1-x}Pu_xB_2$ sont obtenues de la même manière à partir de la solution solide $Np_{1-x}Pu_x$.

L'intérêt, pour la physique des solides, de ces composés réside dans l'opposition entre les propriétés magnétiques des composés binaires PuB_2 et NpB_2. Alors que le premier présente un paramagnétisme peu dépendant de la température, le second s'ordonne ferromagnétiquement en dessous de 200 K.

Les spectres Mössbauer indiquent un fort effet quadripolaire, expliqué par la structure cristallochimique des composés (cf. figure 1-1). Dans la phase ferromagnétique, les moments magnétiques sont orientés perpendiculairement à l'axe c de la structure hexagonale. La température de transition ferromagnétique (température de Curie) décroît lentement lorsque la proportion de plutonium augmente, jusqu'à $x = 30$ %, puis plus rapidement pour disparaître pour $x \geq 67$ %. Des fluctuations ferromagnétiques sont observées autour de la transition.

A l'occasion de cette thèse j'ai développé pour analyser et modéliser les résultats obtenus, le programme d'affinement des spectres Mössbauer utilisant le hamiltonien hyperfin complet, que j'ai étendu par la suite au cas général [2], ainsi qu'un modèle de champ moléculaire dérivé de celui de Weiss pour les composés comprenant deux ions magnétiques différents, modèle qui permet de retrouver avec une bonne précision les distances interatomiques les plus favorables au magnétisme des ions Np^{3+} et Pu^{3+} [3].

2. Post doc au CERN

Au cours des deux ans que j'ai passés au CERN, au sein du groupe de P. Bernard développant les cavités accélératrices supraconductrices, avec une bourse de cet organisme, j'ai travaillé, dans la lignée des compétences acquises durant ma thèse en chimie et physique du solide, sur la recherche de matériaux supraconducteurs à haute température critique.

Suivant une idée de C. Benvenuti, il s'agissait de rechercher d'éventuels composés supraconducteurs symétriques des cuprates découverts par Bednorz et Müller. En résumé nous voulions tester d'éventuelles analogies dans les propriétés de conduction entre, à structure similaire, composés comprenant des ions à couche électronique d quasi pleine (un trou) comme Cu^{2+} ($3d^9$) ou Bi^{4+} ($5d^9$) et composés comprenant des ions à bande d quasi vide (un électron) ou supposée telle, comme Ti^{3+}, V^{4+}, (supposés $3d^1$), Zr^{3+}, Nb^{4+} (supposés $4d^1$)…

Cette idée ne s'est pas avérée fructueuse [4], mais je me console en remarquant que depuis lors, la supraconductivité à haute température n'a pas pour autant, à ma connaissance, trouvé d'applications significatives dans le domaine des hyper fréquences et des cavités accélératrices. Le point positif de ce séjour étant la découverte pour moi à la fois de la physique des particules et du CERN, ce qui a déterminé mon parcours ultérieur.

3. Travaux sur les détecteurs « optiques » de particules

Rejoignant le Département de Physique des Particules Élémentaires, Service des Techniques Instrumentales (DPhPE/STIPE/STD), j'ai été dès lors amené à élargir mes compétences et mon domaine de recherche aux techniques de détection de particules et de rayonnements en général, et en particulier les matériaux pour les détecteurs dits « optiques ».

On range dans cette catégorie les détecteurs dans lesquels l'interaction rayonnement matière se traduit par l'émission de lumière visible (ou « quasi » visible : ultraviolet, infrarouge…) qui doit ensuite parvenir à un photodétecteur. Cette émission de lumière peut se faire par exemple par effet Cherenkov, ou par scintillation dans des matériaux scintillants organiques (liquides ou plastiques) ou inorganiques (les cristaux scintillants). Je me suis, comme il sera montré dans les chapitres suivants, intéressé à ces trois grandes catégories de matériaux.

J'ai fait le choix de classer l'exposé qui suit suivant le type de matériaux : organiques, puis inorganiques, plutôt que par ordre chronologique, ou par type d'applications, ces matériaux s'utilisant aussi bien dans les calorimètres (aussi bien hadroniques qu'électromagnétiques), dans les discriminateurs ou les trajectographes.

Il s'agit d'un domaine essentiellement pluridisciplinaire, puisque, s'appliquant aux recherches fondamentales en physique des particules, astrophysique, physique nucléaire (dont il vaut mieux dès lors bien appréhender les aspects expérimentaux), il touche, non seulement à l'interaction rayonnement matière, mais également aux phénomènes de luminescence (dans les matériaux scintillants), à l'optique, à la physique et à la chimie des matériaux, au vieillissement, à la détection de lumière, à l'électronique de lecture etc., sans oublier les simulations numériques.

3.1. Scintillateurs organiques

Les scintillateurs organiques, tant solides (scintillateurs plastiques) que liquides, sont souvent utilisés pour la détection des rayonnements, notamment dans les détecteurs de traces, hodoscopes et autres instruments destinés à détecter le passage de particules chargées, ou dans des spectromètres ou calorimètres hétérogènes dans lesquels ils constituent le milieu actif. Bien qu'existant dans les catalogues, leurs applications pour la physique nécessitent souvent des développements, tant pour leur mise en œuvre que pour en améliorer, optimiser ou adapter les propriétés. C'est ainsi que j'ai été amené à m'intéresser d'une part aux fibres plastiques scintillantes, dans le cadre notamment des recherches et développements pour les expériences auprès du *large hadron collider* (LHC) au CERN, et d'autre part aux liquides scintillants, pour la spectroscopie des neutrinos.
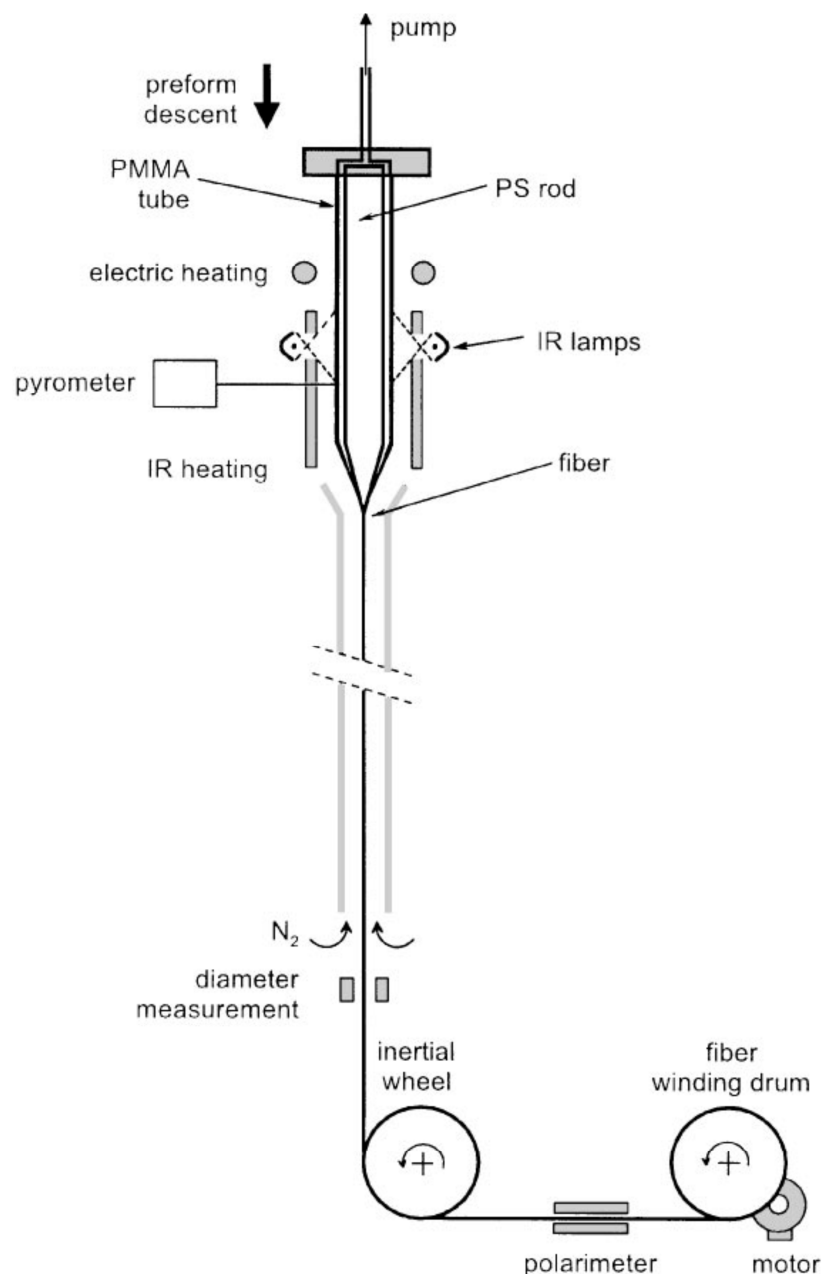
Figure 3-1 :
Schéma du dispositif de tirage de fibres plastiques développé au SED.

3.1.1. Fibres optiques scintillantes

Le DPhPE a fortement contribué dans les années 1980 au développement des fibres scintillantes plastiques, avec en particulier le développement du détecteur de vertex à fibres scintillantes de l'expérience UA2 [5]. Fort de cette expérience, plusieurs projets de recherche et développement ont été poursuivis, au début des années 1990, en vue de définir leurs possibilités d'application dans les futures expériences du LHC et du *superconducting super collider* (SSC) alors en construction au Texas.

J'ai en particulier participé à un programme générique de recherche et développement [6], dans le cadre duquel plus de 50 km de fibres scintillantes plastiques, composés d'un cœur de polystyrène et d'une gaine de polyméthylméthacrylate, ont été tirées avec la méthode des préformes.
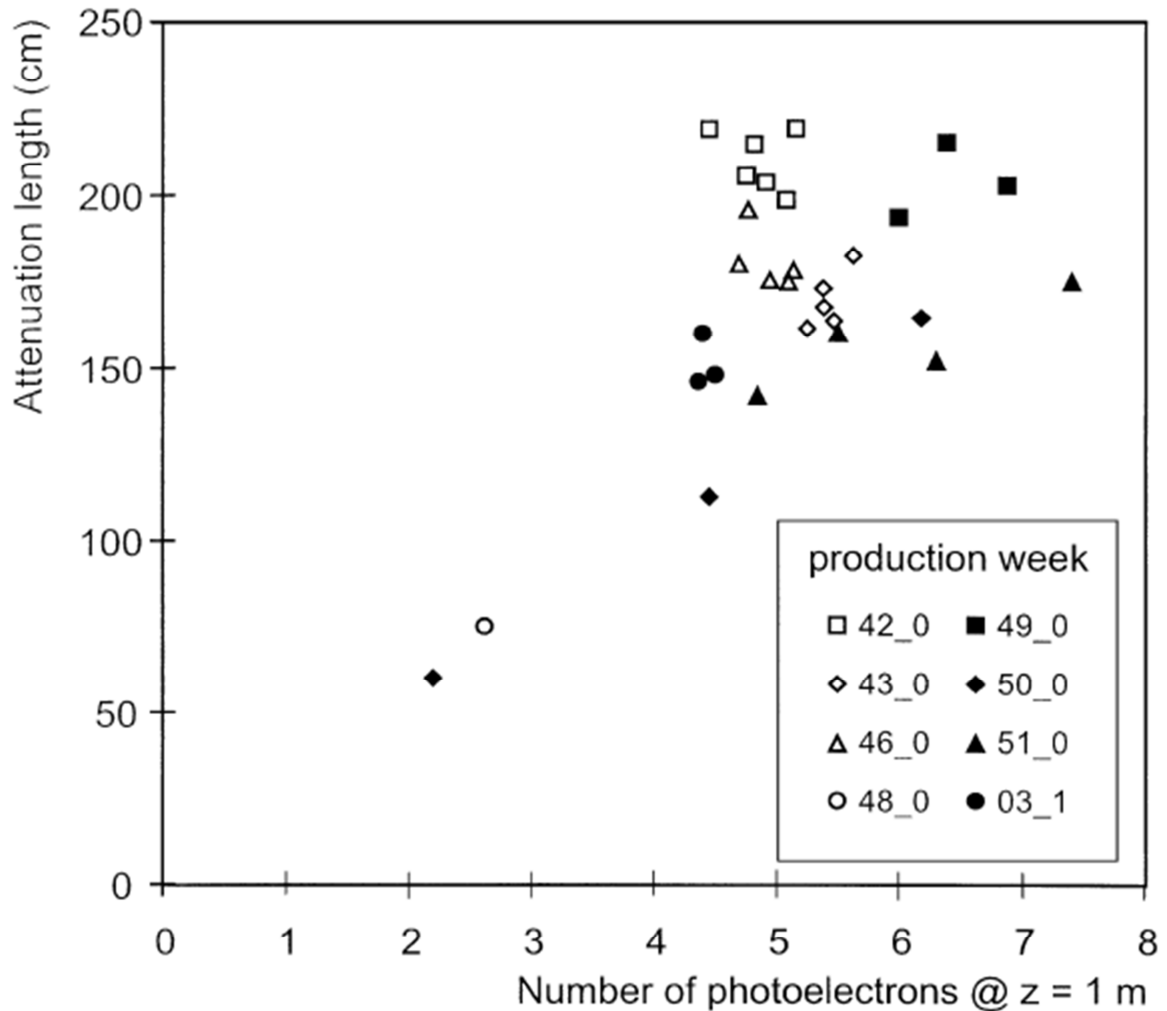
Figure 3-2 :
Corrélation entre longueur d'atténuation et nombre de photoélectrons par particule au minimum d'ionisation dans les lots de production de fibres.

Les propriétés optiques du polymère ont été extensivement mesurées aux différentes étapes de la production pour permettre de qualifier le processus. Il a été montré que la cause principale des pertes de lumière était due à l'absorption dans le polystyrène. Cette absorption est déjà apparente dans les préformes, ce qui montre l'importance de la purification des matières premières et du procédé de polymérisation. La longueur d'atténuation liée à cette absorption est d'environ 3 m, tandis que les pertes de réflexion aux interfaces sont de l'ordre de 10^{-5} à 10^{-4} par réflexion, équivalant à une longueur d'atténuation de 7 m.

L'issue de ce programme démontrait que les facteurs de pertes dans les fibres scintillantes étaient bien compris et qu'on ne pouvait espérer d'améliorations importantes des rendements lumineux, notamment par rapport aux productions industrielles. Il n'était donc plus du ressort d'un laboratoire d'instrumentation en physique des particules d'entreprendre ce type de développement et de fabrication.

Dès lors le laboratoire s'est concentré sur la caractérisation et la mise en œuvre des fibres scintillantes dans des détecteurs pour la physique des hautes énergies. En particulier, la possibilité de construire un détecteur de traces à base de fibres ou de microfibres scintillantes pour les expériences du LHC, a été longuement considérée [7]. Les deux points cruciaux, et du fait desquels cette option n'aura finalement été retenue par aucune des expériences auprès du LHC, étaient la lecture des fibres (dans un espace réduit et sous champ magnétique élevé) et leur tenue sous fort rayonnement.

Je me suis très tôt intéressé à ce dernier point, menant notamment les campagnes d'irradiations gamma sur les fibres scintillantes rapportées dans [7] et [8]. Ces campagnes ont mis en évidence l'accroissement des dégâts d'irradiation dans les plastiques scintillants lorsque le débit de dose est faible. Les dégradations sont en effet plus faibles lorsque les irradiations sont faites à fort débit, ce qui est souvent le cas dans les études, faute de disposer de suffisamment de temps dans les installations d'irradiation.

Ce comportement, opposé à ce qui se produit en général dans les cristaux inorganiques ou dans les composants, est dû à la physicochimie spécifique des matériaux organiques, et en particulier à la diffusion de l'oxygène dans les matériaux. Hormis ce résultat scientifique qui confirmait la relative fragilité des fibres plastiques envers les rayonnements, cette activité m'a permis de prendre contact d'une part avec les laboratoires travaillant sur le sujet, d'autre part avec des services exploitants des installations d'irradiation. Elle a été le début d'une longue collaboration avec l'équipe du réacteur Ulysse de l'INSTN/Saclay, avec laquelle le DAPNIA a mené de nombreuses études d'irradiation neutronique de cristaux scintillants (voir chapitre 3.2), de photodétecteurs etc. Elle a directement motivé l'étude, la construction et l'exploitation de l'installation d'irradiation COCASE dont j'assure la responsabilité.

L'environnement radiatif étant moins critique dans un calorimètre, l'étude et le développement du détecteur de maximum de gerbe du projet d'expérience SDC auprès de l'accélérateur SSC [8] était bien engagée quand ce projet d'accélérateur a été brutalement stoppé, venant mettre un terme aux activités fibres optiques scintillantes au DAPNIA.

3.1.2. Scintillateurs liquides

Un domaine de prédilection en physique pour les scintillateurs liquides, est constitué par la physique des neutrinos, qui nécessite de larges volumes détecteurs, et des conditions de pureté extrêmes vis à vis des contaminations radioactives. En général, les matériaux disponibles dans l'industrie ne répondent pas au cahier des charges, tant par la pureté radioactive que par leurs propriétés optiques insuffisantes. Les expériences Borexino et Double Chooz en sont des exemples [9,10]. Comme nous le verrons, certaines expériences, comme le projet LENS auquel j'ai collaboré, nécessitent par ailleurs le développement de matériaux présentant des propriétés nucléaires spécifiques.

3.1.2.1. Détection des neutrinos solaires, la collaboration Lens

La première génération d'expériences de neutrinos a non seulement confirmé le déficit des neutrinos solaires, mais a transformé cette énigme en un soupçon que les neutrinos doivent changer de saveur (effet MSW) pour expliquer les résultats expérimentaux. Une telle explication implique une masse non nulle pour le neutrino.

Les premières expériences détectant les neutrinos solaires d'énergie inférieure au MeV utilisaient la réaction bêta inverse :

$$\nu_e + {}^A_Z X \rightarrow e^- + {}^A_{Z+1} X$$
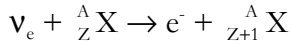
La première expérience, Homestake [11], exploitait la transmutation du chlore 37 en argon 37 :

$$\nu_e + {}^{37}Cl \rightarrow e^- + {}^{37}Ar$$
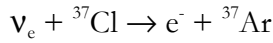
Les expériences Gallex [12] et Sage celle du gallium 71 en germanium 71 :

$$\nu_e + {}^{71}Ga \rightarrow e^- + {}^{71}Ge$$
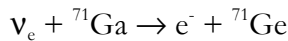
Dans les deux cas il s'agissait d'expériences de comptage (les noyaux finaux, ${}^{37}Ar$ ou ${}^{71}Ge$, instables, étaient comptés par leurs décroissances radioactives). Ces réactions de transmutation par capture de neutrinos ont l'avantage d'avoir des seuils bien déterminé par les états nucléaires initiaux et finaux, et de présenter une grande sélectivité. Par contre elles ne permettent pas d'accéder à l'énergie du neutrino incident, donc interdisent toute spectroscopie. Seule l'intégrale du flux de neutrinos, dans une certaine gamme, est mesurée.

Dans la partie haute énergie du spectre, (> 3 à 5 MeV), on peut utiliser la diffusion du neutrino par l'électron :

$$\nu_e + e^- \rightarrow \nu_e + e^-$$
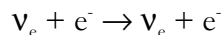
La seconde génération d'expériences porte sur la partie du spectre des neutrinos solaires la plus énergétique, SNO, Kamiokande [13,14].

Pour accéder au spectre de basse énergie, des méthodes plus sophistiquées doivent être envisagés. Raghavan a proposé en 1976 [15] d'utiliser la capture des neutrinos par l'isotope 115 de l'indium suivant la réaction suivante :

$$\nu_e + {}^{115}In \xrightarrow{\text{(seuil 114 keV)}} e_1^- + {}^{115}Sn^*$$
$$\rightarrow {}^{115}Sn + e_2^- / \gamma_2 \ (116 \ keV, \ 4,76 \ \mu s) + \gamma_3 \ (497 \ keV, \ 16 \ ps).$$
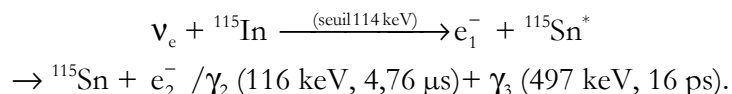
Dans ce type de réaction, la coïncidence retardée entre l'électron primaire e_1^- et la ou les émissions de particules (e ou γ) résultant de la désexcitation du noyau final, (après un temps moyen et avec une énergie bien déterminés) représente une signature en temps réel spécifique de l'interaction d'un neutrino, permettant une bonne réjection des bruits de fond et autorisant une mesure de l'énergie du neutrino.

De nombreuses études ont été menées pour développer des matériaux scintillateurs organiques ou inorganiques incorporant des densités importantes d'indium.

Cependant, jusqu'à ces dernières années, ces études n'ont pas abouti, les propriétés des matériaux scintillateurs obtenues étant insuffisantes pour combattre le bruit de fond intrinsèque dû à la radioactivité bêta de l'indium 115 ($\tau_{\frac{1}{2}} = 4,41 \ 10^{14}$ ans). Nous verrons cependant plus loin que des avancées ont été faites récemment.
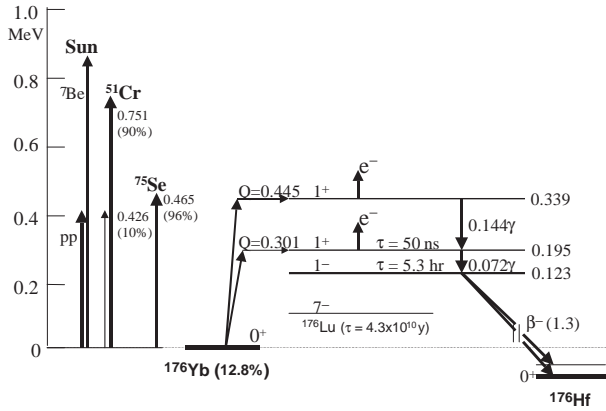
Figure 3-3 :
Niveaux d'énergie et transitions nucléaires dans le noyau d'ytterbium 176, comparaison avec les énergies des neutrinos solaires et de quelques sources de neutrinos.

La découverte en 1997 par le même Raghavan de noyaux présentant des caractéristiques analogues mais stables, à savoir ^{82}Se, ^{160}Gd et ^{176}Yb [16] a relancé les recherches, notamment dans le cadre de la collaboration internationale LENS [17].
Les réactions de capture sont les suivantes :
Pour ^{82}Se :

$$\nu_e + {}^{82}\text{Se} \xrightarrow{\text{(seuil 173 keV)}} e_1^- + {}^{82}\text{Br}^* \rightarrow {}^{82}\text{Br}^m + \gamma_2 \text{ (29 keV, 10,4 ns)}$$
$$\rightarrow {}^{82}\text{Br} + \gamma_3 \text{ (46 keV, 6,1 min)}$$
$$[\rightarrow {}^{82}\text{Kr} + \rightarrow e_2^- \text{ (<3,1 MeV, 35,5 h)}].$$

Pour ^{160}Gd :

$$\nu_e + {}^{160}\text{Gd} \xrightarrow{\text{(seuil 244 keV)}} e_1^- + \gamma_1 + {}^{160}\text{Tb}^* \rightarrow {}^{160}\text{Tb} + \gamma_2 \text{ (64 keV, 87 ns)}$$
$$[\rightarrow {}^{160}\text{Dy} + e_2^- \text{ (<1,84 MeV, 72 j)}].$$

Pour ^{176}Yb :

$$\nu_e + {}^{176}\text{Yb} \xrightarrow{\text{(seuil 301 keV)}} e_1^- (+ \gamma_1) + {}^{176}\text{Lu}^* \rightarrow {}^{176}\text{Lu}^m + \gamma_2 \text{ (72 keV, 50 ns)}$$
$$[\rightarrow {}^{176}\text{Hf} + e_2^- \text{ (<1,3 MeV, 3,7 h)}]$$
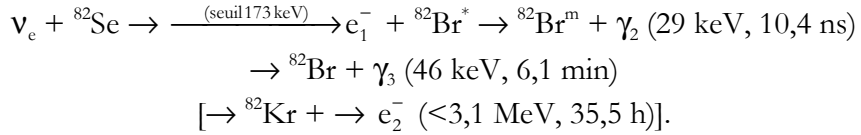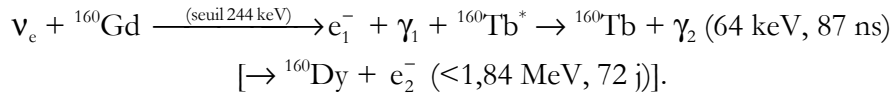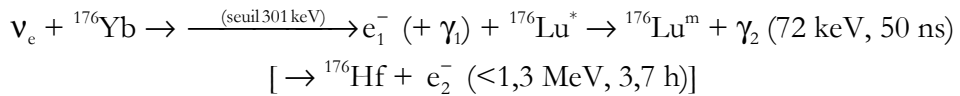
(Les paramètres des décroissances radioactives sont tirés de la base de données NUDAT [18].)
La signature du sélénium 82 est difficilement exploitable dans des scintillateurs. Seules les possibilités des semi-conducteurs et des détecteurs gazeux ont été envisagés pour ce noyau. Par contre, l'ytterbium et le gadolinium ont été étudiés, à la fois incorporés dans des scintillateurs organiques que dans les cristaux scintillants.
Nous nous concentrerons ici sur les développements sur les scintillateurs organiques chargés en Yb, Gd (et In). Les cristaux scintillants seront abordés dans le chapitre 3.2.2.

3.1.2.2. Scintillateurs liquides pour la spectroscopie des neutrinos solaires

La spectroscopie des neutrinos exige des caractéristiques très contraignantes d'un éventuel détecteur. Bien entendu la nécessité d'identifier sélectivement la capture d'un neutrino par rapport au bruit de fond impose des résolutions énergétique, temporelle et spatiale suffisantes : résolutions énergétique et temporelle pour mesurer les particules secondaires des réactions de captures en coïncidence retardée avec l'électron primaire et les distinguer de celui-ci ; résolution spatiale pour limiter le nombre de coïncidences fortuites provenant d'un même volume de

détection. Pour répondre à ces contraintes, un scintillateur, qu'il soit organique ou inorganique, doit avoir un rendement lumineux et une rapidité suffisants.

Malgré un flux colossal les sections efficaces de capture sont extrêmement faibles et les captures extrêmement rares. On estime à environ 5 tonnes d'indium, 20 d'ytterbium ou 40 de gadolinium (de composition isotopique naturelle) la masse nécessaire pour obtenir une capture d'un neutrino solaire par jour… On comprend donc qu'il faut prendre en compte dès le début de l'étude l'aspect quasi industriel que devra prendre *in fine* la réalisation du détecteur.

Il a également été suggéré, notamment pour le gadolinium [19], pour diminuer la masse totale, d'utiliser des éléments enrichis dans l'isotope utile. Les proportions naturelles sont, respectivement, de 8,73(22)% pour ^{82}Se ; 95,71(5)% pour ^{115}In ; 21,86(19)% pour ^{160}Gd et 12,76(41)% pour ^{176}Yb. Dans le cas du gadolinium, cet enrichissement aurait aussi l'effet bénéfique de diminuer la proportion d'isotope 152 radioactif. Les solutions techniques existent (séparation, enrichissement par capture neutronique…), mais le coût est a priori prohibitif, sauf à bénéficier de retombées industrielles extérieures. Ces problèmes de d'enrichissement isotopique, de même que ceux de pureté radioactive, sont tout à fait similaires à ceux rencontrés dans les recherches sur la décroissance double béta [20].

3.2. Scintillateurs inorganiques

3.2.1. Cristaux pour la calorimétrie électromagnétique
Les collaborations Crystal Clear et CMS

3.2.1.1. Introduction

Cette activité de recherche s'est tout d'abord développée de manière générique, sous l'égide de la collaboration Crystal Clear à laquelle le DAPNIA a adhéré peu après sa formation, avec le but de développer un scintillateur dense et rapide pour la calorimétrie haute résolution dans une expérience auprès du LHC. Avec J.-L. Faure, nous avons cherché dès l'origine à développer notre action suivant deux axes : d'une part promouvoir des solutions réalistes et économiques, d'autre part utiliser et développer au mieux nos compétences et les atouts du CEA. Nous avons pour cela renforcé nos moyens de caractérisation optique (spectroscopie optique, bancs d'étude « cosmiques » etc.) et pris l'option stratégique des études d'irradiation pour lesquelles le CEA est particulièrement bien placé : accès au réacteur Ulysse pour les irradiations neutroniques, mise en place de l'irradiateur Cocase pour les irradiations gamma à faible débit de dose.

3.2.1.2. R&D générique, Crystal Clear, CeF$_3$, PbF$_2$…

Tout en participant aux recherches de Crystal Clear sur le fluorure de cérium (CeF$_3$), (voir les références [21] à [30], mes premiers travaux ont portés sur des cristaux potentiellement plus économiques : étude du fluorure de plomb (PbF$_2$) en tant que radiateur Cherenkov [31], pré-étude avec le laboratoire de cristallogenèse du LETI de l'iodure de cadmium (CdI$_2$), ainsi qu'à des tests d'irradiation sur des points critiques comme les colles optiques par exemple [32].

3.2.1.3. Le tungstate de plomb PbWO$_4$

Le tungstate de plomb (PbWO$_4$) a été proposé comme matériau scintillant pour la calorimétrie électromagnétique en 1992, notamment lors de la conférence « Crystal 2000 » qui s'est tenue à Chamonix en septembre [33]. Il a dès ce moment suscité notre intérêt, pour de nombreuses raisons. Tout d'abord sa composition, à Z élevé, sa densité, celle du cuivre, sa cinétique d'émission (temps de décroissance $\tau \approx 15$ ns) et son spectre d'émission (dans le bleu vert) le rendaient particulièrement intéressant pour la calorimétrie électromagnétique à haute énergie nécessaire pour les expériences en projet pour le LHC. Sa longueur de radiation ($X_0 = 0,89$ cm) et son rayon de Molière ($R_m = 2,2$ cm) sont parmi les plus courts que l'on connaisse dans un matériau transparent. Son faible rendement lumineux (5 à 10 photons par MeV, environ 50 fois moins que le BGO), est néanmoins suffisant, aux énergies du LHC, pour permettre sa lecture par les photodiodes à avalanche de grande surface qui commençaient alors à apparaître sur le marché et présentent l'intérêt d'un gain important tout en étant insensibles au champ magnétique.

Mes premiers résultats de mesure de résistance du tungstate de plomb au flux neutronique, présentés en 1994 [22], et aux irradiations gamma à faible débit, présentés en 1995 [28] ont montré que ce matériau pouvait résister à l'environnement radiatif du LHC et constituer une alternative économique au CeF$_3$. On constatait sur les échantillons de laboratoire étudiés (voir la figure 3-4) des propriétés (saturation à faible dose, récupération, etc.) que l'on retrouvera sur les cristaux produits industriellement après plusieurs années de recherches et de développements intensifs.

Ces moyens mis en place et ces études ont permis d'avoir une action décisive pour l'émergence du tungstate de plomb comme candidat pour CMS.
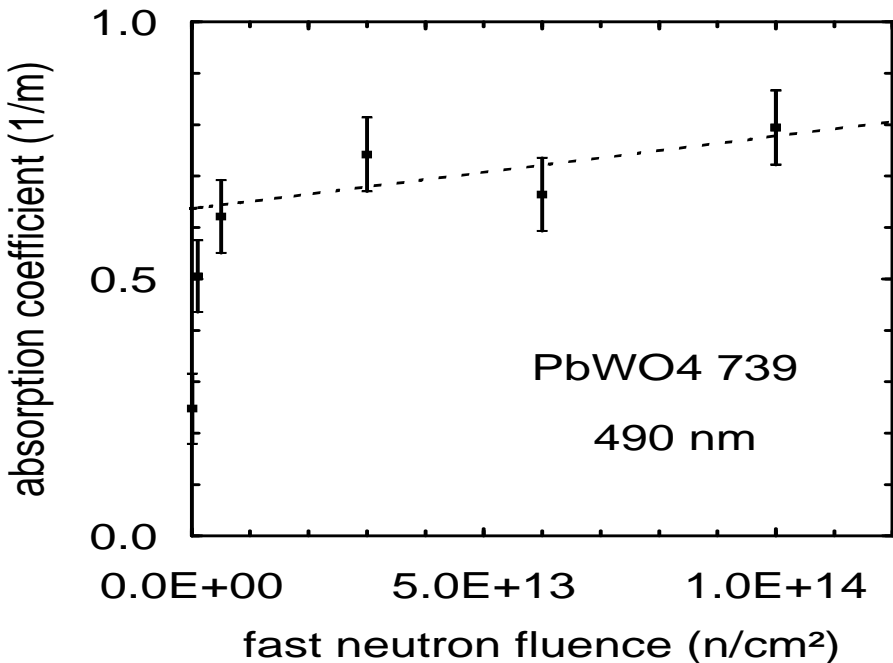
Figure 3-4 : Variation de l'absorption induite à la longueur d'onde d'émission du tungstate de plomb après différentes fluences de neutrons rapides, publié en 1995 ([28]).

L'irradiateur Cocase a été fortement utilisé par un groupe comprenant des physiciens du LAPP, du CERN, de Minsk, Protvino et de Saclay pour caractériser et participer aux efforts d'amélioration de la tenue des cristaux de PbWO$_4$ aux faibles doses [34]. Outre ma participation scientifique et technique, l'accès au centre de Saclay des personnes de nationalité étrangère a nécessité un effort important. L'équipement mis en place, les cristaux caractérisés et les mesures effectuées à cette occasion ont été utilisés largement dans les études sur le système de suivi optique. Dans le même ordre d'idée, les résultats obtenus sur les propriétés d'anisotropie optique du PbWO$_4$ ont des répercussions importantes sur les programmes de simulation développés pour le système de monitoring [35].

Par la suite cette activité s'est orientée naturellement vers le développement du calorimètre électromagnétique de CMS et de son système de suivi optique dont le DAPNIA a pris la responsabilité. La politique suivie a consisté à utiliser nos moyens d'investigation pour participer de manière efficace aux recherches sur la tenue aux radiations et sur la collection de lumière menée par la collaboration CMS/ECAL dans son ensemble, tout en engageant un axe de recherche intense sur le fonctionnement physique du système de suivi optique.

3.2.1.4. Le système de suivi optique du calorimètre de CMS

Les propriétés à faible dose des cristaux de PbWO$_4$ ont des conséquences sur le dessin du calorimètre électromagnétique. Si les performances du calorimètre ne seront pas significativement dégradées au cours du temps, du moins du fait des cristaux scintillants, les variations d'absorption de ceux-ci, faibles mais à courte constante de temps, imposent pour maintenir la précision d'étalonnage du détecteur la réalisation d'un système de suivi optique précis, stable et dont on comprend bien les liens avec la réponse de chaque cristal. Le système de suivi optique est donc

un élément crucial du calorimètre électromagnétique de CMS. Tout en participant aux réflexions et aux travaux visant à la réalisation concrète de ce système, je me suis attaché avec un groupe conjoint SPP/SED aux aspects physiques et optiques de son fonctionnement, le but étant de bien comprendre la corrélation, évidente mais non triviale, entre variations de transparence des cristaux mesurés par le système de suivi et variations du rendement lumineux de scintillation de ces mêmes cristaux, et partant de leur étalonnage. L'extrême importance et la difficulté de ce sujet ont motivé les travaux de ce groupe, que j'ai animé conjointement avec J.-P. Pansart, et la thèse de Marie Géléoc, entreprise à ce propos.

Cette étude a été abordée à la fois du point de vue théorique (modélisation et simulation) et expérimental, à travers plusieurs cycles de mesures et irradiations, tant à Saclay qu'en faisceau test au CERN. Ces travaux ont continué après la soutenance de thèse de M. Géléoc, et débouchés sur des avancées significatives dans la compréhension du problème.

On peut montrer qu'au premier ordre cette corrélation entre rendement lumineux de scintillation et rendement du système de suivi, ou, de manière équivalente, entre variations du coefficient d'étalonnage (rapport entre énergie déposée et signal mesuré) et du signal de suivi lumineux, peut s'exprimer de la façon suivante :

$$\frac{S(t)}{S_0} = \left(\frac{R(t)}{R_0} \right)^{\alpha}$$

où S est le coefficient d'étalonnage du cristal et R le signal de suivi optique à l'instant t, S_0 et R_0 étant leurs valeurs initiales. α est souvent également appelé S/R.

Un modèle plus complexe, que l'on peut qualifier de semi phénoménologique a été développé [36], qui permet de dégager les paramètres optiques importants gouvernant la corrélation des variations de rendement lumineux dans les cristaux de CMS, à savoir longueur d'absorption et propriétés des surfaces du cristal, notamment des extrémités. Il rend compte par exemple du fait que dans des cristaux polis et de grande transparence, une partie notable de la lumière de scintillation parcourt plusieurs fois la longueur du cristal et que, par conséquent, le rendement lumineux est très sensible à de faibles variations de la transparence. La lumière du système de suivi, au contraire, ne parcourt le cristal qu'une fois, ce qui explique des coefficients de corrélation α élevés.

Les coefficients de corrélation α calculés à partir des simulations faites avec le programme Litrani [37] correspondent bien à ceux que l'on observe expérimentalement ($\alpha \sim 1,54$) dans les cristaux CMS de provenance russe [38-40]. La figure 3-5 montre, par exemple, d'une part l'influence sur α de l'environnement du cristal, et d'autre part la stabilisation de ce coefficient introduite par le dépolissage partiel d'une des faces latérales, au prix d'une diminution du rendement lumineux.
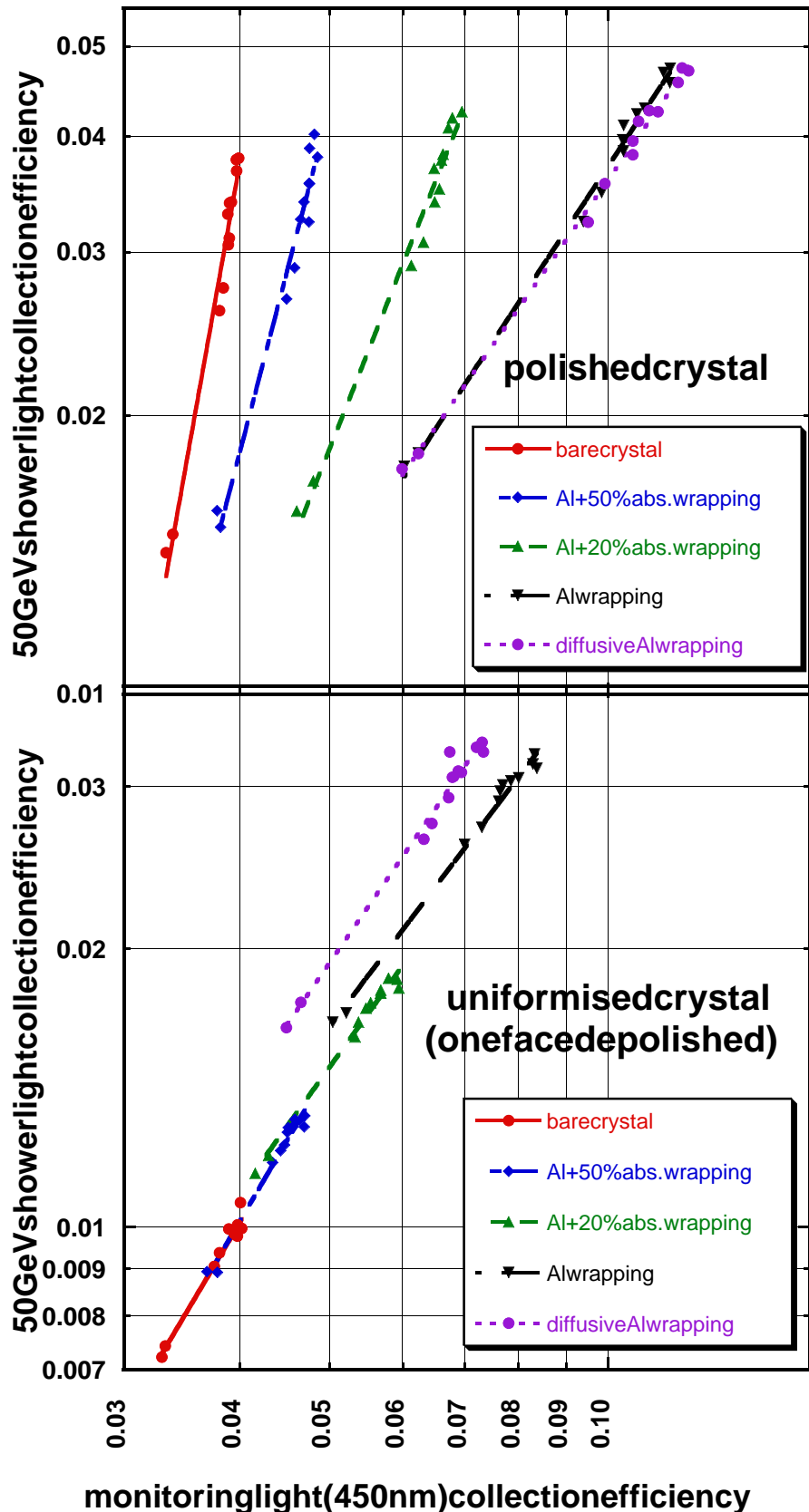
Figure 3-5 : Variation du rendement lumineux de scintillation en fonction du rendement lumineux du système de suivi optique pour diverses configurations du cristal [39]. Le coefficient de corrélation α correspond à la pente des droites.

Toutefois, les écarts de comportement observés entre cristaux de provenance russe et chinoise étaient mal compris dans le cadre de ce modèle. Nous avons été conduits, F.-X. Gentit et moi, à reprendre récemment nos calculs en introduisant l'hypothèse d'une diffusion possible de la lumière dans les cristaux. Les premiers résultats de simulation (voir figure 3-6) montrent effectivement qu'une longueur de diffusion interne peut entrainer une variation importante des coefficients de corrélation. Les valeurs de α inférieures à 1 parfois observées peuvent être expliquées de cette façon.
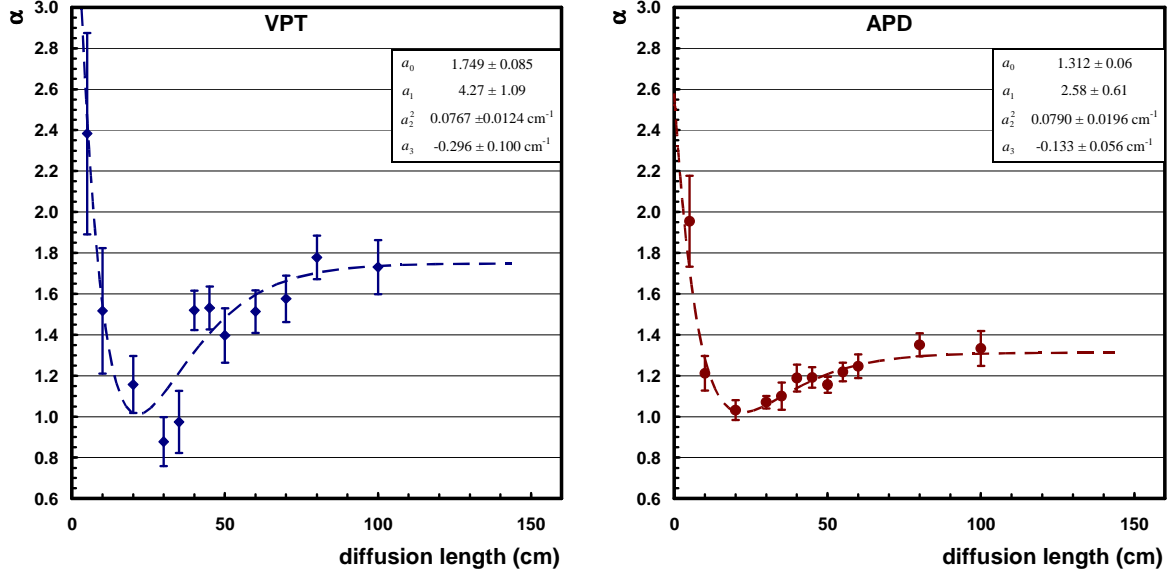
Figure 3-6 : Calcul par Litrani des coefficients de corrélation α en fonction de la longueur de diffusion interne des cristaux pour les bouchons de CMS-ECAL, et fit par la fonction
$$\alpha(x) = a_0 + (a_1 - a_0 + a_3 x)\exp(-a_2^2 x) \text{ [40]}.$$

Outre les aspects intervenants dans le fonctionnement du système de suivi, l'étude de la collection de lumière dans les cristaux scintillants a fait l'objet d'un développement spécifique en collaboration avec le CEA-Limeil à propos des revêtements optiques sol-gel [41]. Bien que finalement non retenu par CMS, ce développement a donné des résultats intéressants, potentiellement utilisables dans l'instrumentation médicale, qui ont motivé le dépôt d'un brevet.

3.2.2. Cristaux pour la spectroscopie des neutrinos solaires

Les travaux menés sur les cristaux scintillants dans les collaborations Crystal Clear et CMS, les liens noués au sein de ces collaborations, les compétences acquises, m'amenèrent naturellement à m'intéresser à la possibilité d'utiliser des cristaux scintillants dans l'expérience LENS.
L'intérêt majeur que présentent les matériaux inorganiques réside dans leur grande densité qui autoriserait, à détectivité égale, un détecteur plus compact, limitant ainsi le volume nécessaire en laboratoire souterrain, et diminuant la taille et donc le coût, des dispositifs extérieurs, blindages actif et passif notamment. Cela limiterait également l'activité des sources radioactives de neutrinos nécessaires à l'étalonnage du détecteur. Le tableau 3-1 montre les volumes de matériau actif qui seraient requis dans les différents cas.

Tableau 3-1 : Comparaison des volumes requis pour un détecteur LENS pour différents scintillateurs à base d'ytterbium.

	Masse volumique	Concentration massique d'Yb	Volume pour 20 tonnes d'Yb
Liquide scintillant	~ 1 g/cm³	10 %	200 m³
YAG :Yb 15%	4,86 g/cm³	12,3 %	33,4 m³
YbAG	6,62 g/cm³	61,4 %	4,9 m³

Un autre avantage des matériaux inorganiques réside dans leur stabilité physique et chimique, au contraire des liquides organiques dont c'est un point préoccupant. Ils sont de ce fait nettement moins contraignants du point de vue sûreté (non volatiles, ininflammables), et on peut envisager d'utiliser des coïncidences retardées plus longues, tant pour l'identification des captures de neutrinos (par exemple la décroissance en 3,7 h du ^{176}Lu^m dans le cas d'un détecteur basé sur Yb) que pour la réjection des bruits de fond.

Dans le même but, la discrimination entre types de particules, notamment entre alpha et gamma, par la reconnaissance des formes de spectres ou par d'autres méthodes, (comme éventuellement l'utilisation de la scintillation infrarouge dans les grenats d'ytterbium) peut rendre de grands services.

L'étroite interaction de ces problèmes et des caractéristiques interdit de conclure rapidement à la faisabilité ou à la non faisabilité d'un détecteur basé sur tel ou tel matériau à la seule connaissance de ses caractéristiques courantes de scintillation telles que le rendement lumineux et la vitesse de décroissance. Telle limite maximale estimée pour un contaminant radioactif dans un liquide scintillant (par exemple ^{235}U < 10^{-16} g/g) pourrait, éventuellement, être assouplie de plusieurs ordres de grandeur dans un scintillateur solide, s'il s'avérait que l'on peut détecter des coïncidences retardées longues et distinguer les particules alpha des rayons gamma.

3.2.2.1. ^{160}Gd

Parmi les éléments proposés, le gadolinium était le seul dont on connaissait des composés formant des matériaux scintillants, il était même d'autant plus intéressant qu'un cristal scintillant, le silicate de gadolinium Gd$_2$SiO$_5$:Ce (GSO) était déjà utilisé industriellement.

Une étude détaillée a été menée sur ce cristal [42], dont le principal résultat a été de mettre en évidence la difficulté de reconnaissance de la signature de l'interaction neutrino. Certains évènements de bruit de fond imitent cette signature, en particulier les décroissances de certains noyaux radioactifs, soit présents en impuretés (notamment la décroissance du thorium 231 présent dans la chaîne de l'uranium 235), soit induits par réaction nucléaire (par exemple la décroissance du gadolinium 153 produit par réaction n/2n sur le gadolinium 154) avec des schémas temporels et énergétiques proches des interactions neutrino et donc non distinguables de celles-ci.

Mais le bruit de fond le plus problématique provient en fait des fluctuations statistiques des impulsions lumineuses de scintillation, qui elles aussi peuvent imiter la signature neutrino []. À scintillateur donné, une meilleure rejection de celles-ci entraîne une perte notable d'efficacité du détecteur (alors que les taux d'interaction sont déjà extrêmement faibles). Un paramètre pertinent est le rendement lumineux du scintillateur par unité de temps. Pour le GSO, 12 000 photons/MeV en environ 50 ns semblent insuffisants, eut égard aux caractéristiques de l'interaction neutrino (87 ns, 64 keV).

De plus, la présence d'un isotope radioactif naturel, émetteur alpha (^{152}Gd, E_α = 2,205 MeV, $\tau_{1/2}$ = 1,08 10^{14} ans), même si sa proportion est très faible (0,20(1)% du gadolinium naturel), est très pénalisante. De même, la présence dans la réaction de capture de quatre niveaux nucléaires possibles pour l'état excité du noyau fils ^{160}Tb complique notablement l'étalonnage d'un éventuel

détecteur : plusieurs sources de neutrinos, d'énergies différentes, devraient être utilisées. Ces deux problèmes ont entraîné assez rapidement l'abandon de ce noyau au profit de l'ytterbium.

3.2.2.2. ^{176}Yb

L'ytterbium avait été initialement exclu des études de matériaux scintillateurs inorganiques pour la spectroscopie des neutrinos. En effet il semblait a priori difficile de pouvoir trouver des scintillateurs rapides et efficaces contenant cet élément, en raison du transfert de charge se produisant en présence de cérium (pressenti comme seul activateur plausible) et supprimant sa luminescence :

$$Yb^{3+} + Ce^{3+} \rightarrow Yb^{2+} + Ce^{4+}$$
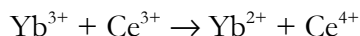
C'est le cas par exemple du silicate d'ytterbium Yb_2SiO_5:Ce, qui ne présente quasiment aucune luminescence alors que ses analogues Y_2SiO_5:Ce (YSO), Gd_2SiO_5:Ce (GSO) et Lu_2SiO_5:Ce (LSO) sont d'excellents scintillateurs [43].

La découverte par l'équipe de G. Carugno de la scintillation ultraviolette rapide dans les grenats d'ytterbium $(Y-Yb)_3Al_5O_{12}$ [44] a montré l'existence possible de scintillateurs rapides incorporant des densités importantes d'ytterbium, ouvrant ainsi la voie à une éventuelle utilisation de ceux-ci pour la spectroscopie des neutrinos solaires.

Les études que nous avons engagés ont porté principalement sur le système des grenats $(Y_{(1-x)}-Yb_x)_3Al_5O_{12}$ et ont permis de confirmer la découverte de G. Carugno. Ce système bénéficie en effet a priori des développements existants sur les grenats d'yttrium, dopés ou non en terres rares, pour l'optique et les lasers. Il faut noter en particulier que, pour ces applications dans les lasers, des monocristaux de YAG:Yb de taille relativement importante sont disponibles sur le marché, avec des concentrations d'ytterbium de l'ordre de 5 à 10 % voire plus élevées.

La structure cristalline des grenats d'aluminium et d'yttrium/ytterbium est cubique faces centrées, groupe d'espace Ia3d. La solution solide entre yttrium et ytterbium existe dans ce système pour toute concentration x. Les ions Y^{3+} et Yb^{3+} ont en effet des rayons ioniques très proches.

À température ambiante, ces composés montrent une photoluminescence et une scintillation très rapide, avec une bande d'émission centrée sur 330 nm et une plus faible autour de 500 nm (voir figure 3-7). L'écart entre ces deux bandes correspond à la différence d'énergie entre les deux premiers états électroniques de l'ion Yb^{3+} : $^2F_{7/2}$ (état fondamental) et $^2F_{5/2}$ (1er état excité).

Le rendement lumineux dépend de la concentration en ytterbium, avec un maximum de l'ordre de 14% du BGO pour une concentration d'ytterbium d'environ 15%.

La variation de la luminescence avec la température présente un comportement peu habituel. La photoluminescence (émission sous excitation ultraviolette) décroît avec la température au-dessus de 100 K, ce qui témoigne de la présence de processus non radiatifs activés par la température en compétition avec les désexcitations radiatives responsables de la luminescence. La radio-luminescence (émission sous excitation X) augmente tout d'abord avec la température pour passer par un maximum vers 100 K et décroître ensuite. Ce comportement est corrélé avec les propriétés de thermoluminescence, qui montrent justement un pic d'émission à cette température. Cela indique que des états excités, peuplés par les excitations de haute énergie mais non par les excitations ultraviolettes, sont piégés à basse température (et donc perdus pour la scintillation) et libérés au-dessus de 100 K.

Le rendement lumineux atteint plusieurs fois celui du BGO dans le composé à 15% d'ytterbium. Cependant, pour les composés à plus haute concentration il est nettement plus faible.
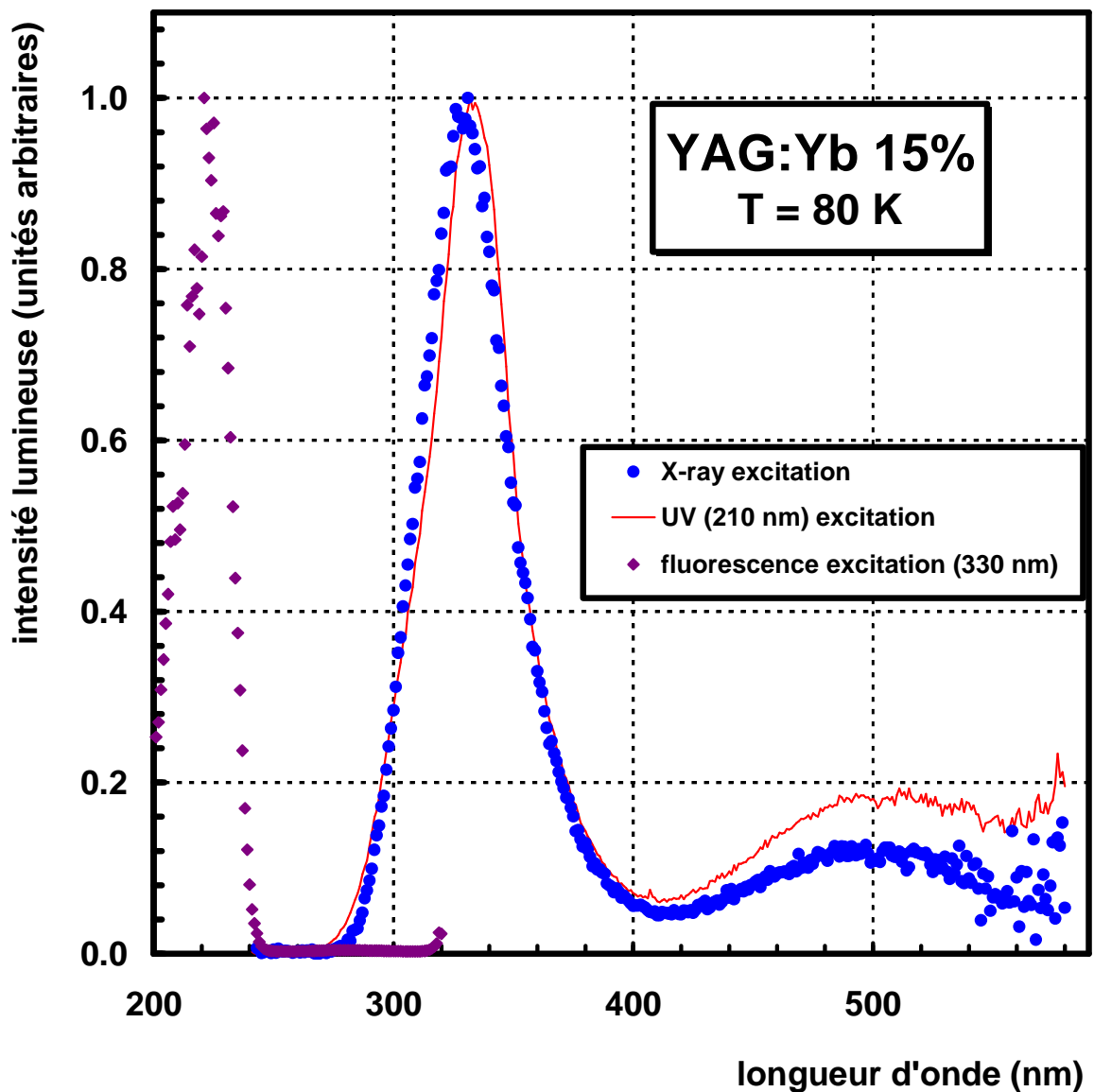
Figure 3-7 :
$Y_{2,55}$-$Yb_{0,45}Al_5O_{12}$: Spectres de photo- et radio-luminescence.
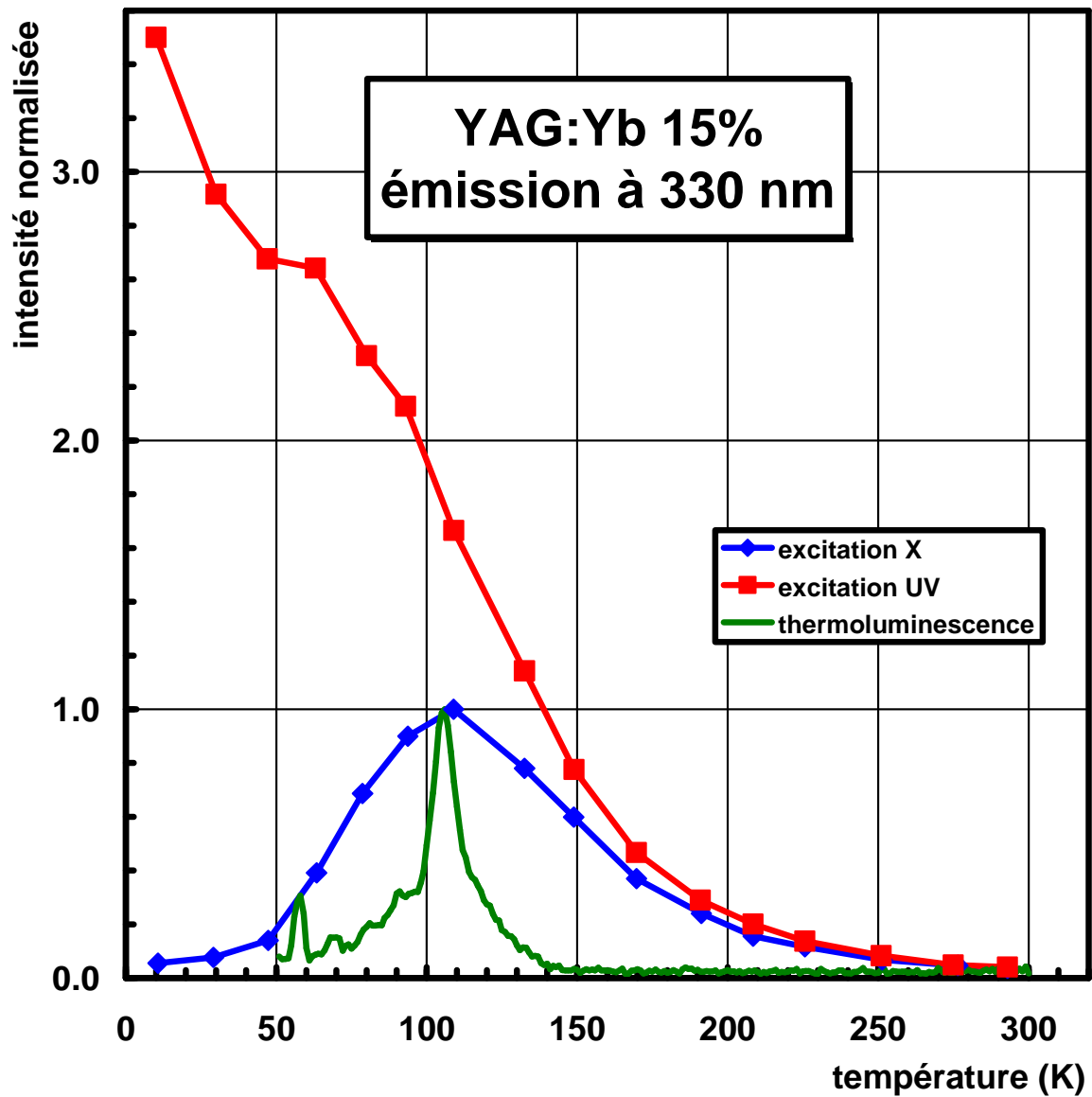
Figure 3-8 :
$Y_{2,55}$-$Yb_{0,45}Al_5O_{12}$: Variation des rendements lumineux et spectre de thermoluminescence en fonction de la température.
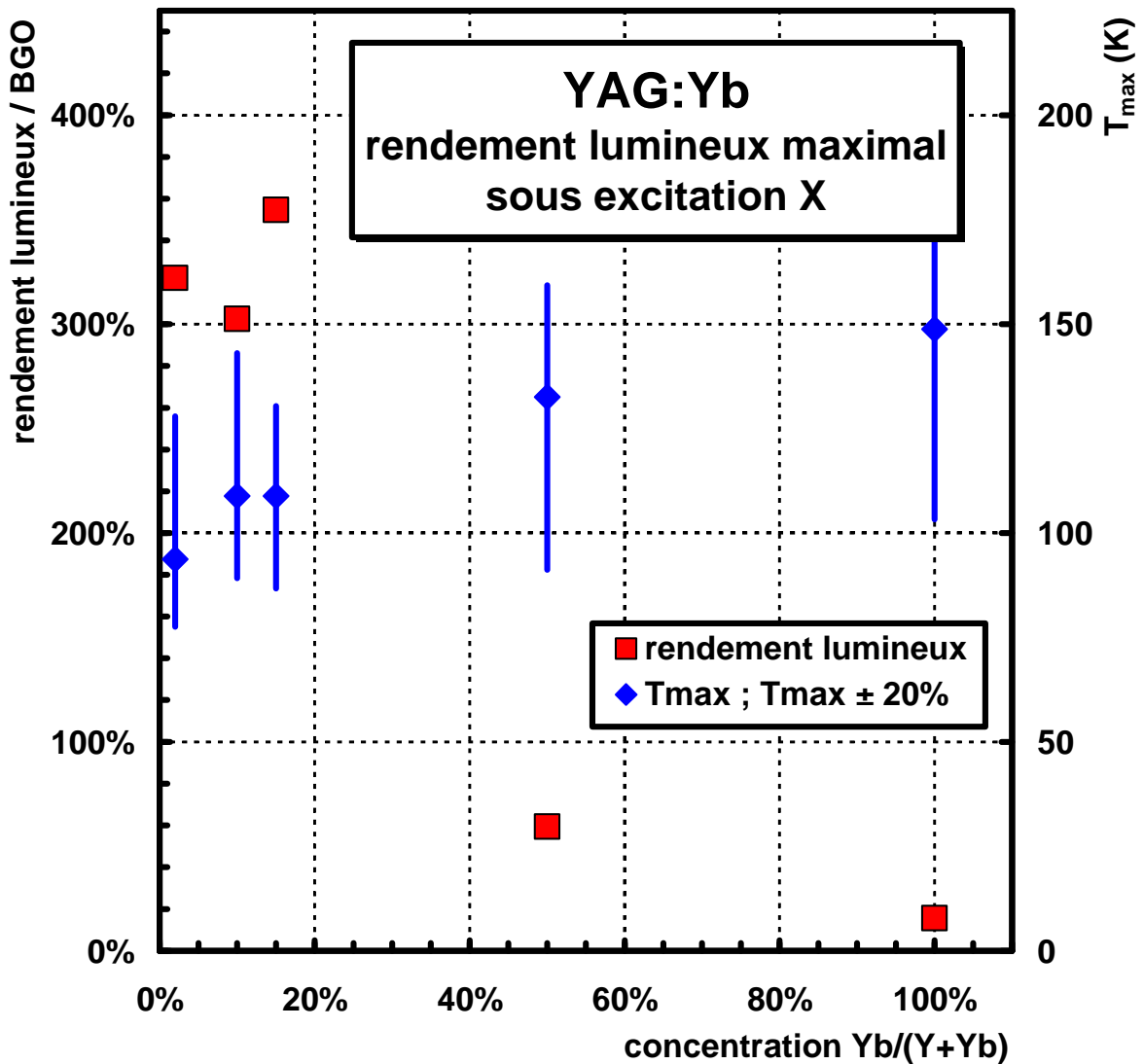
Figure 3-9 :
Y_{3-3x}-$Yb_{3x}Al_5O_{12}$: Rendement lumineux et température du maximum d'émission en fonction de la concentration d'ytterbium x.
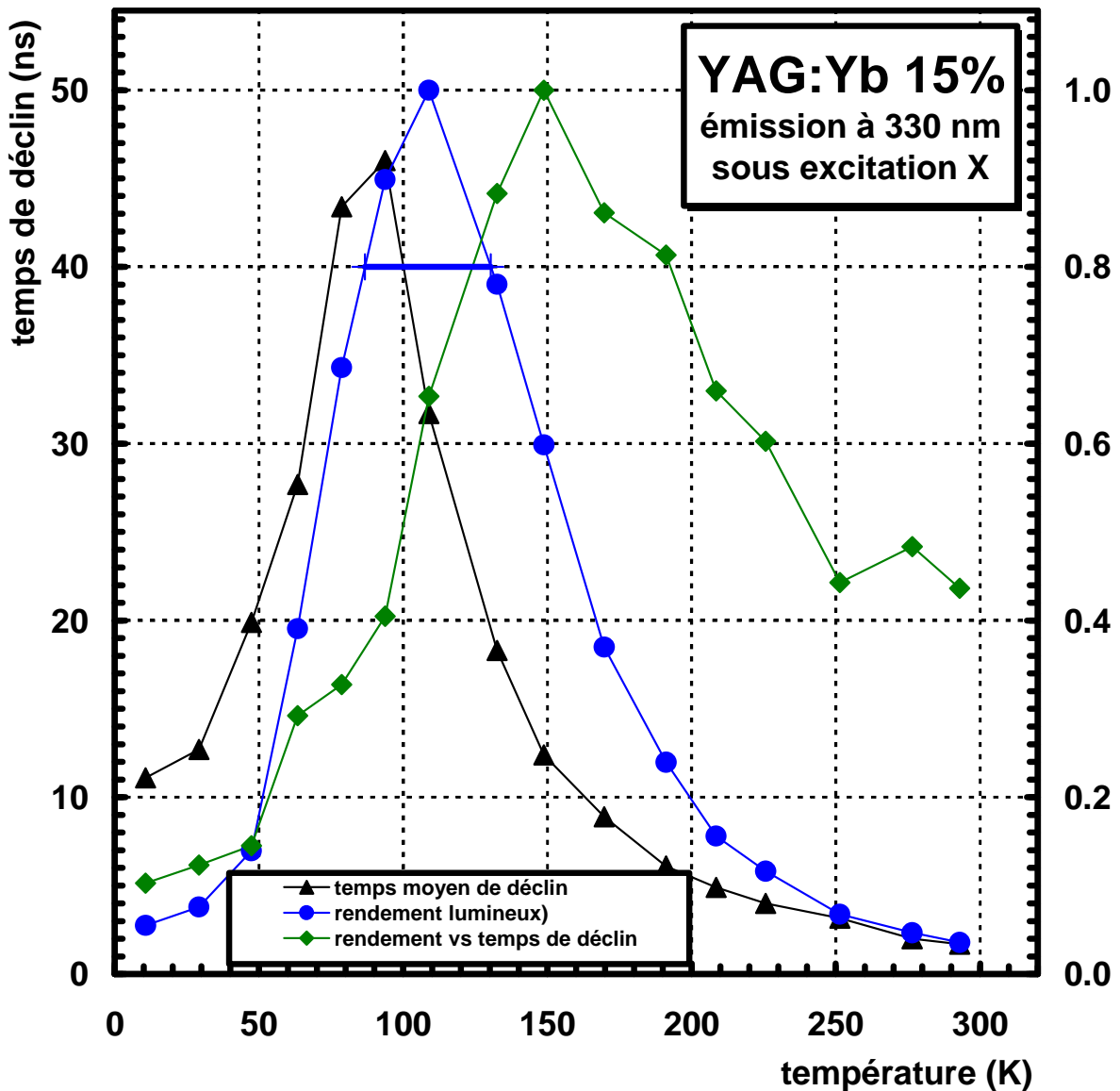
Figure 3-10 :
$Y_{2,55}$-$Yb_{0,45}Al_5O_{12}$: variation du temps de décroissance moyen, du rendement lumineux et du rapport rendement sur temps de décroissance en fonction de la température.

La découverte des propriétés de luminescence et de scintillation intrinsèques de ces oxydes d'ytterbium, intéressantes tant pour la détection des neutrinos, voire la détection des rayonnements en général, qu'en tant que telles pour l'étude fondamentale de la physique de la luminescence [45], a motivé le démarrage de recherches sur d'autres composés à base d'ytterbium. Dans le cadre d'un contrat OTAN que nous avons mené avec le Laboratoire de Physique et Chimie des Matériaux Luminescents de Lyon et le laboratoire de cristallogenèse de l'Académie des Sciences arménienne à Ashtarak, nous avons montrés que cette luminescence se retrouvait également dans de nombreux autres oxydes d'ytterbium. Le tableau 3-2 résume les résultats obtenus dans le cadre de ce contrat.

Tableau 3-2 : Propriétés des scintillateurs ytterbium.

Scintillateur	Rendement lumineux relatif à 300 K (%)	Temps de décroissance à 300 K (ns (fraction, %))	Maximum d'émission (nm)	Densité (g/cm³)	Longueur de radiation X_0 (cm)	Rayon de Molière R_m (cm)	Contenu en ytterbium (g/g)
$Bi_4Ge_3O_{12}$	100	300	505	7,13	1,12	2,23	0
$Y_{2,94}Yb_{0,06}Al_5O_{12}$	9,4	1,8 (74), 15,5 (26)	330				1,7 %
$Y_{2,70}Yb_{0,30}Al_5O_{12}$	12,5	1,7 (71), 19 (29)	330				8,4 %
$Y_{2,55}Yb_{0,45}Al_5O_{12}$	12,7	1,6 (67), 17 (33)	330	4,86	2,96	2,66	12,3 %
$Y_{1,50}Yb_{1,50}Al_5O_{12}$	5,4	1,5 (71), 13 (29)	330	5,57	2,12	2,44	36,1 %
$Yb_3Al_5O_{12}$	4,4	1,0 (66), 15 (34)	330	6,62	1,50	2,18	61,4 %
$Y_{2,94}Yb_{0,06}Ga_5O_{12}$	24,8	1,1 (9), 7,8 (41), 50,4 (50)					1,3 %
$Y_{2,55}Yb_{0,45}Ga_5O_{12}$	4,5	1,0 (10), 9,9 (31), 53,6 (59)					9,2 %
$Yb_3Ga_5O_{12}$	5,5	1,0 (15), 9,7 (34), 47,8 (53)		7,74	1,27	1,90	49,0 %
$Y_{0,92}Yb_{0,08}AlO_3$	7,3						8,1 %
$LaYbO_3$	1,6	0,53 (62), 16 (38)		8,16	1,02	1,94	48,1 %

L'étude de l'application des YAG:Yb et autres scintillateurs à base d'ytterbium pour la détection des neutrinos solaires n'a pas été menée dans le détail. Si on compare avec le GSO (voir paragraphe 3.2.2.1 ci-dessus), à 120 K un détecteur basé sur un YAG:Yb 15-20% présenterait de meilleures caractéristiques avec toutefois l'inconvénient majeur de la température cryogénique. À température ambiante, la diminution drastique du rendement lumineux n'est que partiellement compensé par le temps de décroissance très faible.

Toutefois il convient de noter que les données n'ont pour le moment été obtenues qu'avec des cristaux de laboratoire, de petite taille et dont la fabrication n'a pas été optimisée. On peut penser qu'au prix de développements spécifiques, certaines améliorations peuvent être obtenues. Par ailleurs, l'émission infrarouge intense de ces matériaux apporte un élément nouveau, qu'il serait intéressant d'étudier plus précisément, pour éventuellement s'en servir pour améliorer les performances de détection (résolution en énergie notamment) voire de discrimination entre différents rayonnements.

C'est un vaste champ de recherche qu'il ne m'a pas été donné de poursuivre, en raison notamment du recentrage de l'intérêt des physiciens des neutrinos sur, dans un premier temps, l'indium comme cible d'interaction, et dans un second temps sur les neutrinos de plus haute énergie, suite notamment aux résultats des expériences SuperKamiokande et SNO.

Même si l'intérêt pour la spectroscopie des neutrinos solaires de basse énergie est devenu moins immédiat, une nouvelle classe de scintillateurs, les scintillateurs à l'ytterbium, a commencé à être étudiée. Il est satisfaisant de noter que, même si c'est sur une échelle relativement réduite, ces études se poursuivent ailleurs dans la communauté des scintillateurs [46].

3.2.2.3. [115]In

En dépit de nombreuses tentatives, les développements de détecteurs à base d'indium n'avaient pas débouchés sur des matériaux de performances suffisantes pour permettre la réalisation d'un détecteur de neutrinos. Dans le domaine des cristaux scintillants, le même problème de transfert de charge qu'avec Yb^{3+} apparaît entre Ce^{3+} et In^{3+}, interdisant l'emploi du cérium comme activateur. Parmi les matériaux riches en indium, $InBO_3$:Tb montre une luminescence relativement intense mais longue [47], le titanate In_2TiO_5 [48], le tungstate In_6WO_{12} [49], les silicate et germanate $In_2Si_2O_7$ et $In_2Ge_2O_7$ [50], tous scintillateurs intrinsèques, présentent une

émission lumineuse insuffisante de même que, plus récemment étudiés, les matériaux dopés suivants : tantalate InTaO$_4$:Tb ou :Ce, gallate InGaO$_3$:Tb ou indate d'yttrium YInO$_3$:Tb [51].

Les progrès accomplis par la collaboration LENS dans le développement de liquides organiques scintillants chargés en éléments métalliques, notamment ytterbium, ainsi que les inconvénients de cet élément comparé à l'indium pour la spectroscopie des neutrinos ont permis de relancer l'idée de l'utilisation de ce métal [42,52] et partant les recherches et développements, notamment dans le domaine des cristaux scintillants.
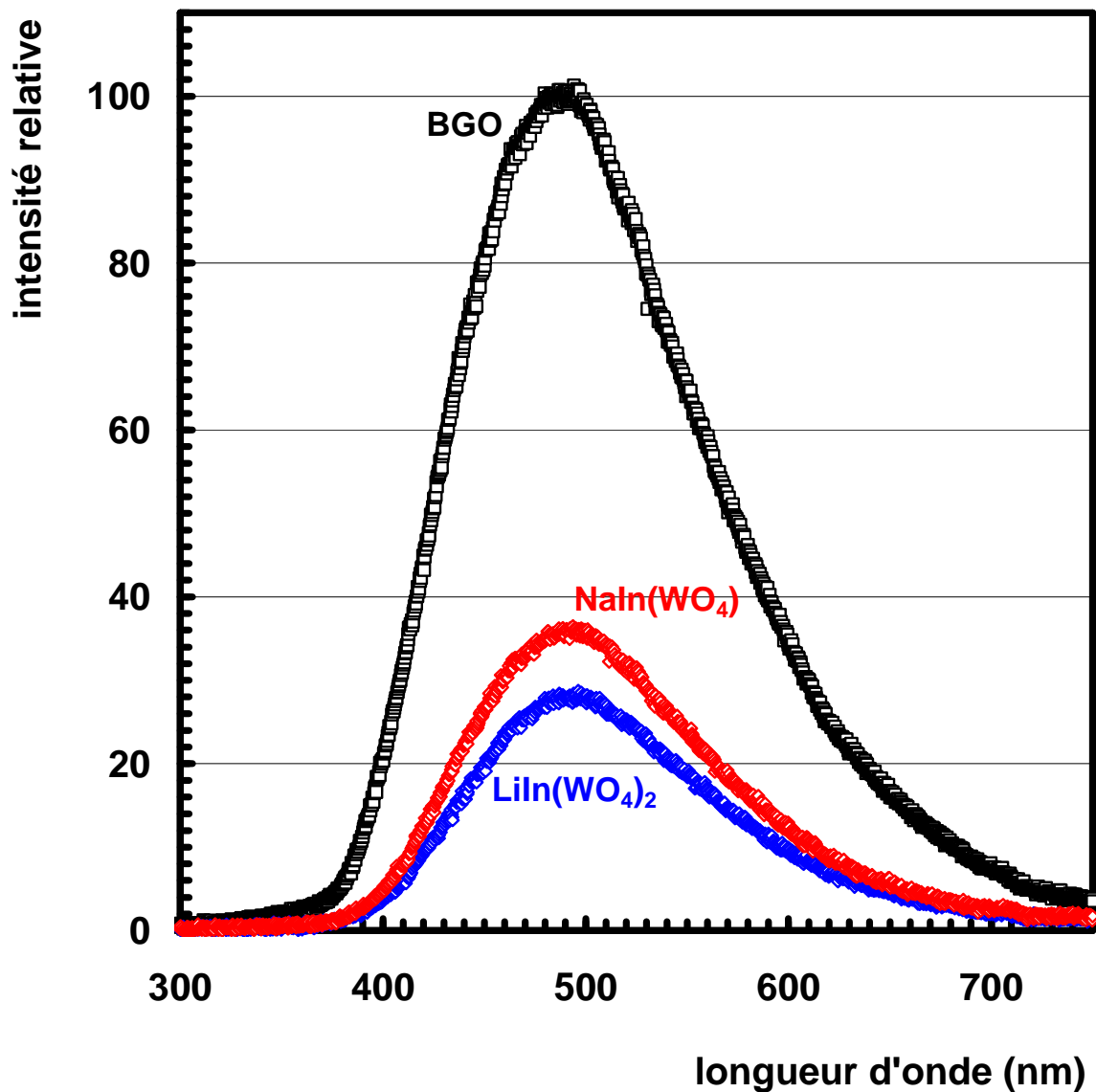
Figure 3-11 :
Spectres d'émission de NaIn(WO$_4$)$_2$ et LiIn(WO$_4$)$_2$, comparaison avec BGO mesuré dans les mêmes conditions.
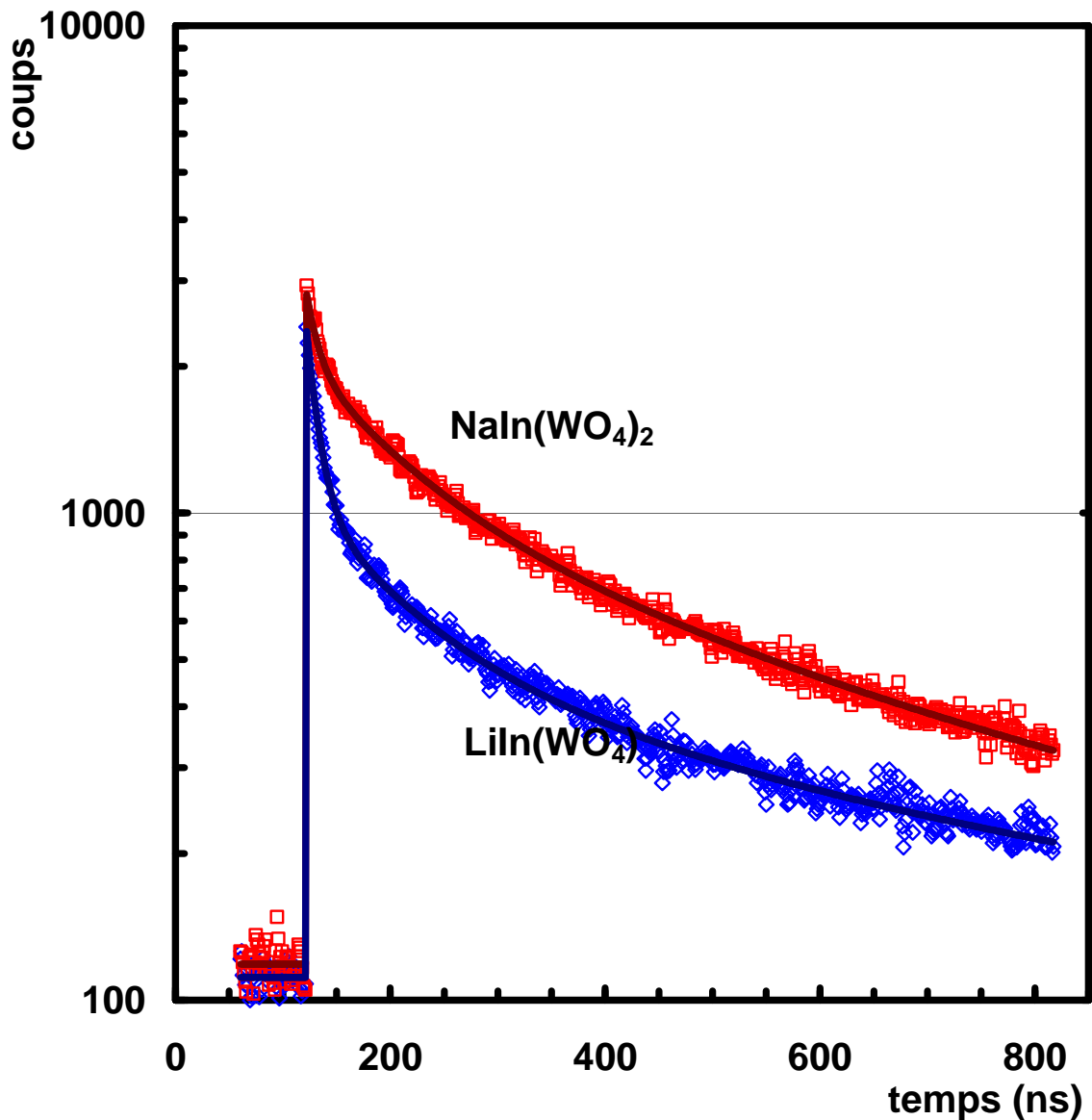
Figure 3-12 :
Spectres de décroissance lumineuse dans NaIn(WO$_4$)$_2$ et LiIn(WO$_4$)$_2$, et ajustements par une
somme de trois exponentielles (voir tableau 3-3).

Réalisées dans le cadre d'un contrat INTAS avec l'INP de Minsk, nos investigations ont porté sur
les tungstates mixtes NaIn(WO$_4$)$_2$ et LiIn(WO$_4$)$_2$, synthétisés sous forme de poudre, qui se sont
révélés présenter des caractéristiques de scintillation proches du BGO, avec un spectre d'émission
centré sur 490 nm (voir figure 3-11.), des intensités lumineuses proches du tiers de celui-ci, donc
de l'ordre de 2700 photons/MeV, et des décroissances pouvant se décomposer en trois
composantes d'environ 10, 100 et 500 ns (voir la figure 3-12 et le tableau 3-1) [53].

Tableau 3-3 : Propriétés des tungstates mixtes d'indium et de sodium ou de lithium.

Scintillateur	Rendement lumineux relatif (%)	Temps de décroissance (ns (fraction, %))	Maximum d'émission (nm)	Densité (g/cm^3)	Longueur de radiation X_0 (cm)	Rayon de Molière R_m (cm)	Contenu en indium (g/g)
$Bi_4Ge_3O_{12}$	100	300	505	7,13	1,12	2,25	0
$NaIn(WO_4)_2$	36	11,2 (3,4) 94,6 (17,1) 448 (79,5)	490	7,14	1,23	2,12	18,1 %
$LiIn(WO_4)_2$	27	11,6 (10,9) 94,0 (18,7) 494 (70,4)	490	7,46	1,16	2,05	18,6 %

Deux hypothèses peuvent être formulées sur l'origine de la scintillation. La plus naturelle et probable est celle de transfert de charge dans les groupes WO_6^{6-}, comme dans la plupart des tungstates. On peut aussi suggérer que la luminescence est due à la recombinaison $In^{4+}(4d^9) \rightarrow In^{3+}(4d^{10})$. Il est cependant prématuré de conclure sur les mécanismes et les caractéristiques de la luminescence dans ces matériaux et partant sur leur utilisation pour la spectroscopie des neutrinos. D'une part les propriétés des matériaux sous forme monocristalline peuvent différer notablement de celles des poudres polycristallines. D'autre part, en ce qui concerne la détection des neutrinos, l'étude de la pureté radioactive, vis à vis notamment du potassium 40, élément chimiquement très proche du sodium et du lithium, reste cruciale, même si la radioactivité de l'indium lui-même reste dominante. Dans ce contexte, des possibilités de discrimination entre rayonnements seraient, là aussi, très attractives. Comme pour les cristaux à base d'ytterbium, le recentrage des recherches en physique des neutrinos a entraîné l'arrêt, (probablement provisoire...) des études sur ces matériaux.

3.3. Détecteurs à effet Cherenkov

Les photons Cherenkov sont émis par une particule chargée traversant un matériau transparent à une vitesse βc supérieure à la vitesse de la lumière c/n dans ce matériau (n étant son indice de réfraction) suivant un angle $\theta = \arccos(\beta/n)$ par rapport à la trajectoire de la particule, et avec une polarisation située dans le plan formé par les deux directions.

Cette propriété géométrique est exploitée dans des dispositifs de reconnaissance de particules, ou dans des discriminateurs de trajectoire, et notamment dans le Trigger Optique imaginé par G. Charpak, Y. Giomataris et L. Lederman [54], sur lequel j'ai travaillé.

Le but de ce dispositif était de fournir une information rapide permettant de sélectionner dans une expérience sur cible fixe les trajectoires de particules secondaires issues de désintégrations de particules primaires, et donc présentant un « paramètre d'impact » non nul par rapport à la cible, contrairement aux trajectoires issues de celle-ci (voir figure 3-13).
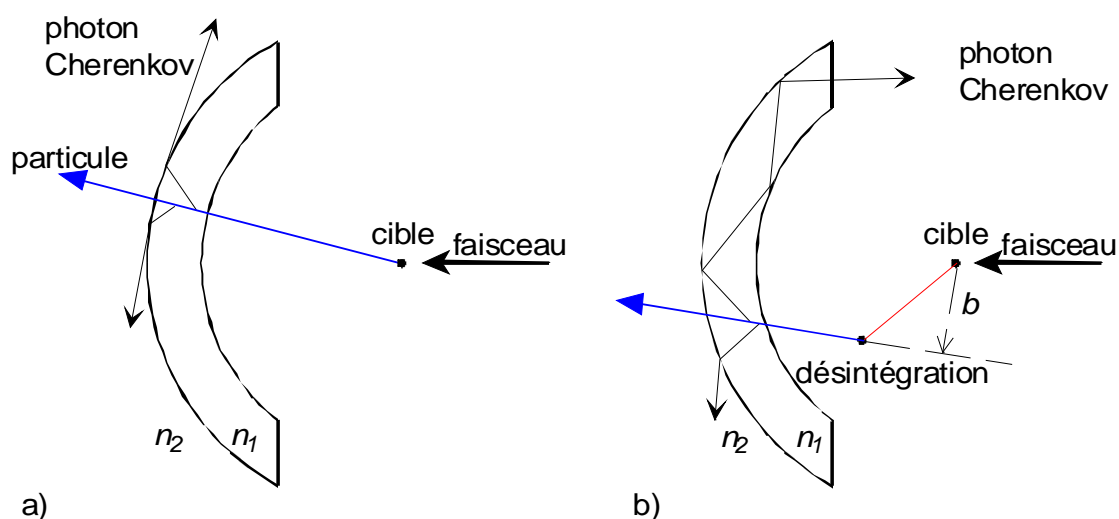
Figure 3-13 :
Schéma de principe du trigger optique.

Le principe repose sur les propriétés géométriques de la lumière Cherenkov créée dans une coupelle transparente en forme de coquille sphérique centrée sur la cible. Moyennant certaines conditions entre les indices de réfraction de la coupelle et du milieu extérieur, les photons Cherenkov provenant d'une particule sans paramètre d'impact peuvent parvenir à la surface extérieure suivant un angle d'incidence inférieur à l'angle critique de réflexion totale, et être progressivement réfractés, alors qu'une partie des photons provenant d'une particule à paramètre d'impact peuvent être en réflexion totale, et guidés dans la coupelle jusqu'à sa tranche où ils pourront être détectés et fournir un signal.

Ce dispositif a fait l'objet d'études par la collaboration RD30 [55-57], études théoriques, recherches de matériaux, tests en faisceau… avec des résultats prouvant la validité du principe (cf. figure 3-14). Tout d'abord avec un matériau simple (le fluorure de lithium LiF) placé dans l'air, puis avec des dispositifs en silice ou en saphir placés dans des liquides d'indice ou couverts de couches minces optiques [58,59]. La thèse d'Alain Delbart effectuée sous ma direction a grandement contribué à ces résultats.
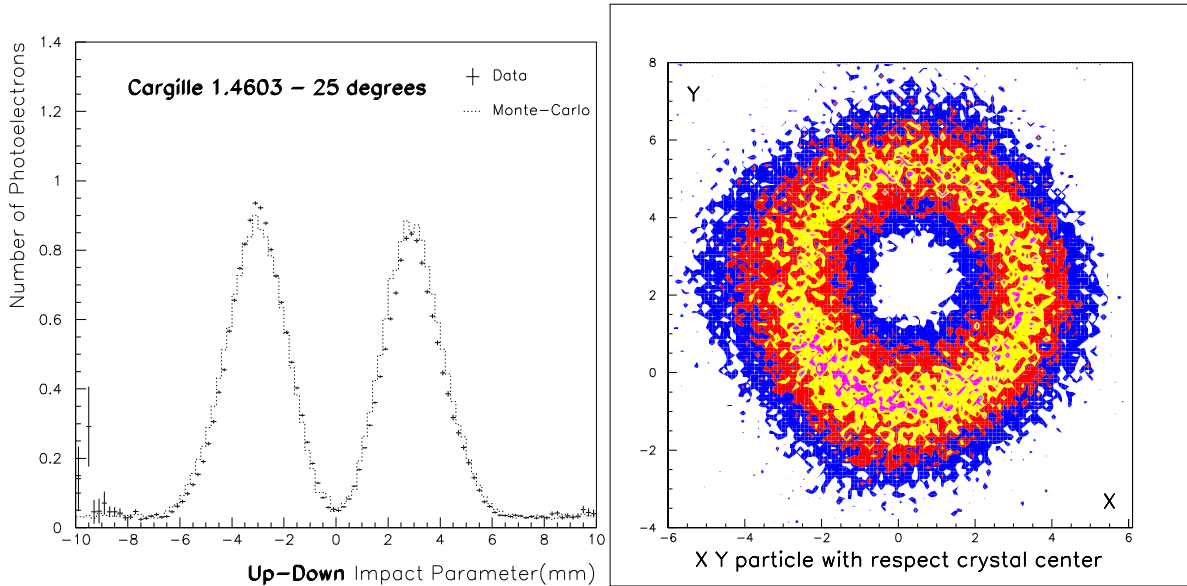
Figure 3-14 :
Trigger optique saphir/liquide d'indice :
droite : réponse du détecteur (en photoélectron par particule) suivant une coupe verticale ;
gauche : vue 2D montrant la réjection des trajectoires à paramètres d'impact faible (le détecteur
est ici centré sur (~0,5 mm, ~2,5 mm).

Nous noterons également l'étude théorique systématique de l'effet Cherenkov dans les milieux anisotropes effectuée à cette occasion par A Delbart et J. Derré [60], voir Figure 3-15. Outre une avancée sur ce point théorique peu et mal étudié, elle a facilité la compréhension des propriétés optiques des milieux anisotropes, abordées pour le $PbWO_4$ de CMS et le programme de simulation optique Litrani (cf. chapitre 3.2.1.3).

Dans des cas particuliers, comme par exemple la calorimétrie électromagnétique à haute énergie ou la discrimination de trajectoires de particules chargées, l'effet Cherenkov peut également être utilisé dans des matériaux transparents mais non scintillants.
Nous citerons l'exemple du fluorure de plomb PbF_2, qui se compare bien aux cristaux scintillants utilisés en physique des hautes énergies du point de vue transparence et densité mais qui n'est pas scintillant (en dépit de quelques supputations infondées). Il a fait l'objet d'études infructueuses en vue d'y induire une scintillation par des dopages appropriés [61], pour finalement être proposé comme matériau actif pour le calorimètre électromagnétique de CMS [31]. L'avantage de la lumière Cherenkov est d'être instantanée, par contre le rendement lumineux est extrêmement faible (dans le tungstate de plomb, pourtant peu performant en terme de rendement lumineux, le rapport entre lumière Cherenkov et lumière de scintillation est estimé à 15 % [62]). Par contre dans un calorimètre électromagnétique, la largeur de la gerbe électromagnétique effectivement mesurée est inférieure du fait du seuil Cherenkov.
Ce rapport entre lumière Cherenkov et lumière de scintillation dépend du type de particules. Il est maximal, à énergie donnée, pour les électrons et photons, et décroit pour les hadrons. On envisage maintenant de mesurer séparément dans un même détecteur lumière de scintillation et Cherenkov, soit en séparant spectralement les deux types de lumière (la lumière Cherenkov pique dans l'ultraviolet), soit par reconnaissance de forme (la lumière Cherenkov étant instantanée au contraire de la scintillation), ce qui permettrait la réalisation de calorimètres hadroniques homogènes de haute solution. C'est le concept de calorimètres à double lecture développé notamment dans le projet DREAM [63].
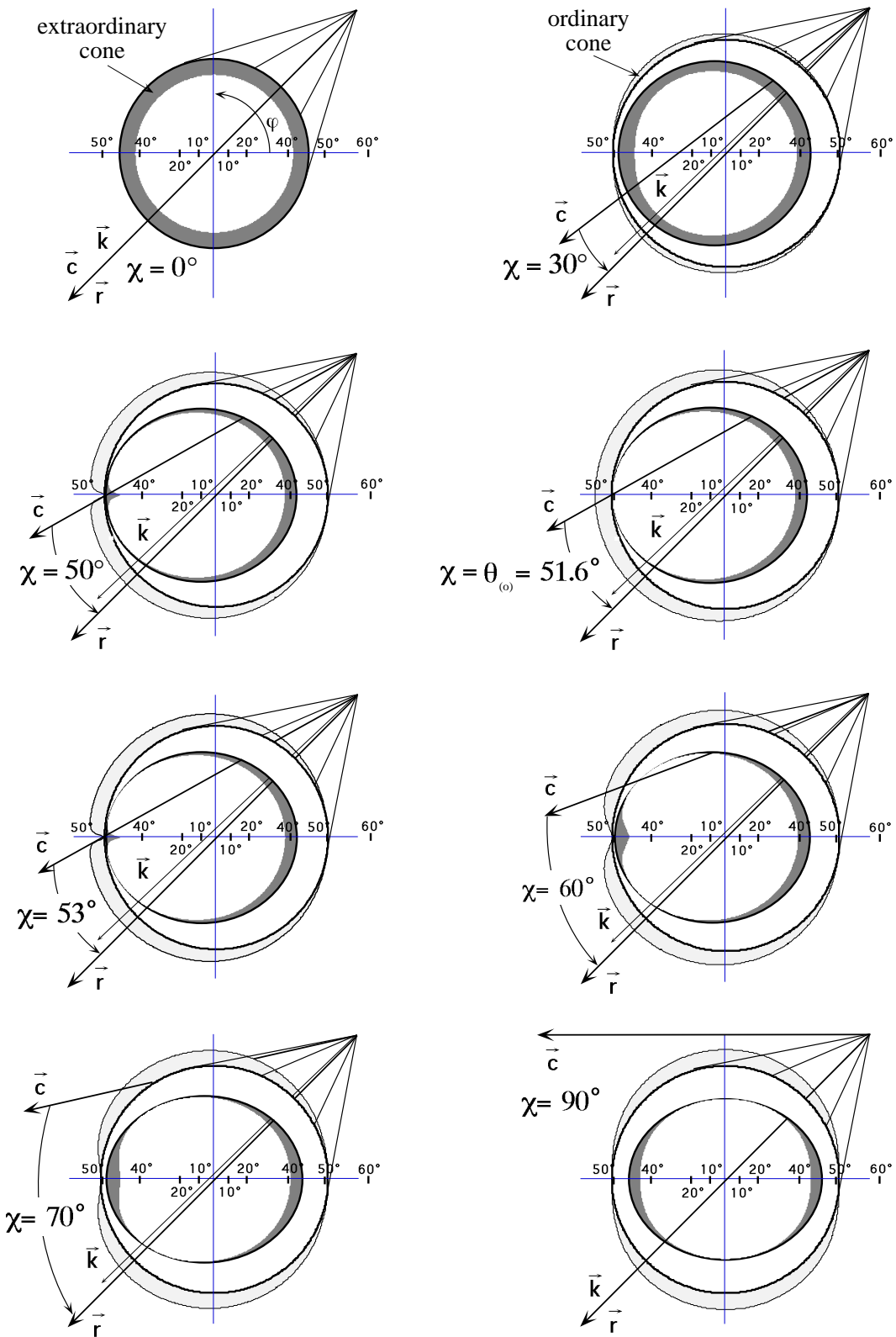
Figure 3-15 :
Cônes théoriques de lumière Cherenkov ordinaire (en gris) et extraordinaire (en noir) pour des trajectoires de particules relativistes à différents angles χ dans un cristal de NaNO₃ [60].

4. Travaux sur les détecteurs CdTe, modélisations avec GEANT4

4.1. Détecteurs CdTe

Ces dernières années, mon intérêt s'est porté sur les détecteurs semi-conducteurs en tellurure de cadmium (CdTe) développés par le groupe « hautes énergies » du Service d'Astrophysique de l'IRFU.

Fort de l'expérience acquise avec la caméra ISGRI embarquée sur le satellite INTEGRAL [64] le SAp développe des détecteurs CdTe à anode segmentée. Outre les avantages du CdTe (densité, grande résistivité permettant le fonctionnement à température ambiante), le concept d'anode segmenté permet de s'affranchir dans une large mesure du problème dit de « déficit balistique ».

Dans un détecteur semi-conducteur, le signal est formé par la charge électrique induite sur les électrodes par la migration en sens opposés des charges, négatives (électrons) vers l'anode et positives (trous) vers la cathode créées par le rayonnement. Dans des semi-conducteurs comme le CdTe, les mobilités des deux types de porteurs, par ailleurs faibles comparativement à celles du silicium, diffèrent d'un ordre de grandeur, ce qui induit une variation de la forme du signal électrique suivant l'endroit où a eu lieu l'interaction. Une interaction près de la cathode engendrera une impulsion plus courte, car essentiellement due à la dérive des électrons, qu'une interaction près de l'anode, pour laquelle le signal sera dû aux trous, 10 à 20 fois plus lents. Cet effet est particulièrement important dans un détecteur planaire épais, ce qui se traduit dans le cas d'une électronique de lecture classique, à mise en forme et mesure de l'amplitude ou de l'intégrale de l'impulsion, par une perte de résolution importante de la mesure de l'énergie déposée. Dans ISGRI, ce problème a été corrigé en mesurant simultanément amplitude et temps de montée des impulsions par une électronique de lecture spécifique. Les corrélations entre ces deux paramètres permettent de faire une correction de pertes de charges qui restore en partie la résolution de la mesure. [65].

Toutefois, dans des configurations d'électrodes non standards, et en particulier lorsqu'elles sont segmentées, le signal électrique induit ne se calcule plus si simplement. Dans le cas particulier d'une anode pixellisée, par exemple, ce n'est pas le champ électrique réel qui doit être utilisé mais celui qui serait créé par le seul pixel considéré, tous les autres étant portés au potentiel de la cathode. Dans ce cas le signal n'est induit que lorsque les électrons parviennent au voisinage de l'anode, et l'on s'affranchit ainsi des fluctuations de collection de charge dues au déficit balistique [66,67]. On obtient ainsi pour le même prix des détecteurs à haute résolution à la fois spatiale et spectrale. On n'a cependant rien sans rien, cela se fait au détriment de la résolution temporelle, le temps de transit des charges jusqu'au voisinage de l'anode étant dépendant, lui aussi, de la position de l'interaction dans le volume du détecteur.

Sont développés conjointement, en collaboration avec le Sédi l'électronique intégrée de lecture (Asic Idef-X [68]) et l'intégration des éléments détecteurs et de leur électronique en modules (Caliste [69]) pouvant être assemblés pour former par exemple un plan focal de télescope à rayons X de grande résolution spectrale et spatiale.

Au sein de ce groupe, j'ai plus particulièrement pris en charge le développement des simulations numériques de l'interaction rayonnement matière avec GEANT4 [70]. Ces études ont deux buts principaux. D'une part elles permettent d'évaluer les propriétés des détecteurs dans leur environnement présumé. Couplées aux calculs numériques de champ et de transport de charges (voir le chapitre 5 de la thèse de Bob Dirks [66]) elles permettent de modéliser les formes d'impulsion. D'autre part, elles fournissent, comme nous le verrons plus particulièrement dans la section suivante pour le projet Simbol-X, une aide précieuse à la conception des expériences.

4.2. Simbol-X

Simbol-X est un projet de télescope spatial sensible dans la gamme des 0,5 à 80 keV [71]. Il utilise deux satellites volant en formation, emportant l'un un miroir à incidence rasante, l'autre le plan focal où sont placés les détecteurs. Ce concept permet d'obtenir une longueur focale de 20 à 30 m, nécessaire à la focalisation des rayons X au-dessus de 10 keV, et donc d'envisager une amélioration de plus de deux ordres de grandeurs tant en sensibilité qu'en résolution angulaire par rapport aux techniques d'imagerie non focalisantes de type masque codé.

Le plan focal de Simbol-X [72] est composé de deux détecteurs, un détecteur en silicium de type DepFet, de 128×128 pixels ($0,6 \times 0,6 \ \mu m^2$), fonctionnant de 0,5 à environ 20 keV, placé au-dessus d'un détecteur CdTe (ou CdZnTe) composé de 64 modules Caliste de 16×16 pixels ($0,6 \times 0,6 \ \mu m^2$ également) chacun, pour la gamme de 15 à 80 keV.

Pour atteindre les objectifs scientifiques de la mission, un bruit de fond inférieur à 10^{-4} coups cm^{-2}s^{-1}keV^{-1} est nécessaire dans chacun des détecteurs, ce qui est bien inférieur à ce que l'on observe dans les missions précédentes. Les deux sources principales de bruit sont le rayonnement X cosmique diffus et les interactions entre particules chargées de haute énergie, majoritairement des protons, avec les matériaux. En ce qui concerne le bruit induit par le rayonnement électromagnétique, cela implique un blindage efficace dimensionné pour être étanche en dessous de 200 à 300 keV, et gradué pour absorber en cascade les raies de fluorescence, ainsi qu'un collimateur de mêmes performances. La réduction du bruit induit par les particules chargées repose par contre sur un dispositif actif d'anticoïncidence, qui doit allier efficacité de réjection et compacité pour ne pas être soumis à un taux de comptage aveuglant les détecteurs.

Plusieurs modèles du détecteur, et plus largement de la charge utile, du satellite et du miroir ont été développés avec GEANT4, et utilisés pour évaluer les différentes contributions aux bruits de fond des détecteurs.
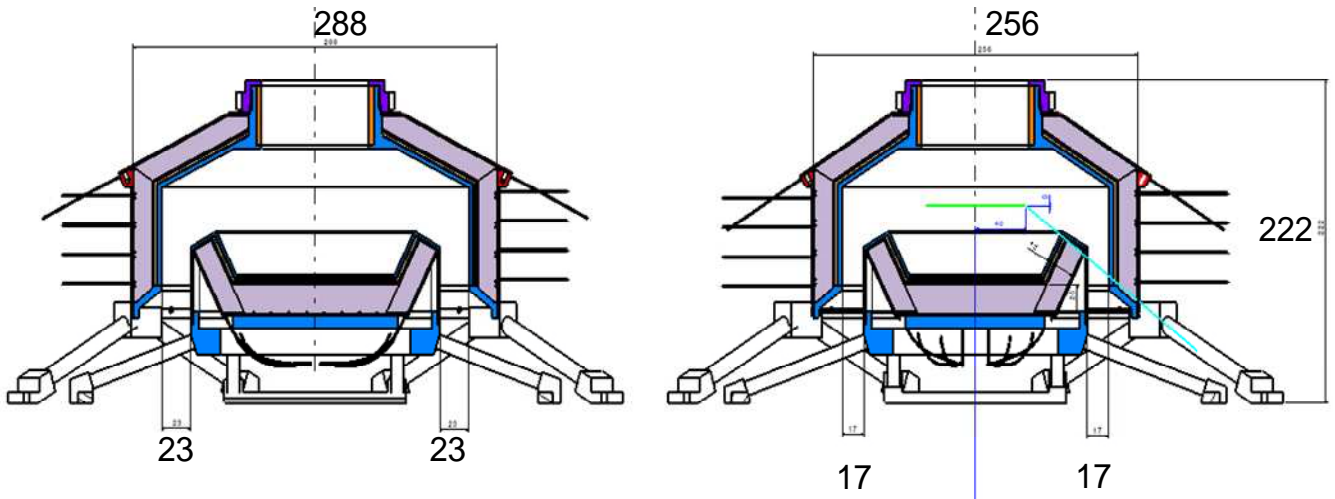
Figure 4-1 :
Schéma du plan focal de Simbol-X.

La réponse des instruments aux flux cosmiques de photons et de protons a été calculée pour différentes compositions, épaisseurs, positions des matériaux actifs (anticoïncidence) et passifs (collimateur, blindages et structures). Divers schémas de réjection sont étudiés : coïncidences entre éléments actifs, reconnaissances de formes dans les détecteurs, etc.

Tableau 4-1 : Bruit de fond dans Simbol-X calculé dans la version de base du plan focal.

Détecteur	Origine du bruit de fond	Taux de comptage après anticoïncidence (10^{-4} cts cm^{-2}s^{-1}keV^{-1})	Taux de comptage sans anticoïncidence (10^{-4} cts cm^{-2}s^{-1}keV^{-1})
LED	Protons cosmiques	0,9 – 1,8	35 – 70
	X et γ cosmiques	0,5	0,5
	radioactivité	0,1	0,1
	Total	**1,5 – 2,4**	36 – 71
HED	Protons cosmiques	0,9 – 1,8	55 – 110
	X et γ cosmiques	0,6	0,6
	radioactivité	0,1	0,1
	Total	**1,6 – 2,5**	56 – 111

Les états d'avancement successifs de ces travaux sont décrits dans les références [73-75]. Les derniers calculs sur un modèle optimisé, terminés juste avant l'abandon du projet par le CNES, montrent, après une réévaluation des facteurs de normalisation utilisés, que les performances estimées sont compatibles avec les critères demandés, laissant même marge à de nouvelles optimisations, notamment du collimateur. Ces dernières études vont être menées à leur terme, en vue d'une utilisation dans de futures propositions d'expériences
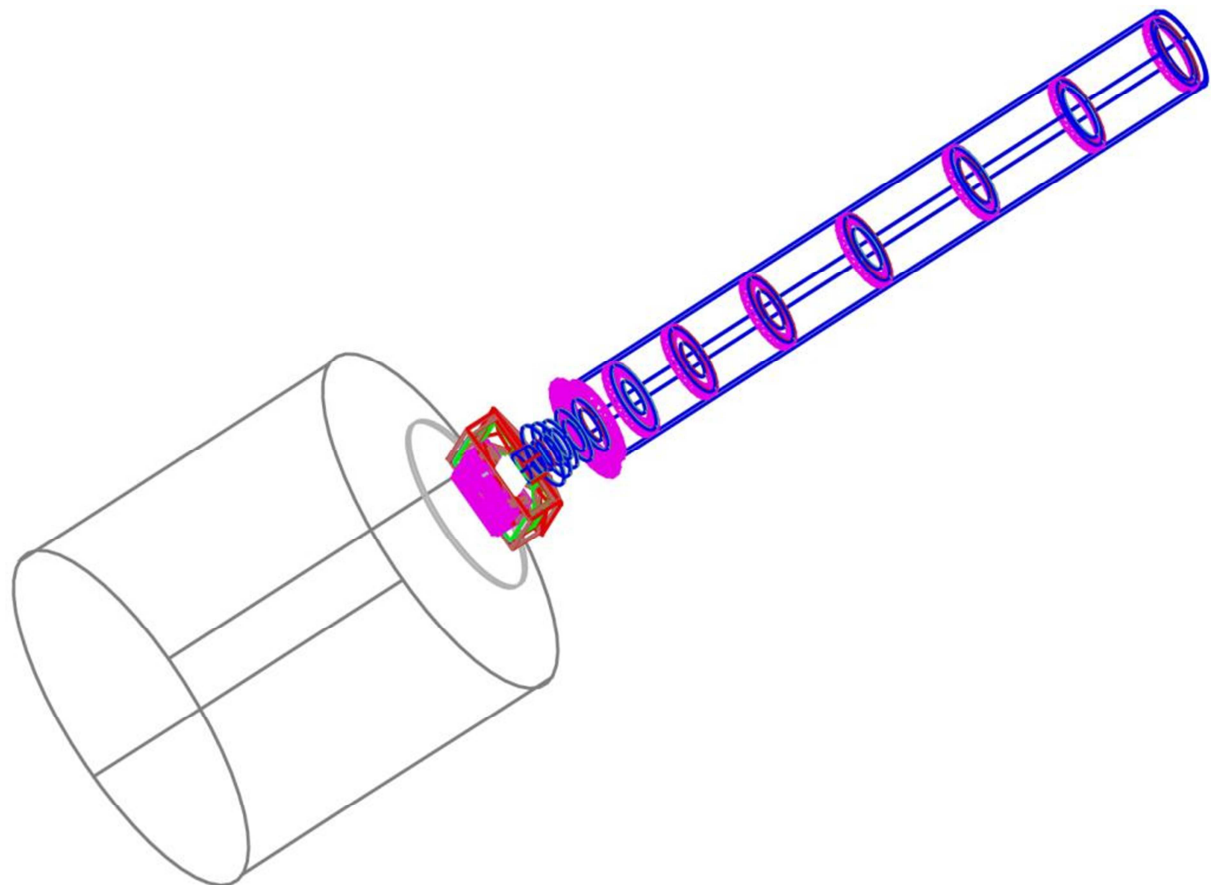
Figure 4-2 :
Modèle GEANT4 du satellite détecteur de Simbol-X (version 6.2).

5. Perspectives

En premier lieu la R&D sur les détecteurs CdTe à anode pixellisée, ou, plus précisément, des éléments modulaires détecteurs/électronique de lecture « Caliste » se poursuit. En particulier, se pose avec la génération des modules de 256 pixels la question d'optimiser les méthodes d'étalonnage. Le problème est de déduire des spectres expérimentaux obtenus par illumination par une source radioactive ou par un générateur X les paramètres d'étalonnage, de linéarité, voire d'efficacité et de rendement, d'une manière simple, robuste, automatisable et transposable « à bord », que ce soit dans l'espace ou dans des caméras autonomes sur terre. Ce thème n'est pas sans me rappeler mes travaux de fin de thèse sur l'analyse des spectres Mossbauer.

Les recherches et développements menées pour les détecteurs du plan focal de SIMBOL-X ont suscitées un vif intérêt dans la communauté des astrophysiciens des hautes énergies, et plusieurs équipes nous ont sollicités.
C'est ainsi que dans la mission ASTRO-H, télescope à rayons X multi-instruments développé par l'agence spatiale japonaise, (JAXA) et dont le lancement est prévu en 2014, nous sommes impliqués dans deux des instruments : le HXI (imageur à rayons X durs) et le SGD (détecteur de rayons gamma mous). Le premier est un télescope à focalisation fonctionnant entre 5 et 80 keV. Il comprend similairement à SIMBOL-X un plan focal composé d'un premier imageur en silicium pour la partie basse énergie et d'un second en CdTe pour la partie haute et un blindage actif. Le second est un télescope Compton à petit champ de vue fonctionnant dans une gamme de 10 à 600 keV. Il comprend des empilements de détecteurs silicium à piste et CdTe pixellisés, perpendiculaires à la ligne de vue, et latéraux pour les plans silicium, ainsi qu'un blindage actif en BGO.

À court terme j'interviens dans les études, les modélisations et simulations des bruits de fond et l'optimisation des blindages passifs et actifs, à titre principal en ce qui concerne le HXI et en soutien à nos collaborateurs japonais pour le SGD. Ces études s'étendront naturellement, à moyen terme, à l'étalonnage des instruments, au sol et en vol : mesures, définition des algorithmes, etc.

Par ailleurs le HXI d'Astro-H est une préfiguration de l'instrument homonyme proposé pour la mission International X-ray Observatory (IXO), grand observatoire spatial à rayons X étudié conjointement par l'ESA, la NASA et la JAXA, pour l'horizon 2015-2025. Notre participation à sa conception et à sa réalisation constitue donc une base de départ solide pour une R&D à long terme.

Enfin, une collaboration germano russe nous a récemment sollicités, pour participer à l'instrument ART-XC, télescope à rayons X dans la gamme de 6 à 30 keV embarqué sur la mission spatiale SRG dont le lancement est prévu en 2013. Bien qu'encore en discussion, notre participation se situerait dans les mêmes thèmes que décrit ci-dessus : étude et développement d'un détecteur CdTe et de son électronique, dont l'attrait serait de pouvoir abaisser le seuil bas de la caméra, et en ce qui me concerne directement, modélisation et simulation du détecteur et de l'instrument.

On le voit, les besoins en simulations et modélisations de détecteurs CdTe X et gamma embarqués ne se sont pas réduits, au contraire, avec l'arrêt du programme SIMBOL-X. Mon projet serait de fédérer et d'étoffer une petite équipe autour de ces thèmes, suffisante en nombre et ouverte pour ne pas se consacrer qu'à la programmation abstraite, mais également aux études,

mesures et développements sur ces détecteurs et dans les domaines de physique auxquels ils répondent.

D'autant que, parallèlement, je souhaite ne pas perdre mon acquis en ce qui concerne les cristaux scintillants et la calorimétrie. Au moment où le LHC entre enfin en opération, je reste en contact avec l'expérience CMS, en participant notamment aux « shifts » pour le calorimètre électromagnétique, et au retour d'expérience quant au fonctionnement de celui-ci.

Dans le même ordre d'idée, je suis de près les évolutions en ce qui concerne les cristaux scintillants, et plus généralement les méthodes de détection pour la calorimétrie tant électromagnétique qu'hadronique.

Dans un premier temps, l'amélioration probable du LHC (le projet de « Super » LHC), va nécessiter la reprise des études de tenue et de durcissement aux rayonnements des cristaux et circuits électroniques.

À plus long terme, des programmes de recherche et développement actuellement en phase préparatoire, vont se concrétiser pour les futures expériences auprès des accélérateurs linéaires « post LHC » tel que le CLIC ou l'ILC. En calorimétrie le concept de « double lecture » pour mesurer séparément les parts électromagnétique et hadronique des interactions dans un même matériau scintillateur me semble être une voie très prometteuse. La collaboration Crystal Clear envisage des programmes de recherche dans lesquelles les compétences de l'IRFU pourraient être mises à contribution, en particulier en ce qui me concerne pour la partie modélisation/simulation et pour les études sous différents rayonnements.

Dans un autre domaine expérimental, la recherche d'évènements rares (neutrinos, matière noire etc.) le lancement d'un programme concerté centré sur les cristaux inorganiques est en discussion au sein de Crystal Clear.

Conclusion

En guise de conclusion de ce mémoire, je mettrais l'accent sur deux aspects cycliques des recherches en matière d'instrumentation, deux cycles rencontrés dans mes travaux, et que j'espère avoir transcrits ici.

J'ai la chance d'avoir pu participer à la réalisation du calorimètre électromagnétique de l'expérience CMS quasiment depuis ses tous premiers balbutiements : Premiers programmes de recherche génériques sur les scintillateurs denses et rapides au sein de la collaboration Crystal Clear, puis, dans la collaboration CMS, développement du tungstate de plomb, de sa mise en œuvre dans le calorimètre électromagnétique, modélisation et simulations pour en mieux comprendre le fonctionnement etc.
Au moment où des données sortent maintenant quotidiennement de l'expérience, un nouveau cycle s'amorce, en vue de la génération suivante. Il sera, sans doute, au moins aussi long en années… L'encadrement d'une thèse sur le système de suivi optique du calorimètre électromagnétique de CMS, avec notamment sa partie simulation optique, les développements de modèles semi-empiriques, ainsi que la maitrise ou la connaissance des outils d'irradiation, me permettent de l'envisager avec optimisme.

D'autres cycles de recherche et développement n'ont pas été à leur terme, le détecteur n'ayant pas été finalement réalisé. Ils laissent cependant, je pense, des résultats, tant sur le plan des matériaux que des concepts, qui seront, ou en tout cas pourront être, utilisés un jour. Je pense en particulier aux travaux menés pour le « trigger optique » de Georges Charpak, par l'encadrement d'une thèse ayant donné lieu à d'intéressants développements dans le domaine des couches minces optiques et dans la théorie de l'effet Cherenkov en milieu anisotrope, ainsi qu'au projet LENS, par les travaux que j'ai conduits dans le cadre de contrats INTAS et OTAN sur les scintillateurs à base d'ytterbium et d'indium.

En ce qui concerne les détecteurs imageurs au tellure de cadmium, le cycle en cours, préparé dès le précédent qui a culminé avec le lancement de la mission INTEGRAL, (laquelle produit toujours des données, et pour quelques années encore), cherche encore son aboutissement. Nul doute qu'à plus ou moins court terme nous verrons voler une expérience spatiale emportant une caméra X à haute résolution spatiale et spectroscopique.

Le second cycle, mais est-ce un cycle ou plutôt un réseau d'interactions ?, je le situerais entre expérimentation, modélisation, simulations numériques. J'espère avoir témoigné que dans ce domaine aussi, ces trois aspects étaient importants, et surtout, justement, les interactions entre eux.
Sans se départir de la physique, car on est souvent tenté de considérer le résultat des calculs comme plus vrais que la réalité. Mais aussi, inversement, il n'est pas forcément facile, dans une foule de paramètres et de propriétés dûment mesurés, d'en discerner la pertinence et la hiérarchie quant au résultat que l'on veut atteindre.

Enfin, j'ai la fierté et le plaisir de penser qu'à mon niveau, j'ai pu participer et contribuer modestement à une grande œuvre à la fois culturelle, sociale, internationale et pacifique.

Références

[1] R. Chipaux, « Recommandations pour le calcul de la non stoechiométrie à partir du paramètre cristallin », Note technique SEFCA n° 93 (1986), 9 p.

[2] R. Chipaux, Computer Physics Communications 60 (1990) 405-415.

[3] R. Chipaux, A. Blaise and J.-M. Fournier, Journal of Magnetism and Magnetic Materials 84 (1990) 132-142.

[4] C. Benvenuti and R. Chipaux, Journal of the Less common Metals 164 165 (1990) 884-891.

[5] R.E. Ansorge *et al.*, Nucl. Instr. and Meth. A 265 (1988) 33-79.

[6] Ph. Rebourgeard *et al.*, Nucl. Instr. and Meth. A 427 (1999) 543-567.

[7] J.-P. Baton, R. Chipaux, J.-P. Pansart, J. Poinsignon, P. Rebourgeard, J.-F. Thomas, « Scintillating fibers for tracking at LHC », Rapport DAPNIA 92-01 (1992), 37 p.

[8] J.-F. Laporte *et al.*, « The shower maximum detector for SDC », in Proceedings of the Workshop on Scintillating Fiber Detectors SciFi93, Notre-Dame (USA), 24-28 octobre 1993, A.D. Bross, R.C. Ruchti, M.R. Wayne eds., World Scientific (1993).

[9] Borexino collaboration, G. Alimonti *et al.*, Astropart. Phys. 16 (2002) 205-234.

[10] F. Suekane, for the Double Chooz Collaboration, Nucl. Instr. and Meth. A, 623 (2010) 440-441.

[11] R. Davis, Prog. Part. Nucl. Phys. 32 (1994) 13-32.

[12] W. Hampel, Phil. Trans. R. Soc. Lond. A 343 (1994) 3-13 ;
      Gallex Collaboration, W. Hampel *et al.*, Phys. Lett. B 447 (1999) 127-133.

[13] The Super-Kamiokande Collaboration, S. Fukuda *et al.*, Nucl. Instr. and Meth. A 501 (2003) 418-462.

[14] The SNO Collaboration, J. Boger *et al.*, Nucl. Instr. and Meth. A 449 (2000) 172-207.

[15] R.S. Raghavan, Phys. Rev. Letters 37 (1976) 259.

[16] R.S. Raghavan, Phys. Rev. Letters 78 (1997) 3618.

[17] J. Bouchez, « The Lens project: a real-time measurement of the low energy solar neutrino spectrum », in « proc. of the VIII International Neutrino Telescopes Workshop », Venise (Italy), 23-26 février 1999 (non publié) ;
      M. Cribier, Nuclear Physics B (Proc. Suppl.) 87 (2000) 195-197.

[18] http://www.nndc.bnl.gov/nndc/nudat/ (2003).

[19] M. Cribier, « Deposit of isotopically modified gadolinium suitable to detect solar neutrinos », rapport interne DAPNIA/SPP 99-09, 1999, 6p.

[20] M.C. Chen Journal of Physics: Conference Series 136 (2008) 022035.

[21] Crystal Clear Collaboration, Nucl. Instr. and Meth A 332 (1993) 373-394.

[22] R. Chipaux *et al.*, Nucl. Instr. and Meth. A 345 (1994) 440-444.

[23] O. V. Buyanov *et al.*, Nucl. Instr. and Meth. A 349 (1994) 62-69.

[24] H. Hillemanns *et al.*, *in* « Scintillator and phosphor materials », eds. M.J. Weber, P. Lecoq, R.C. Ruchti, C. Woody, W.M. Yen and R. Y. Zhu, Mat. Res. Soc. Symp. Proc. Vol. 358, 117-122, 1994.

[25] R. Chipaux *et al.*, *in* « Scintillator and phosphor materials », eds. M.J. Weber, P. Lecoq, R.C. Ruchti, C. Woody, W.M. Yen and R. Y. Zhu, Mat. Res. Soc. Symp. Proc. Vol. 358, 481-486, 1994.

[26] T. Beckers *et al.*, *in* Proc. 5th int. conf. on calorimetry in high-energy physics, eds. H.A. Gordon and D. Rueger, World Sci. Singapore, 1995, 89-96.

[27] E. Auffray *et al.*, *in* Proc. int. conf. on advanced technology and particle physics, eds. E. Borchi, S. Majevski, J. Huston, A. Penzo and P.G. Rancoita, Nuclear Physics B (Proc. Suppl.) 44 (1995) 57 62.

[28] R. Chipaux, O. Toson, *in* Proc. int. conf. on Inorganic Scintillators and their Applications, SCINT 95, eds. P. Dorenbos and C.W.E. van Eick, Delft University Press, Delft, 1996, 274-277.

[29] E. Auffray *et al.*, Nucl. Instr. and Meth. A 378 (1996) 171-178.

[30] E. Auffray *et al.*, Nucl. Instr. and Meth. A 383 (1996) 367-390.

[31] J.-L. Faure, « A Cerenkov EM-calorimeter for CMS, using PbF_2 crystals », CMS TN-1992/020 (1992).

[32] R. Chipaux, A. Soyer, rapport DAPNIA/SED 95-01, CMS/TN 95-032, (1995) 16 p.

[33] L. Nagornaya and V. Ryzhikov, « Fast scintillators based on large "heavy" tungstate single crystals »,
      in « Heavy scintillators for scientific and industrial applications, proceedings of the "Crystal 2000" international workshop », F. De Notaristefani, P. Lecoq and M. Schneegans eds, Chamonix, September 1992, Editions Frontières, Gif sur Yvette, ISBN 2-86332-128-5, 1993 ; pp 367-374 ;
      M. Kobayashi *et al.*, « $PbWO_4$ scintillator as room temperature », *ibidem*, pp 375-379 ;
      V.A. Kachanov *et al.*, « Study of characteristics of real-size $PbWO_4$ crystal cells for precise em-calorimeters to be used at LHC energies », *ibidem*, p 381.

[34] A.N. Annenkov *et al.*, *in* Proc. 7th int. conf. on calorimetry in high-energy physics (ICCHEP 97), Tucson, AZ, 9-14 Nov. 1997, pp 484-491.

[35] Saclay group, « ECAL calibration: Use of the light monitoring system », Note CMS TN-1996/036 (1996).

[36] R. Chipaux, M. Géléoc, Nucl. Instr. and Meth. A 451 (2000) 610-622.

[37] F.-X. Gentit, Nucl. Instr. and Meth. A 486 (2002) 35-39 ; http://gentit.home.cern.ch/gentit/litrani/.

[38] R. Chipaux, *in* Proc. 5th int. conf. on inorganic scintillators and their applications, SCINT 99, ed. V.V. Mikhailin, M.V. Lomonosov Moscow State University, 2000, 639-642.

[39] R. Chipaux, F.-X. Gentit, Nucl. Instr. and Meth. A 486 (2002) 48-54.

[40] R. Chipaux and F.-X. Gentit, *IEEE Transactions on Nuclear Science*, 57 (2010) 1460-1464.

[41] R. Chipaux, M. Géléoc, P. Belleville, B. Lambert, IEEE Transactions on Nuclear Science 47 (2000) 2020-2023.

[42] J.-F. Cavaignac, J. Lamblin, A. Stutz, B. Vignon, « Reconnaissance de la signature des neutrinos solaires dans le cadre du projet LENS », Institut des Sciences Nucléaires de Grenoble, ISN 99-105, 1999, 7p ; J. Lamblin « Étude de la faisabilité d'un détecteur de neutrinos solaires à l'aide d'un cristal de gadolinium », Institut des Sciences Nucléaires de Grenoble, ISN 99-108, 1999, 28p.

[43] D.W. Cooke *et al.*, J. Lumin. 79 (1998) 185-190.

[44] P. Antonini, G. Bressi, G. Carugno, D. Iannuzzi, Nucl. Instr. and Meth. A 460 (2001) 469–471 ; G. Bressi, G. Carugno, E. Conti, C. Del Noce, D. Iannuzzi, Nucl. Instr. and Meth. A 461 (2001) 361–364.

[45] K. Zuber, Phys. Letters B485 (2000) 23.

[46] Voir par exemple les présentations aux conférences SCINT 2003 : A. Yoshikawa *et al.*, Nucl. Instr. and Meth. A 537 (2005) 76-80 ; Grigory Shirinyan *et al.*, *ibidem*, 134-138 ; et SCINT 2005 : N. Guerassimova, « Charge-transfer luminescence of ytterbium-doped sesquioxides », J. Pejchal, « Luminescence of Yb-doped YAlO3 and Lu3Al5O12. », *in* « Scint 2005, Proc. 8th Int. Conf. on Inorganic Scintillators », A. Getkin and B. Grinyov eds, Alushta, Crimée, 2005.

[47] J.-P. Chaminade *et al.*, J. Cryst. Growth 99 (1990) 799 ; T. Gaedwand *et al.*, J. Phys. Chem. Solids 55 (1994) 501.

[48] T. Gaedwand *et al.*, Mat. Res. Bull., 28 (1993) 1051-1060.

[49] T. Gaedwand *et al.*, Mat. Lett., 18 (1993) 64-68.

[50] Y. Messous *et al.*, Nucl. Instr. and Meth. A 354 (1995) 527-529.

[51] M. Balcerzyk *et al.*, « Search for indium and thallium based high density scintillators », Nuclear Science Symposium, Lyon, 15-20 octobre 2000, Conference Record, vol 1 6/25-6/29, 2000.

[52] R.S. Raghavan « pp solar neutrino spectroscopy: return of the indium detector », Bell-Labs-Tech-Memo:-10009622-010606-19TM, Jun 2001. 4pp, hep-ex/0106054.

[53] A. Borisevich, R. Chipaux, J.-F. Cavaignac and M.V. Korzhik, Nucl. Instr. and Meth. A 537 (2005) 228-231.

[54] G. Charpak, Y. Giomataris and L. Lederman, Nucl. Instr. and Meth. A 306 (1991) 439-445

[55] G. Charpak *et al.*, « Study of an optical trigger to be used for beauty search in fixed target mode at the LHC », CERN/DRDC/91-32 (1991).

[56] G. Charpak *et al.*, « Addendum to the proposal DRDC/P30, Optical discriminator to be used for beauty search in fixed target mode at the LHC: experimental results and perspectives », CERN/DRDC/92-53 (1992).

[57][G. Charpak *et al.*, « RD30 – Status Report: Study of an Optical Trigger to be used for beauty search in fixed target mode at the LHC », CERN/DRDC/93-56 (1993).

[58] M. Atac *et al.*, Nucl. Instr. and Meth. A 367 (1995) 372-376.

[59] N. Leros *et al.*, Nucl. Instr. and Meth. A 387 (1997) 88-91.

[60] A. Delbart, J. Derré, R. Chipaux, The European Physical Journal D 1 (1998) 109-116.

[61] Crystal Clear Collaboration, « Crystal Clear Collaboration Status Report », CERN/DRDC/93-31, (1993).

[62] N. Akchurin *et al.*, Nucl. Instr. and Meth. A 582 (2007) 474-483.

[63] N. Akchurin *et al.*, Nucl. Instr. and Meth. A 536 (2005) 29-51; R. Wigmans, Nucl. Instr. and Meth. A 617 (2009) 129-133.

[64] F. Lebrun *et al.*, « ISGRI: The CdTe gamma-ray camera onboard INTEGRAL », *in* : « Exploring the gamma-ray universe. Proceedings of the Fourth INTEGRAL Workshop », 4-8 septembre 2000, Alicante, Espagne, éditeur: B. Battrick, éditeurs scientifique: A. Gimenez, V.Reglero et C. Winkler. ESA SP-459, Noordwijk: ESA Publications Division, ISBN 92-9092-677-5, 2001, p. 591-594.

[65] O. Limousin, « Mise en œuvre et étude des propriétés spectrales de la gamma-caméra ISGRI », thèse de doctorat, Université Toulouse III – Paul Sabatier, 27 novembre 2001.

[66] B.P.F Dirks, « Study and modeling of the new generation Cd(Zn)Te X- and gamma-ray detectors for space applications », thèse de doctorat, Université Paris VII – Denis Diderot, 23 novembre 2006.

[67] A. Meuris, « Etude et optimisation du plan de détection de haute énergie en Cd(Zn)Te de la mission spatiale d'astronomie X et gamma Simbol-X », thèse de doctorat, Université Paris VII – Denis Diderot, 30 septembre 2009.

[68] O. Limousin *et al.*, IEEE Trans. Nucl. Science 52 (2005) 1595-1602 ; O. Gevin *et al.*, IEEE Trans. Nucl. Science 56 (2009) 2351-2359.

[69] A. Meuris *et al.*, Nucl. Instr. and Meth. 610 (2009) 154-157.

[70] S. Agostinelli *et al.*, Nucl. Instr. and Meth. A 506 (2003) 250-303 ;
      J. Allison *et al.*, IEEE Trans. Nucl. Science 53 (2006) 270-278.
[71] P. Ferrando *et al.*, « Simbol-X: mission overview », Proc. SPIE, 6266-17 (2006).
[72] B.P.F. Dirks *et al.*, « The focal plane of the Simbol–X space mission », Proc. SPIE 6276-45 (2006).
[73] C. Tenzer *et al.*, Proceedings of SPIE Volume 6266 II, 2006, Article number 626620.
[74] R. Chipaux *et al.*, Mem. S.A.It. 79 (2008) 234-238.
[75] C. Tenzer *et al.*, AIP Conf. Proc. 1126, « Symbol-X: Focusing on the Hard X-ray Universe, 2d International
      Symposium », eds P. Ferrando and J. Rodriguez, 2009, pp 65-68.

Annexes

55

A. Liste des publications

Revues à comité de lecture.

[p1]   S. Bouffard, R. Chipaux, D. Jérome and K. Bechgaard,
« Pinning of charge density waves in irradiated TTF-TCNQ »,
Solid State Communications 37 (1981) 405-408.

[p2]   R. Chipaux, G. Cécilia, M. Beauvy et R. Troc,
« Capacité thermique à haute température de UBe_{13}, $ThBe_{13}$ et UB_4 »,
Journal of the Less-common Metals, 121 (1986) 347-351.

[p3]   J. Larroque, R. Chipaux et M. Beauvy,
« Synthèses de composés d'actinides binaires et ternaires à partir de leurs oxydes »,
Journal of the Less-common Metals 121 (1986) 487-496.

[p4]   R. Chipaux, D. Bonnisseau, M. Bogé and J. Larroque,
« Crystallographic and Mössbauer investigations on $Np_{1-x}Pu_xB_2$ »,
Journal of Magnetism and Magnetic Materials 74 (1988) 67-73.

[p5]   R. Chipaux, J. Larroque and M. Beauvy,
« Study of the neptunium-plutonium diboride system »,
Journal of the Less-common Metals 153 (1989) 1-7.

[p6]   R. Chipaux, A. Blaise and J.-M. Fournier,
« Magnetic properties of the pseudo-binaries $Np_{1-x}Pu_xB_2$, extension of the Curie-Weiss model for di-magnetic solid solutions »,
Journal of Magnetism and Magnetic Materials 84 (1990) 132-142.

[p7]   R. Chipaux,
« MOSPLV, a program for simulation of complex Mössbauer spectra in polycrystalline samples »,
Computer Physics Communications 60 (1990) 405-415.

[p8]   C. Benvenuti and R. Chipaux,
« Search of superconductivity in ternary oxides based on d^1 ions »,
Journal of the Less-common Metals 164-165 (1990) 884-891.

[p9]   G. Charpak, R. Chipaux, J. Derré *et al.*,
« Experimental study of an impact-parameter optical discriminator »,
Nuclear Instruments and Methods in Physics Research A332 (1993) 91-99.

[p10]   Crystal Clear Collaboration,
« Further results on cerium fluoride crystals »,
Nuclear Instruments and Methods in Physics Research A332 (1993) 373-394.

[p11]   R. Chipaux, J.-L. Faure, P. Rebourgeard, G. Dauphin, J. Safieh,
« Behaviour of CeF_3 scintillator in a LHC-like environment »,
Nuclear Instruments and Methods in Physics Research A345 (1994) 440-444.

[p12]   O. V. Buyanov, R. Chipaux, A. A. Fyodorov *et al.*,
« A first electromagnetic calorimeter prototype of $PbWO_4$ crystals »,
Nuclear Instruments and Methods in Physics Research A349 (1994) 62-69.

[p13]   H. Hillemanns, E. Auffray, I. Dafinei *et al.*,
« First results of CeF_3 crystals in a test beam »,
Mat. Res. Soc. Symp. Proc. 358 (1994) 117-122.

[p14]   R. Chipaux, J.-L. Faure, J.-P. Pansart *et al.*,
« Study of neutron damage resistance of some scintillating crystals and associated photodetectors with the nuclear reactor ULYSSE »,
Mat. Res. Soc. Symp. Proc. 358 (1994) 481-486.

[p15]   C. Kochowski *et al.*,
« RD30 – study of an optical trigger proposed for a beauty search in fixed target mode at the LHC »
Nuclear Instruments and Methods in Physics Research A351 (1994) 193-196.

[p16]   E. Auffray *et al.*,
« Test beam results of a cerium fluoride crystal matrix »,
in Proc. int. conf. on advanced technology and particle physics,
eds. E. Borchi, S. Majevski, J. Huston, A. Penzo and P.G. Rancoita,
Nuclear Physics B (Proc. Suppl.) 44 (1995) 57-62.

[p17] M. Atac, G. Charpak, R. Chipaux, A. Delbart *et al.*,
« The development of the optical discriminator »,
Nuclear Instruments and Methods in Physics Research A367 (1995) 372-376.

[p18] E. Auffray *et al.*,
« Performance of a cerium fluoride crystal matrix measured in high-energy particle beams »,
Nuclear Instruments and Methods in Physics Research A378 (1996) 171-178.

[p19] E. Auffray *et al.*,
« Extensive studies of CeF_3 crystals, a good candidate for electromagnetic calorimetry at future accelerators »,
Nuclear Instruments and Methods in Physics Research A383 (1996) 367-390.

[p20] G. Alexeev *et al.*,
« Studies of lead tungstate crystal matrices in high energy beams for the CMS electromagnetic calorimeter at the LHC »,
Nuclear Instruments and Methods in Physics Research A385 (1997) 425-434.

[p21] N. Leros, J.-P. Perroud, R. Chipaux, A. Delbart *et al.*
« An optical discriminator for hyperon physics »,
Nuclear Instruments and Methods in Physics Research A387 (1997) 88-91.

[p22] N. Fourches, P. Abbon, R. Chipaux, E. Delagnes *et al.,*
« Thick film SOI technology: characteristics of devices and performance of circuits for high-energy physics at cryogenic temperatures; effects of ionizing radiation »,
Nuclear Instruments and Methods in Physics Research A401 (1997) 229-237.

[p23] A. N. Annenkov *et al.*,
« Systematic study of the $PbWO_4$ crystal short term instability under irradiation »,
Radiation Measurements 29 (1998) 27-38.

[p24] A. Delbart, J. Derré, R. Chipaux,
« Cherenkov radiation emission in uniaxial optical materials »,
The European Physical Journal D 1 (1998) 109-116.

[p25] E. Auffray *et al.*,
« Beam test of lead tungstate crystal matrices and a silicon strip preshower detector for the CMS electromagnetic calorimeter »,
Nuclear Instruments and Methods in Physics Research A412 (1998) 223-237.

[p26] Ph. Rebourgeard, F. Rondeaux, J.-P. Baton, G. Besnard *et al.*,
« Fabrication and measurements of plastic scintillating fibers »,
Nuclear Instruments and Methods in Physics Research A427 (1999) 543-567.

[p27] D. Neyret *et al.*,
« A photon calorimeter using lead tungstate crystals for the CEBAF Hall A Compton polarimeter »,
Nuclear Instruments and Methods in Physics Research A443 (2000) 231-237.

[p28] R. Chipaux, M. Géléoc,
« Modelisation and simulation of the light collection in the CMS lead tungstate crystals »,
Nuclear Instruments and Methods in Physics Research A451 (2000) 610-622.

[p29] R. Chipaux, M. Géléoc, P. Belleville, B. Lambert,
« Sol-gel coating of scintillating crystals »,
IEEE Transactions on Nuclear Science 47 (2000) 2020-2023.

[p30] R. Chipaux, G. André, A. Cousson,
« Crystal structure of lead tungstate at 1.4 and 300 K »,
Journal of Alloys and Compounds 325 (2001) 91-94.

[p31] R. Chipaux, X.-F. Gentit,
« Simulation of light collection in the CMS lead tungstate crystals with the program Litrani: coating and surface effects »,
Nuclear Instruments and Methods in Physics Research A486 (2002) 48-54.

[p32] R. Chipaux *et al.*,
« Ytterbium-based scintillators, a new class of inorganic scintillators for solar neutrino spectroscopy »,
Nuclear Instruments and Methods in Physics Research A486 (2002) 228-233.

[p33] N. Guerassimova *et al.*,
« Charge transfer luminescence and spectroscopic properties of Yb^{3+} in aluminium and gallium garnets »,
Nuclear Instruments and Methods in Physics Research A486 (2002) 278-282.

[p34] A. Borisevich, R. Chipaux, J.-F. Cavaignac and M.V. Korzhik,
« New class of indium-containing room temperature inorganic scintillators »,
Nuclear Instruments and Methods in Physics Research A537 (2005) 228-231.

[p35] O. Limousin, O. Gevin, F. Lugiez, R. Chipaux, E. Delagnes, B. Dirks, B. Horeau,
« IDeF-X ASIC for Cd(Zn)Te spectro-imaging systems »,
IEEE Transactions on Nuclear Science 52 (2005) 1595-1602.

[p36] The CMS Electromagnetic Calorimeter Group, P. Adzic *et al.*,
« Results of the first performance tests of the CMS electromagnetic calorimeter »,
The European Physical Journal C 44 (2006) 1-10.

[p37] The CMS Electromagnetic Calorimeter Group, P. Adzic *et al.*,
« Reconstruction of the signal amplitude of the CMS electromagnetic calorimeter »,
The European Physical Journal C 46 (Suppl. 1), (2006) 23-35.

[p38] G.L. Bayatian, S. Chatrchyan, G. Hmayakyan, *et al.*
« CMS physics technical design report, volume II: Physics performance »,
Journal of Physics G - Nuclear and Particle Physics, 34 (2007) 995-1579.

[p39] P. Adzic *et al.*,
« Energy resolution of the barrel of the CMS Electromagnetic Calorimeter »,
Journal of Instrumentation, 2 (2007) P04004.

[p40] M. Anfreville *et al.*,
« Laser monitoring system for the CMS lead tungstate crystal calorimeter »,
Nuclear Instruments and Methods in Physics Research, A594 (2008) 292-320.

[p41] R. Chipaux, U. Briel, A. Bulgarelli, L. Foschini, E. Kendziorra, C. Klose, M. Kuster, P. Laurent, C. Tenzer,
« Status of the Simbol-X detector background simulation activities »,
Mem. S.A.It. 79 (2008) 234-238.

[p42] The CMS Collaboration, S. Chatrchyan *et al.*,
« The CMS experiment at the CERN LHC »,
Journal of Instrumentation, 3 (2008) S08004.

[p43] The CMS Electromagnetic Calorimeter Group, P. Adzic *et al.*
« Intercalibration of the barrel electromagnetic calorimeter of the CMS experiment at start-up »,
Journal of Instrumentation, 3 (2008) P10007.

[p44] CMS HCAL/ECAL Collaborations, S. Abdullin *et al.*,
« The CMS barrel calorimeter response to particle beams from 2 to 350 GeV/c »,
The European Physical Journal C - Particles and Fields, 60 (2009) 359-373.

[p45] A. Abdo et al,
« The on-orbit calibration of the Fermi Large Area Telescope »,
Astroparticle Physics 32 (2009) 193-219.

[p46] W.B. Atwood, A.A. Abdo, M. Ackermann *et al.*,
« The large area telescope on the Fermi gamma-ray space telescope mission »,
The Astrophysical Journal, 697 (2009) 1071-1102.

[p47] The CMS Collaboration,
« Commissioning of the CMS experiment and the cosmic run at four tesla »,
Journal of Instrumentation, 5 (2010) P03001.

[p48] The CMS Collaboration
« Measurement of the muon stopping power in lead tungstate »,
Journal of Instrumentation, 5 (2010) P03007.

[p49] The CMS Electromagnetic Calorimeter Group, P. Adzic *et al.*,
« Radiation hardness qualification of $PbWO_4$ scintillation crystals for the CMS electromagnetic calorimeter »,
Journal of Instrumentation, 5 (2010) P03010.

[p50] The CMS Collaboration
« Performance and operation of the CMS electromagnetic calorimeter »,
Journal of Instrumentation, 5 (2010) T03010.

[p51] The CMS Collaboration
« Time reconstruction and performance of the CMS electromagnetic calorimeter »,
Journal of Instrumentation, 5 (2010) T03011.

[p52] R. Chipaux and F.-X. Gentit,
« Transparency variations and calibration in CMS electromagnetic calorimeter crystals: Monte-Carlo studies »,
IEEE Transactions on Nuclear Science, 57 (2010) 1460-1464.

Actes de colloques et de conférences

[c1] R. Chipaux, M. Beauvy, D. Bonnisseau and A. Blaise,
« Structure and magnetic properties of the solid solutions of the diborides of neptunium and plutonium »,
in Proc. 9th int. symp. on boron, borides and related compounds,
ed. H. Werheit, Universität Duisburg, 1987, 393-396.

[c2] R. Chipaux,
« The optical discriminator - A guided Cherenkov light device for a very fast triggering on impact parameter in a fixed target experiment »,
Nuclear Science Symposium and Medical Imaging Conference 1993 conference records, pp 430-431.

[c3] « Y. Giomataris *et al.*,
The optical trigger for beauty research, recent developments and perspectives »,
AIP Conf. Proc. 272, « The XXVIth International Conference on High Energy Physics »,
ed J.R. Sanford, 1993, 1738-1742.

[c4] T. Beckers *et al.*,
« Test results of a CeF$_3$ crystal matrix »,
in Proc. 5th int. conf. on calorimetry in high-energy physics,
eds. H.A. Gordon and D. Rueger, World Sci. Singapore, 1995, 89-96.

[c5] R. Chipaux, O. Toson,
« Resistance of lead tungstate and cerium fluoride to low rate gamma irradiation or fast neutrons exposure »,
in Proc. int. conf. on Inorganic Scintillators and their Applications, SCINT 95,
eds. P. Dorenbos and C.W.E. van Eijk, Delft University Press, Delft, 1996, 274-277.

[c6] A.N. Annenkov, E. Auffray, R. Chipaux, G.Yu. Drobyshev, A.A. Fedorov, M. Géléoc, N.A. Golubev,
M.V. Korzhik, P. Lecoq, A.A. Lednev, A.B. Ligun, O.V. Misevich, V.B. Pavlenko, J.P. Peigneux,
A.V. Singovsky,
« Control of lead tungstate crystals radiation hardness through optical transmission measurements »,
in Proc. 7th int. conf. on calorimetry in high-energy physics (ICCHEP 97), Tucson, 9-14 Nov. 1997, 484-491.

[c7] E. Auffray *et al.*,
« Certifying procedures for lead tungstate crystal parameters during mass production for the CMS ECAL »,
Nuclear Science Symposium 1998 conference records, pp 508-513.

[c8] R. Chipaux, M. Géléoc,
« Optical anisotropy effects in lead tungstate crystals »,
in Proc. 5th int. conf. on inorganic scintillators and their applications, SCINT 99, ed. V.V. Mikhailin,
M.V. Lomonosov Moscow State University, 2000, 629-635.

[c9] A. Cousson, W. Paulus and R. Chipaux,
« Determination of the crystal structure of lead tungstate by neutron diffraction »,
in Proc. 5th int. conf. on inorganic scintillators and their applications, SCINT 99, ed. V.V. Mikhailin,
M.V. Lomonosov Moscow State University, 2000, 636-638.

[c10] R. Chipaux,
« Light collection in the CMS lead tungstate crystals : relation between monitoring and calibration variations »,
in Proc. 5th int. conf. on inorganic scintillators and their applications, SCINT 99, ed. V.V. Mikhailin,
M.V. Lomonosov Moscow State University, 2000, 639-642.

[c11] R. Chipaux *et al.*,
« Ytterbium-based compounds as fast and dense inorganic scintillators »,
Nuclear Science Symposium 2001 conference records, pp 966-970.

[c12] Bob P. F. Dirks, Olivier Limousin, Philippe R. Ferrando and Rémi Chipaux,
« 3D modeling of Cd(Zn)Te detectors for the Simbol-X space mission »,
Proc. SPIE, Vol. 5501, 412 (2004); doi:10.1117/12.584936.

[c13] R. Chipaux, M.V. Korzhik, A. Borisevich, P. Lecoq, C. Dujardin,
« Behaviour of PWO scintillators after high fluence neutron irradiation »,
in SCINT 2005, Proc. 8th int. conf. on inorganic scintillators and their use in scientific and industrial applications, A. Getkin and B. Grinyiv eds., Institute for Single Crystals, Kharkov, Ukraine, 2006, 369-371.

[c14] C. Tenzer, E. Kendziorra, A. Santangelo, M. Kuster, P. Ferrando, P. Laurent, A. Claret, R. Chipaux,
« Monte Carlo simulations of stacked X-ray detectors as designed for Simbol-X »,
Proc. SPIE, Vol. 6266, 62662O (2006); doi:10.1117/12.671929.

[c15] A. Meuris *et al.*,
« The high energy detector of Symbol-X »,
AIP Conf. Proc. 1126, « Symbol-X: Focusing on the Hard X-ray Universe, 2nd International Symposium »,
eds P. Ferrando and J. Rodriguez, 2009, pp 25-30.

[c16] M. Civitani, S. Djalal, J.-M. Le Duigou, O. La Marle, R. Chipaux,
« Simbol-X formation flight and image reconstruction »
AIP Conf. Proc. 1126, « Symbol-X: Focusing on the Hard X-ray Universe, 2nd International Symposium »,
eds P. Ferrando and J. Rodriguez, 2009, pp 65-68.

[c17] C. Tenzer *et al.*,
« Status of the Simbol–X background simulation activities »,
AIP Conf. Proc. 1126, « Symbol-X: Focusing on the Hard X-ray Universe, 2nd International Symposium »,
eds P. Ferrando and J. Rodriguez, 2009, pp 75-78.

[c18] Marta Civitani, Sophie Djalal and Rémi Chipaux,
« Optimization of detectors positioning with respect to flying dynamics for future formation flight missions »,
Proc. SPIE, Vol. 7437, 74370E (2009), doi :10.1117/12.827974.

[c19] S. Hauf, M. Kuster, M.G. Pia, *et al,*
« Progress and Validation of Geant4 Based Radioactive Decay Simulation Using the Examples of Simbol-X
and IXO »,
Nuclear Science Symposium 2009 conference record, pp 2060-2065.

Principales autres publications.

Principaux rapports, publications internes, propositions d'expérience etc.

[r1] R. Chipaux,
« étude de la conductivité de TTF-TCNQ irradié »,
Rapport de stage de DEA de Sciences des matériaux, Paris VI, mars-juin 1980, 39 p.

[r2] R. Chipaux,
« Les effets de cisaillement dans les cristaux colloïdaux »,
Rapport de stage de DEA de physique des solides, Paris XI, mars-avril 1981, 15 pages, (et 11 photographies
dont les plus significatives ont été publiées par P. Pieranski dans *Contemp. Phys.* 24 (1983) 25-73 et dans *La
Recherche* 175 (1983) 312, sans que l'auteur des clichés soit crédité…).

[r3] R. Chipaux,
« Recommandations pour le calcul de la non-stœchiométrie à partir du paramètre cristallin »,
Note technique SEFCA n° 93 (1986), 9 p.

[r4] R. Chipaux, J. Larroque et B. Tournois,
« Synthèse et caractérisation des diborures de neptunium et de plutonium »,
Note technique SEFCA n° 100 (1986), 15 p.

[r5] R. Chipaux et J. Larroque,
« Elaboration et caractérisation de borures et oxyséléniures d'actinides (Pu et Np) »,
Rapport d'Activité DECPu, 2e semestre 1986, p 87-109.

[r6] R. Chipaux, « Contribution à l'étude de la cristallochimie et des propriétés électroniques des borures
d'actinides », Thèse de doctorat, Université d'Aix Marseille II, octobre 1987, 170 p, rapport CEA-R-5435.

[r7] G. Charpak, Y. Giomataris, C. Joseph, C. Morel, J.-P. Perroud, M.T. Tran, R. Chipaux, J. Derré,
C. Kochowski, Y. Lemoigne, S. Loucatos, P. Rebourgeard,
« Study of an optical trigger to be used for beauty search in fixed target mode at the LHC »,
Proposition CERN/DRDC/91-32, (1991).

[r8] J.-P. Baton, R. Chipaux, J.-P. Pansart, J. Poinsignon, P. Rebourgeard, J.-F. Thomas
« Scintillating fibers for tracking at LHC »,
Rapport DAPNIA 92-01 (1992), 37 p.

[r9] G. Charpak, Y. Giomataris, C. Joseph, C. Morel, J.-P. Perroud, M.T. Tran, R. Chipaux, J. Derré,
C. Kochowski, Y. Lemoigne, S. Loucatos, P. Rebourgeard,
« Addendum to the proposal DRDC/P30, Optical discriminator to be used for beauty search in fixed target
mode at the LHC: experimental results and perspectives »,
Proposition CERN/DRDC/92-53, (1992).

[r10] Crystal Clear Collaboration,
« Crystal Clear Collaboration Status Report »,
Rapport CERN/DRDC/93-31, (1993).

[r11] G. Charpak *et al.*,
« RD30 – Status Report: Study of an Optical Trigger to be used for beauty search in fixed target mode at the
LHC »,
Rapport CERN/DRDC/93-56, (1993).

[r12] Crystal Clear Collaboration,
       « Crystal Clear Collaboration Status Report »,
       Rapport CERN/DRDC/94-53, (1995).

[r13] R. Chipaux, A. Soyer,
       « Study of some optical glues in a LHC-like environment »,
       Rapport DAPNIA/SED 95-01, CMS/TN 95-032, (1995) 16 p.

[r14] R. Chipaux,
       « Numerical formulæ for the refractive index of lead tungstate »,
       Note CMS TN-1995/184, (1995) 5 p.

[r15] Saclay group,
       « ECAL calibration: Use of the light monitoring system »,
       Note CMS TN-1996/036 (1996).

[r16] Crystal Clear Collaboration,
       « R&D for the study of new, fast and radiation hard scintillators for calorimetry at LHC/RD18 »,
       CERN/LHCC/96 019.

[r17] R. Chipaux *et al.*,
       « Ytterbium-based compounds as fast and dense inorganic scintillators »,
       Conf. Records of the IEEE 2001 Nuclear Science Symposium, San Diego (USA),
       4-10 novembre 2001, N27 2.

[r18] C. Pédrini, N. Guerassimova, C. Dujardin, N. Garnier, A.G. Petrosyan, I.A. Kamenskikh, V.V. Mikhailin,
       A.N. Belsky, R. Chipaux,
       « Charge transfer luminescence of ytterbium containing crystals »,
       9th Europhysical Conference on Defects in Insulating Materials, EURODIM 2002,
       30 juin – 5 juillet, 2002, Wrocław, Poland.

[r19] Saclay group,
       « The CMS-ECAL monitoring system: data generation, acquisition and processing at LHC »,
       Note CMS IN-2002/012 (2002) 10 p.

[r20] C. Pédrini *et al.*,
       « Scintillators based on Yb charge transfer luminescence: what is the status? »,
       SCINT 2003, 7th International Conference on Inorganic Scintillators and Industrial Applications,
       Valencia, Espagne, 8-12 septembre 2003.

[r21] « Radiation Induced Effects in a Monolithic Active Pixel Sensor : The Mimosa8 Chip »,
       N. Fourches, M. Besançon, R. Chipaux, Y. Li, P. Lutz, F. Orsini,
       arXiv:0805.3934v1 [physics.ins-det]

[r22] F.X. Gentit, R. Chipaux,
       « Results of Litrani concerning the S/R ratio of the ECAL crystals »,
       Note CMS DN-2008/008 (2009).

Présentation orales dans des conférences et séminaires

[s1] « Quelques propriétés physico-chimiques des actinides… »,
      17e Séminaire des Lecques, Les-Lecques, 16 mai 1986.

[s2] « Propriétés cristallochimiques et magnétiques des solutions solides $Np_{1-x}Pu_xB_2$ »,
      Soutenance de thèse, Université d'Aix-Marseille II, faculté de Luminy, 8 octobre 1987.

[s3] « La formation par la recherche comme expérience professionnelle »,
      Forum national « SPORE-87 », Toulon, 5-7 novembre 1987.

[s4] « Recherche de nouveaux composés supraconducteurs »,
      LEPES, Grenoble, 9 novembre 1989.

[s5] « Recherche de composés supraconducteurs à base d'ions d^1 »,
      LMPTM, Villetaneuse, 22 janvier 1990.

[s6] « Propriétés magnétiques des diborures de neptunium, de plutonium et de leurs solutions solides »,
      Institut Curie, Section de Physique et Chimie, Paris, 6 février 1990.

[s7] « Optical triggering for beauty physics »,
      18th INFN Eloisatron Project Workshop, « Image Processing for Future High Energy Physics Detectors »,
      Erice (Italie), 13-18 novembre 1991. (avec J.-P. Perroud.)

[s8] « Un discriminateur optique pour l'étude de la physique des mésons B en cible fixe »,
      13es Journées Nationales d'Optique Guidée, Marseille, 26-27 mai 1993.

[s9]   « Le Discriminateur Optique »,
         Dapnia, Saclay, 22 juin 1993.

[s10]   « The Optical Discriminator: a guided Cherenkov-light device for a very fast triggering on impact parameter
         in a fixed target experiment »,
         IEEE 1993 Nuclear Science Symposium, San-Francisco (USA), 3 novembre 1993.

[s11]   « Study of neutron damage resistance of some scintillating crystals and associated photodetectors with the
         nuclear reactor Ulysse »,
         Symposium on Scintillator and Phospor Materials, MRS '94 Spring Meeting, San-Francisco (USA),
         6-8 avril 1994.

[s12]   « Resistance of lead tungstate and cerium fluoride to low rate gamma irradiation or fast neutrons exposure »,
         SCINT95, International Conference on Inorganic Scintillators and their Applications, Delft,
         28 août-1er septembre 1995.

[s13]   « Le Discriminateur optique : des symétries fondamentales aux lois de Fresnel »,
         Horizons de l'Optique 1995, Palaiseau, 8 novembre 1995.

[s14]   « Sol-gel coating of scintillating crystals »,
         International Conference on Inorganic Scintillators and their Applications, SCINT 97,
         Shanghai, Chine, 22 septembre 1997.

[s15]   « Ytterbium based scintillators, a new class of inorganic scintillators for solar neutrino spectroscopy »
         SCINT 2001, International Conference on Inorganic Scintillators and their Applications,
         Chamonix, France, 18 septembre 2001.

[s16]   « Ytterbium-based crystals as fast and dense inorganic scintillators »,
         IEEE 2001 Nuclear Science Symposium, San Diego, USA, 9 novembre 2001.

[s17]   « Les cristaux scintillants pour la détection des particules »,
         Journée SÉDI/DIMRI, 14 mars 2002.

[s18]   « Cristaux scintillants pour la détection de particules, de la recherche au développement… »,
         Institut de Chimie de la Matière Condensée, Bordeaux, 3 avril 2002.

[s19]   « Scintillators R&D for solar neutrino spectroscopy: the LENS project »,
         INFN-Padoue, Italie, 31 mai 2002.

[s20]   « Ytterbium-containing crystals: when laser materials appear as fast and dense inorganic scintillators »,
         Conference on Laser Physics – 2002, 15 octobre 2002, Ashtarak, Arménie.

Présentations par affiches dans des conférences

Seules sont mentionnées les présentations assurées personnellement et non celles dont je n'étais
que signataire.

[a1]   R. Chipaux, J. Larroque and M. Beauvy,
         « Actinide-boron phase-diagram investigations »,
         16es Journées des Actinides, Eibsee (RFA), avril 1986.

[a2]   R. Chipaux, J. Larroque, M. Beauvy, A. Blaise and D. Bonnisseau,
         « Synthesis and magnetic properties of the diborides of neptunium and plutonium »,
         17es Journées des Actinides, Chexbres (Suisse), mars 1987.

[a3]   C. Benvenuti and R. Chipaux,
         « Search of superconductivity in ternary oxides based on d^1 ions »,
         Symposium on High T_c Superconductor Materials, E-MRS Spring Meeting, Strasbourg, 29 mai-1er juin 1990.

[a4]   G. Charpak, Y. Giomataris, C. Joseph, C. Morel, J.-P. Perroud, M.T. Tran, R. Chipaux, J. Derré,
         C. Kochowski, Y. Lemoigne, S. Loucatos et P. Rebourgeard,
         « Étude d'un discriminateur optique pour la recherche en physique des particules »,
         12es Journées Nationales d'Optique Guidée, Paris, 23-24 janvier 1992.

[a5]   A. Delbart et R. Chipaux,
         « Développement de couches minces pour le discriminateur optique »,
         Horizons de l'Optique 1995, Palaiseau, 7-9 novembre 1995.

[a6]   P. Besson *et al.*,
         « How to rely the variations of calibration and transmission parameters in ageing scintillating crystals »,
         International Conference on Inorganic Scintillators and their Applications, SCINT 97,
         Shanghai, Chine, 22-25 septembre 1997.

[a7] R. Chipaux, M. Géléoc, P. Belleville, B. Lambert,
« Sol-gel coating of scintillating crystals »,
IEEE 1998 Nuclear Science Symposium, Toronto (Canada), 11 novembre 1998.

[a8] R. Chipaux,
« Optical characterisation of scintillating crystals for high energy physics »
Colloquium Optical Spectroscopy, COSP'99, Überlingen, Allemagne, 12-14 avril 1999.

[a9] R. Chipaux and M. Géléoc,
« Optical anisotropy effect in lead tungstate crystals »,
International Conference on Inorganic Scintillators and their Applications, SCINT 99,
Moscou, Russie, 16-20 août 1999.

[a10] A. Cousson, W. Paulus and R. Chipaux,
« Determination of the crystal structure of lead tungstate by neutron diffraction »,
International Conference on Inorganic Scintillators and their Applications, SCINT 99,
Moscou, Russie, 16-20 août 1999.

[a11] R. Chipaux,
« Light collection in the CMS lead tungstate crystals: relation between monitoring and calibration variations »,
International Conference on Inorganic Scintillators and their Applications, SCINT 99,
Moscou, Russie, 16-20 août 1999.

[a12] R. Chipaux, F.-X. Gentit,
« Simulation of light collection in the CMS lead tungstate crystals with the program Litrani: coating and surface effects »,
SCINT 2001, International Conference on Inorganic Scintillators and their Applications,
Chamonix, France, 16-21 septembre 2001.

[a13] R. Chipaux, M.V. Korzhik, A. Barisevich, P. Lecoq,
« Damage of lead tungstate after very high neutron fluence »,
SCINT 2003, 7th International Conference on Inorganic Scintillators and Industrial Applications,
Valence, Espagne, 8-12 septembre 2003.

[a14] R. Chipaux, M.V. Korzhik, A. Borisevich, P. Lecoq, C. Dujardin,
« Behaviour of PWO scintillator after high fluence neutron irradiation »,
SCINT 2005, 8th International Conference on Inorganic Scintillators and Industrial Applications,
Alushta, Crimée, Ukraine, 19-23 septembre 2005.

[a15] R. Chipaux, U. Briel, A. Bulgarelli, L. Foschini, E. Kendziorra, C. Klose, M. Kuster, P. Laurent, C. Tenzer,
« Status of the Simbol-X detector background simulation activities »,
International Workshop Simbol-X: the hard X-ray universe in focus, I
Bologne, Italie, 14-16 mai 2007.

[a16] R. Chipaux and F.-X. Gentit,
« Transparency variations and calibration in CMS electromagnetic calorimeter crystals: Monte-Carlo studies »,
SCINT 2009, 10th international conference on inorganic scintillators and their applications,
Jeju, Corée, 8-12 juin 2009.

B. Cours de DEA

De 1994 à 1999 : Cours sur les détecteurs à semi-conducteurs, et examens associés du DEA « Modélisation et Instrumentation en Physique » des universités de Paris VI, VII, XII et de l'INSTN.

C. Encadrements de doctorants

Responsable CEA de deux thèses de doctorat financées par des contrats CEA de formation par la recherche :

> Thèse de M. Alain Delbart, « Le Trigger Optique : un discriminateur à effet Cherenkov pour la physique des particules. Réalisation et caractérisation de couches minces dont l'indice de réfraction autorise la discrimination sur un large domaine spectral. », thèse de l'Université d'Aix-Marseille III soutenue le 19 juin 1996, mention très honorable avec félicitations, jury : G. Charpak (président), J.-P. Borgogno (rapporteur), R. Chipaux, F. Flory, J. Mugnier (rapporteur), J.-P. Perroud.

> Thèse de Melle Marie Géléoc, « Étude du système de suivi optique des cristaux scintillants du calorimètre électromagnétique de l'expérience CMS », thèse de l'Université de Paris VI soutenue le 4 septembre 1998, mention très honorable, jury : F. Gires (président), R. Chipaux, J.-C. Clémens (rapporteur), J.-L. Faure, P. Gadenne, J.-P. Peigneux (rapporteur).

Dans les deux cas les doctorants ont été embauchés au CEA à la suite de leur thèse.

Participation à l'encadrement des thèses de Bob Dirks (« Study and modeling of the new generation Cd(Zn)Te X- and gamma-ray detectors for space applications », Paris VII, 2003-2006) et d'Aline Meuris (« Étude et optimisation du plan de détection de haute énergie en Cd(Zn)Te de la mission spatiale d'astronomie X et gamma SIMBOL-X », Paris VII, 2006-2009).

D. Encadrements de stagiaires

J'encadre régulièrement, quand les programmes et calendriers s'y prêtent, des stagiaires universitaires, de niveau allant de seconde année d'IUT à la maîtrise ou au DEA.

« Superviseur étranger » du jeune chercheur biélorusse Andreï Barisevitch, de l'Institut des problèmes Nucléaires de Minsk, dans le cadre de son contrat INTAS YSF07 (Young Scientists Fellowships) (2002-2003), accueil et encadrement lors de ses séjours à Saclay et à Lyon en 2003.

E. Activités de diffusion de l'information scientifique

Organisation de conférences

Membre du comité d'organisation de la « *IXth International Conference on Calorimetry in High Energy Physics - CALOR2000* », LAPP, Annecy, 9 au 14 octobre 2000

Membre du comité d'organisation de la « *VIth International Conference on inorganic Scintillators and their Use in scientific and industrial Applications, SCINT 2001* », Chamonix, 16 au 21 septembre 2001. J'y ai plus particulièrement assuré la coordination scientifique et technique de l'édition des comptes-rendus, parus en 2002 dans le numéro 486 de la revue *Nuclear Instruments and Methods in Physics Research A.*

Séminaires d'instrumentation du DAPNIA

De 1995 à 2004 j'ai assuré l'organisation des séminaires d'instrumentation du DAPNIA. En tout j'ai organisés 48 séminaires, dans des domaines très variés touchant à l'instrumentation pour la physique en général, que ce soit dans les domaines des détecteurs, des accélérateurs, de l'informatique, de l'organisation, etc.

Comité éditorial du journal ScintillationS de l'IRFU.

Depuis avril 1995, je participe au comité éditorial du journal de l'IRFU, *ScintillationS*. Tous les deux ou trois mois depuis la création du département en 1992 (83 numéros parus à ce jour), ce journal présente pour le plus large public l'actualité de l'activité de l'IRFU et ses résultats majeurs.
Le comité éditorial, dirigé par J. Martin jusqu'en 2006, puis par J.-L. Sida, suscite les articles, s'assure de leur qualité et de leur adéquation à la ligne éditoriale et au lectorat du journal, ainsi que des relectures et corrections. ScintillationS est tiré à 1500 exemplaires dont 850 sont diffusés à l'extérieur de l'IRFU vers les autres laboratoires du CEA, du CNRS, de l'Université, les média etc.

F. Autres activités scientifiques

Participation à des jurys de thèse, revues d'articles et de propositions de recherche.

Outre les deux thèses mentionnées plus haut, j'ai été membre du jury de la thèse de Gleb Drobyshev, « Optimisation des paramètres de scintillation des cristaux de tungstate de plomb pour leur application dans la calorimétrie électromagnétique de haute précision », thèse conjointe de l'Université de Savoie et de l'Université de Minsk, Biélorussie, soutenue le 12 avril 2000 à Minsk, mention très honorable, jury : V.G. Barischevski (président), R. Chipaux, M.V. Korzhik, A.S. Kourilin (rapporteur), J.-M. Moreau, J.-P. Peigneux, E.A. Rudak (rapporteur).

Outre l'édition des comptes-rendus de la conférence SCINT 2001 (voir ci-dessus), j'évalue régulièrement des articles scientifiques pour les revues *Nuclear Instruments and Methods in Physics Research A* et *IEEE Transactions on Nuclear Science*, ainsi que plus épisodiquement pour d'autres journaux scientifiques.

Évaluateur auprès de l'INTAS de 2003 à 2007 et dans ce cadre ait été amené périodiquement à évaluer des réponses aux appels à propositions de cet organisme. (L'INTAS a terminé ses activités et est en liquidation depuis début 2007).

Responsabilités diverses

Conseils et comités

Membre à plusieurs reprises des « Conseil d'Unité » (CU) et « Comité scientifique et technique » du SEDI (CSTS) et amené dans ce dernier cas à faire des rapports sur des projets qui lui était soumis, et à le représenter dans d'autres comités scientifiques de service.

Moyens d'irradiation

Responsable de la construction en 1994, (et de ses différents déplacements…) et de l'exploitation depuis cette date de l'irradiateur Cocase de l'IRFU, irradiateur au ^{60}Co destiné à des études et tests de matériaux, composants électroniques, détecteurs etc., à faible débit de dose. Parmi les tests effectués, citons les cristaux scintillants pour CMS, l'électronique durcie DMILL, des matériaux pour BaBar, des bolomètres pour la mission Herschell, les asic IdefX et Maroc, etc.

G. Publications

[p17] M. Atac, G. Charpak, R. Chipaux, A. Delbart *et al.*,
« The development of the optical discriminator »,
Nuclear Instruments and Methods in Physics Research A367 (1995) 372-376.

[p23] A. N. Annenkov *et al.*,
« Systematic study of the $PbWO_4$ crystal short term instability under irradiation »,
Radiation Measurements 29 (1998) 27-38.

[p32] R. Chipaux *et al.*,
« Ytterbium-based scintillators, a new class of inorganic scintillators for solar neutrino spectroscopy »,
Nuclear Instruments and Methods in Physics Research A486 (2002) 228-233.

[p49] The CMS Electromagnetic Calorimeter Group, P. Adzic *et al.*,
« Radiation hardness qualification of $PbWO_4$ scintillation crystals for the CMS electromagnetic calorimeter »,
Journal of Instrumentation, 5 (2010) P03010.

[p52] R. Chipaux and F.-X. Gentit,
« Transparency variations and calibration in CMS electromagnetic calorimeter crystals: Monte-Carlo studies »,
IEEE Transactions on Nuclear Science, 57 (2010) 1460-1464.

ELSEVIER

The development of the optical discriminator

M. Atac[f,g], G. Charpak[a], R. Chipaux[c], A. Delbart[c],
J. Derre[c], Y. Giomataris[c,*], T. Hill[e], C. Joseph[b], D.M. Kaplan[d], C. Kochowski[c],
N. Leros[b], S. Loucatos[c], J.-P. Perroud[b], Ph. Rebourgeard[c], E.I. Rosenberg[e]

[a]CERN-AT-ET, Geneva, Switzerland
[b]Lausanne University , Switzerland
[c]CEA, DSM, DAPNIA, CE Saclay, France
[d]Northern Illinois University , USA
[e]Iowa State University , USA
[f]University of California at Los Angeles, USA
[g]Fermilab, Batavia, IL, USA

The RD30 Collaboration

Abstract

New results from the tests of the impact parameter discriminator by the RD30 Collaboration are presented. The device, based on the detection of Cherenkov light produced in a thin crystal, is able to cope with extremely high rates in the GHz range and sign tracks with non-zero impact parameter at a first trigger level. We report experimental results obtained with a sapphire shell surrounded by a liquid cladding compensating chromatic dispersion. An excellent signal to background ratio has been obtained and the sensitivity at low impact parameters reaches the requirements for efficient B-meson selection. The use of such a device for hyperon selection will also be discussed.

1. Introduction

Many of the interesting physics questions at the high luminosity proton accelerators require an efficient and fast selection of rare events out of background events occurring at a much higher rate. Following an idea in Ref. [1], the optical discriminator is a device sensitive to the main characteristics of a B-meson event produced in a fixed target experiment by a proton accelerator. The idea is to detect the Cherenkov light emitted in a thin crystal shell by charged particles and retain those particles having a sizeable impact parameter b with respect to the production vertex. The development of such a device started in 1992 as R&D experiment CERN-RD30 [2]. Another potential application of the optical trigger is the fast selection of long-lived particles. An example is the new E871-FNAL fixed-target experiment at the Tevatron. The experiment will perform a search for CP violation in hyperon decays. The aim is to fully reconstruct 4×10^9 Ξ and ($\bar{\Xi}$) decays in order to achieve a sensitivity for the relevant asymmetry in decay angular distribution parameters of about 10^{-4}.

These events should be selected among a four order of magnitude higher rate of background events estimated to be about 40 MHz. Therefore the use of the optical discriminator with a subnanosecond time resolution can be a precious tool for the first trigger level.

2. The principle of the optical discriminator and first results

The principle of the optical discriminator (OD) is illustrated in Fig. 1. The radiator is a thin crystal with a refractive index n_1, shaped as a shell limited by two concentric spheres and surrounded by a medium of refractive index n_2. Particles emerging from a small target located at the center of curvature of the crystal produce Cherenkov light in the crystal which is refracted and lost, while for particles off-center part of the light is internally reflected and can reach the exit surface of the crystal and be detected. To optimize the light collection, the exit face is shaped along a cone with an angle matching the Cherenkov one. In order to avoid the detection of charged particles coming from the target, i.e. with an impact parameter $b = 0$, the refractive indices have to satisfy the

---

* Corresponding author. E-mail ioa@cernvm. cern.ch
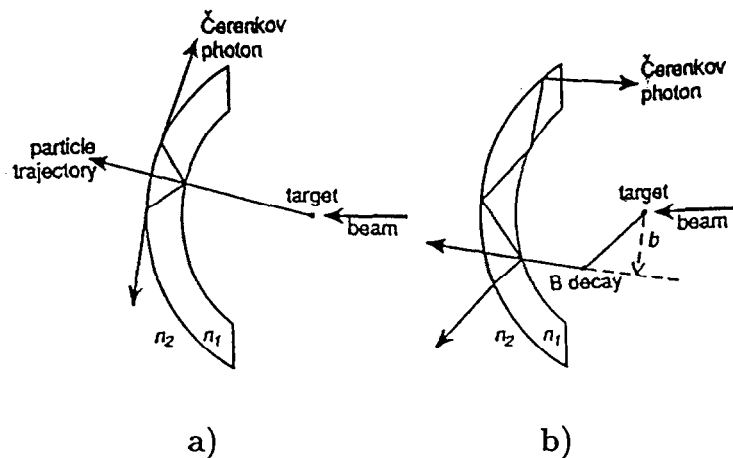
Fig. 1. The principle of the optical discriminator: a particle with zero impact parameter (a) produces Cherenkov light refracted through the outer surface of the crystal, whereas for a particle with a non-zero impact parameter (b), part of the Cherenkov light is internally reflected and trapped.

condition:

$$n_1^2 - n_2^2 = 1 - \varepsilon, \tag{1}$$

with ε small and positive. When a single crystal is used in air or vacuum, $n_2 = 1$, and n_1 has to be close to, but lower than $\sqrt{2}$. The principle was tested in 1992 using a single crystal shell. A LiF shell (thickness 3 mm, diameter 60 mm, spherical radius 100 mm) was placed at the first

focus of an ellipsoidal mirror, the light was guided to a PMT whose photocathode was located at the second focus. Details of this test can be found in Ref. [3]. The distribution of the signal is shown in Fig. 2 as a function of the up–down signed impact parameter. The agreement with the Monte-Carlo simulation is good. However, the LiF achromaticity in ε is poor, and the small b values induced in B-events cannot be reached with this material.

A second prototype using the same crystal but read out
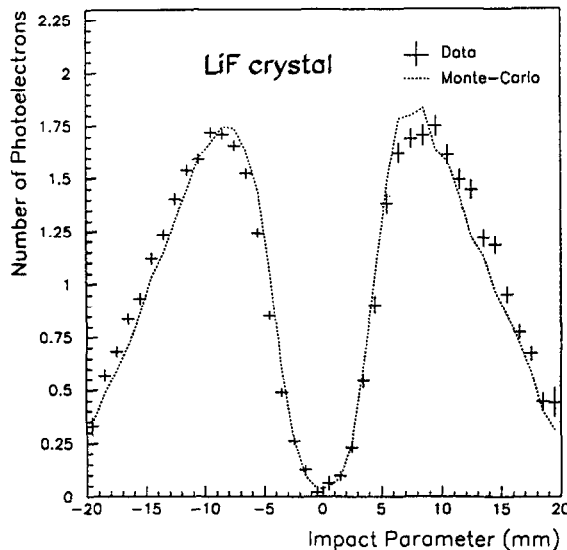
Fig. 2. Amplitude of the signal as a function of the signed impact parameter, data (crosses) and Monte Carlo (line). The impact parameter is given with a positive sign if the impact is above the center of the sphere, negative otherwise.
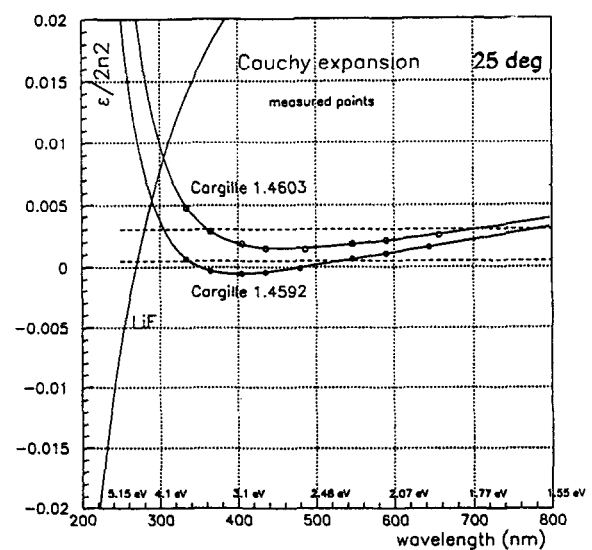

Fig. 3. The variation of the quantity $\varepsilon/2n_2$ as a function of the wavelength for two liquids (Cargille 1.4603 and Cargille 1.4592) used as cladding on sapphire, and for LiF in Air.
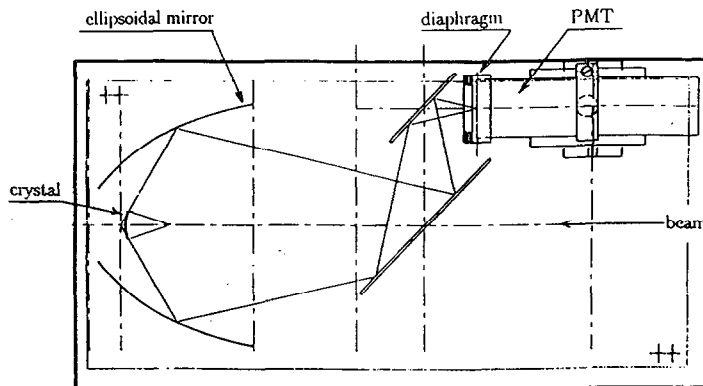
Fig. 4. The set-up used for the sapphire + liquid beam test.

through fibers was also tested and gave a similar result [4]. In order to obtain a good sensitivity to very small impact parameters, but to avoid background from minimum bias tracks coming from the optical centre, the minimum impact parameter must be small but greater than some lower limit. To achieve such a performance, the idea explored by the RD30 Collaboration was to balance a high index crystal (sapphire) by an appropriate lower index material (liquid or solid) in order to obtain a compensation of the relative index dispersion. Fig. 3 shows the quantity $\varepsilon/2n_2$ as a function of the wavelength for two different liquids used as cladding to a sapphire crystal. The result is quite promising: the large chromaticity of the sapphire

crystal is well balanced by the liquid index dispersion: $\varepsilon/2n_2$ is flat in a wide wavelength range. This quantity is equal to the minimum incident angle of a track giving collected light. It is very small, of the order of 10^{-3} for the useful visible and near UV region.

This optical set-up was tested as a prototype in a beam, as described in the next section.

3. The experimental tests

The sapphire + liquid setup is shown in Fig. 4. It has the following main components: a sapphire crystal, a vessel
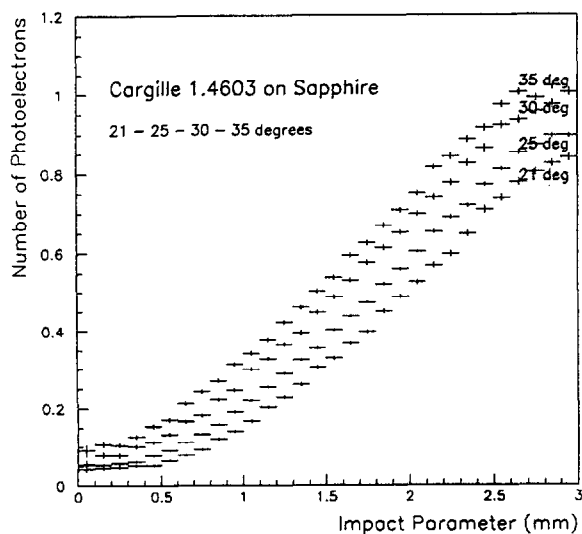

Fig. 5. Collected signal versus the impact parameter for various temperatures of the liquid.
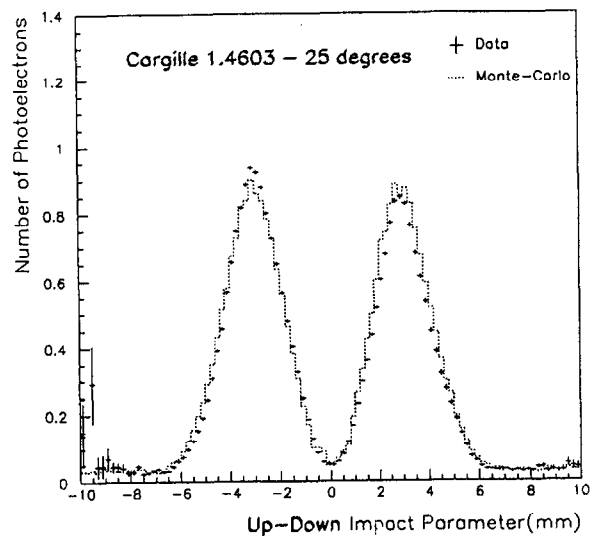

Fig. 6. Amplitude of the signal versus signed impact parameter in the vertical plane, for the sapphire + liquid device at 25°.

enclosing the liquid cladding, an ellipsoidal mirror, two flat mirrors, and a photomultiplier. The crystal is a section of a spherical shell with 50 mm radius of curvature, 1.5 mm thickness, and a diameter of 30 mm. The outgoing light from the crystal is focussed by the ellipsoidal mirror on the photomultiplier via the two flat mirrors. The vessel enclosing the liquid was filled with a siloxane liquid [5], circulated by a closed-loop circulation/temperature-regulation system. In this configuration the sapphire crystal is the Cherenkov radiator having a refractive index n_1. Its external spherical face is immersed in a liquid medium of refractive index n_2 (condition (1) needs to be satisfied at the external face only).

Since the refractive index of the liquid is sensitive to temperature variations, we used temperature regulation to optimize the response. Fig. 5 shows the signal as a function of the impact parameter obtained for different temperatures of the liquid. The minimum impact parameter shifts to lower values with increasing temperature. This gives a great flexibility to our procedure, since the minimum impact parameter can be tuned by varying the temperature of the circulating liquid.

Fig. 6 shows the distribution of the signal as a function of the signed impact parameter in the horizontal plane. Data points are compared to Monte-Carlo simulation. An excellent agreement is obtained. The signal rises to its maximum value at 3 mm and then falls down at larger impact parameters. The fall is due to the limited light collection acceptance, which can be tuned by varying a diaphragm in front of the photomultiplier. For the present
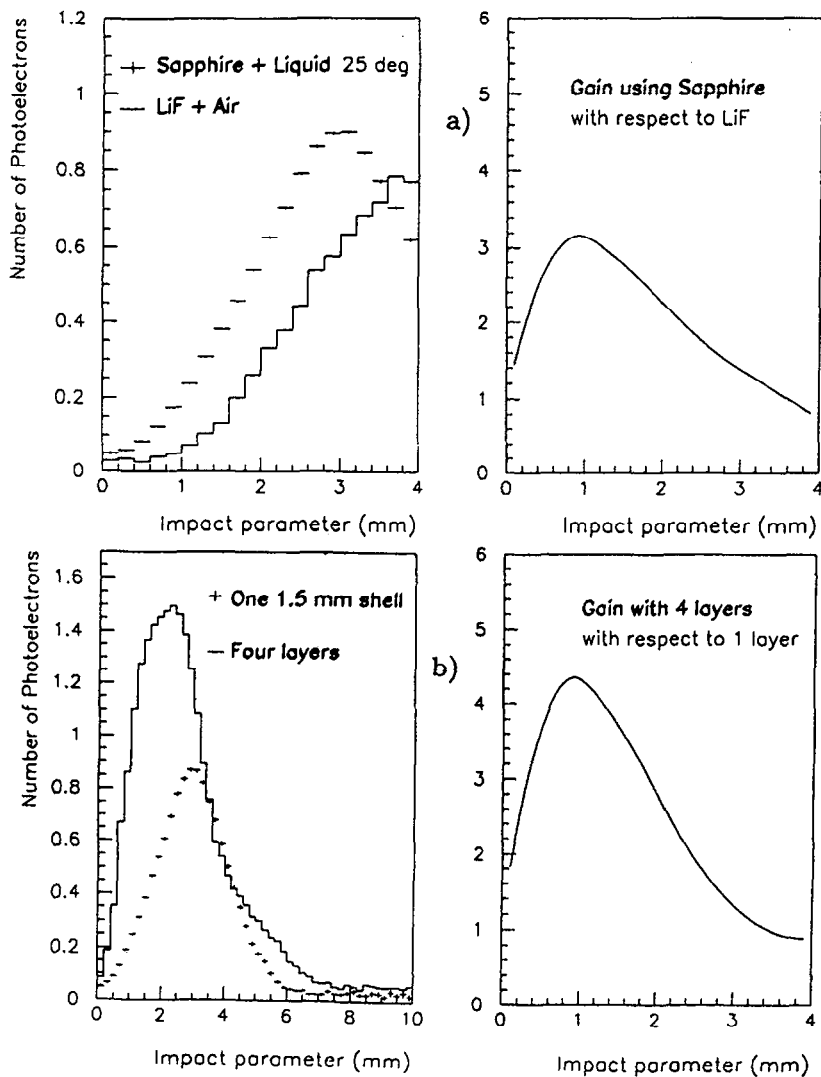

Fig. 7. (a) Evolution of the sensitivity of the optical trigger from the LiF to the sapphire + liquid, and (b) expected performance using a 4-layer sapphire + liquid object.

study the diameter of the diaphragm was 40 mm. The background tail at large impact parameter gives an upper limit of the delta rays contribution. The Monte-Carlo simulation program gives a similar flat distribution independent of the particle impact, in agreement with the observed tail. This background level is measured to be only 0.03 photoelectrons and is quite small compared to the maximum signal of about 1 photoelectron.

The rise of the signal observed is quite steep but not yet optimum for B-meson detection; it is mainly due to the thickness of the crystal, the second reason being the contribution of the chromaticity in ε. The effect of the thickness can be improved by using a multilayer crystal, having several thinner shells with the same total thickness as the crystal. In this configuration the signal at small impacts is roughly multiplied by the number of layers. A projective multilayer prototype with four thin sapphire crystals (400 μm) [6] is under investigation to be tested this year. Thinner crystals down to 150 μm are possible using present technology. Fig. 7a shows the evolution of the sensitivity of the optical trigger from the first LiF prototype to the sapphire + liquid and Fig. 7b the expected performance using the four layer object. The side figure gives the gain obtained in each step.

In usual accelerator vacuum conditions, a solid cladding is easier to use. The problem is to find such a solid having good mechanical and optical properties and deposited in reproductible conditions. A promising technique is the SOLGEL one: solution of a precursor material (SOL) which is gelled (GEL) at ambiant temperature and giving stable depositions. An active collaboration is in progress with specialized laboratories [8].

4. Conclusions – outlook

The results obtained with a sapphire + liquid prototype are very encouraging. They establish the optical discriminator as a new promising technique able to select low impact parameter particles, like B-mesons, in fixed target experiments. The sensitivity to small impact parameters has been greatly improved by using two dispersion-compensating materials. A multilayer prototype that is being designed will allow us to push the sensitivity to lower impacts.

Concerning physics applications, the LHC-committee decision, in June 1994, to recommend only collider beauty experiments has prevented for the time being the application of the novel technique in a fixed target B experiment. On the other hand, simulations are going on to study the merit of the optical trigger for hyperon selection in a Tevatron fixed target environment [7]. A sapphire crystal with 30 cm dimension, 3 mm thickness located at about 17 m from the target is simulated, using the program which finely reproduces our experimental results. With the same
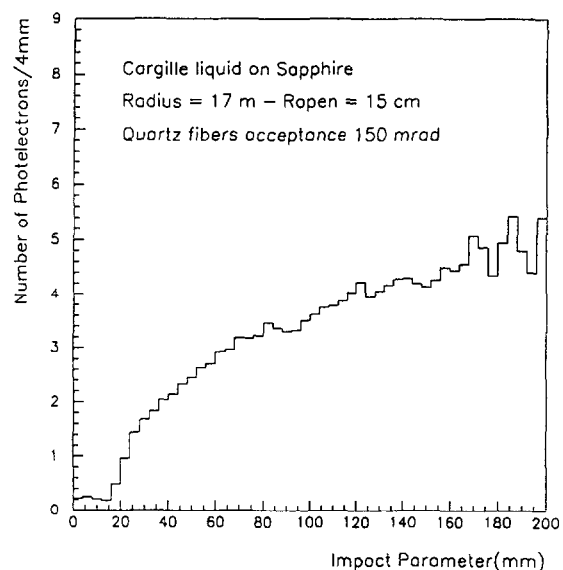

Fig. 8. Simulated signal for the E871 Hyperon Experiment.

siloxane liquid the result is quite promising; as is shown in Fig. 8, the signal starts rising at 15 mm impact parameter up to about 4 photoelectrons at high impact values, with a small background level for small impacts. The efficiency can be high for most of the hyperons having impacts of several centimeters. The low background will certainly allow us to achieve high rejection factors for the minimum bias events. In this direction a study is under way to find out the efficiency and the rejection expected when such a trigger is used for the E871-FNAL experiment.

References

[1] G. Charpak, Y. Giomataris and L. Lederman, Nucl. Instr. and Meth. A 306 (1991) 439.
[2] CERN/DRDC/P30 (20 August 1991);
    CERN/DRDC/92-53 Addendum (5 November 1992);
    CERN/DRDC/93-56 Status Report (20 December 1993).
[3] G. Charpak, R. Chipaux, J. Derre, Y. Giomataris, C. Joseph, C. Kochowski, S. Loucatos, J.-P. Perroud, Ph. Rebourgeard, M. Steininger, M.T. Tran and M.C.S. Williams, Nucl. Instr. and Meth. A 332 (1993) 91.
[4] C. Kochowski, Nucl. Instr. and Meth. A 351 (1994) 193.
[5] R.P. Cargille Laboratories, 55 Commerce Road, Cedar Grove, New Jersey, 07009-1289, USA.
[6] Crystals manufactured by Victor Kyburz AG, CH-2553 Safnern, Switzerland.
[7] J. Antos et al., Search for CP violation in the Decays of Ξ/Ξ̄ and Λ/Λ̄ Hyperons Fermilab Proposal P-871 (March 26, 1994).
[8] H.G. Floch and J-J. Priotton, Am. Ceram. Soc. Bull. 69 (7) (1990) 1141;
    P.F. Belleville and H.G. Floch, SPIE 1848 (1993) 290.

Pergamon

SYSTEMATIC STUDY OF THE SHORT-TERM INSTABILITY OF PBWO₄ SCINTILLATOR PARAMETERS UNDER IRRADIATION

A. N. ANNENKOV[a], E. AUFFRAY[b], R. CHIPAUX[c], G. YU DROBYCHEV[d,g],
A. A. FEDOROV[d], M. GÉLÉOC[c], N. A. GOLUBEV[f], M. V. KORZHIK[d], P. LECOQ[b],
A. A. LEDNEV[e], A. B. LIGUN[a], O. V. MISSEVITCH[d], V. B. PAVLENKO[d],
J-P. PEIGNEUX* and A. V. SINGOVSKI[b,e]

[a]Bogoroditsk Techno-Chemical Plant, 301800 Bogoroditsk Tula Reg., Russia, [b]CERN, 1211 Geneva,
Switzerland, [c]DSM/DAPNIA/SED, CEA-Saclay, Gif-sur-Yvette Cedex, France, [d]Institute for Nuclear
Problems, Minsk, Belarus, [e]Institute for High Energy Physics, Sapukhov RU-142284 Protvino, Moscow
Region, Russia, [f]Institute for Nuclear Research, Moscow, Russia and [g]LAPP, F-74941 BP110 Annecy-
le-Vieux, France

Abstract—The effect of irradiation on lead tungstate PbWO₄ (PWO) scintillator properties has been studied at different irradiation facilities. Lead tungstate crystals, grown with the oxide content in the melt tuned to the stoichiometry of pure sheelite or sheelite-like crystal types and doped with heterovalent, trivalent and pentavalent impurities, have been studied in order to optimize their resistance to irradiation. A combination of a selective cleaning of raw materials, a tuning of the melt from crystallization to crystallization and a destruction or compensation of the point-structure defects has to be used to minimize the short-term instability of PWO parameters under irradiation. © 1998 Elsevier Science Ltd. All rights reserved

1. INTRODUCTION

The CMS (Compact Muon Solenoid) Collaboration (CMS, 1994) R&D efforts related to lead tungstate PbWO₄ (PWO) scintillator technology development have already led to the reproducible production of a quite transparent, fast scintillator with acceptable light yield. In spite of significant progress in the improvement of PWO scintillation properties, the prototype technology for the production of PWO crystals with an acceptable level of transmission damage under irradiation is still under development. To solve this problem, a systematic study of the variation under irradiation of PWO crystal properties, mainly produced in Russia, has been organized at different facilities. It allowed a fast or detailed investigation mode of the parameter changes for full-sized PWO elements (23 cm in length) at different dose rates. Such an organization made possible two research levels: a fast check of the produced crystals and a detailed investigation of the most important samples.

For a high-precision calorimeter, the scintillator's light output must remain unchanged under irradiation in order to prevent non-uniformities of

the crystal response due to a non-uniform irradiation. Moreover, the variation of the crystal response cannot exceed a few per cent and must be slow in order for the monitoring system to correct for these variations with a precision of about 0.2% (Saclay Group, 1996). Thus a short-term instability of the scintillator parameters dependent on dose rate or accumulated dose is not acceptable for the design of a precise calorimeter.

Although damage to the transmission of 23 cm-long PWO scintillation elements is detectable and can achieve some tens of a per cent in the worst case, the value of the absorption induced by irradiation is rather small and does not exceed a few inverse meters corresponding to an attenuation length of more than one meter for the majority of crystals. Even for the worst crystals, the total concentration of the damaged defects is of an order of magnitude of 10^{17} cm^{-3} to be compared to the lattice atom density of 10^{22} cm^{-3}. At such a level of defect content in crystals obtained from standard raw materials, the separate contribution of the impurities and of the point-structure defects to be recharged under irradiation cannot be distinguished. Although the separated contribution of the impuri-

---

*To whom all correspondence should be addressed.

ties could easily be studied by increasing their concentration, this is not possible for the point-structure defects.

Another aspect is related to the damage kinetics which describes the equilibrium between the damage/recovery processes and establishes the acceptable amount of the different kinds of defects. The transmission damage kinetics have already been described elsewhere (Annenkov *et al.*, 1997).

In this paper the stability of the scintillating centers under irradiation is established and the conclusion is that the damage results from the attenuation of the scintillation light by color centers. The origin of the damaged centers is discussed. Also the results of a systematic investigation of the tuning of crystal growth conditions (stoichiometry scan) based on 56 full-sized crystals produced by the Bogoroditsk Techno-Chemical Plant in Russia are presented. Ways to suppress or compensate the remaining defects by specific doping of PWO crystals are proposed. For the last point the results based on a large statistical sample of full-sized crystals are presented in Annenkov *et al.* (1998)

2. MEASUREMENTS AND IRRADIATION FACILITIES

The changes of absorption in the sample due to the irradiation are evaluated using the radiation-induced absorption coefficient k_{ind} defined as:

$$k_{ind} = (1/L)\ln[T_0(\lambda)/T(\lambda)] \qquad (1)$$

where $T(\lambda)$ stands for the transmission after the irradiation, $T_0(\lambda)$ stands for the initial transmission, L is the length of the PWO sample. A clear correlation was observed for each crystal between the collected light loss measured at the back of the crystal on a photomultiplier tube (PMT) and the longitudinal transmission loss characterized by the induced absorption coefficient k defined in [1]. The number of photons detected on the PMT before (N_0) and after irradiation (N) is given at the first order by:

$$N_0 = I_0 \times \exp(-k \times L_{mean}) \qquad (2)$$

$$N = I \times \exp[-(k + k_{ind}) \times L_{mean})] \qquad (3)$$

where I_0 and I are the scintillation yields, not necessarily equal before and after irradiation, L_{mean} is the mean free path for photons between the point of emission and the PMT, k is the initial absorption coefficient at the wavelength of peak emission of PWO (about 500 nm) and k_{ind} is the induced absorption coefficient at the same wavelength after irradiation. Strictly speaking, [2] and [3] are first order approximations of more complex equations (Besson *et al.*, 1997). In particular, with this formalism, L_{mean} is a function of the transparency of the crystal, given by k and k_{ind}, of its other optical characteristics (surface quality, coating or wrapping) and of the photodetector. L_{mean} decreases when k (or $k + k_{ind}$) increases. However, for a small induced absorption, it can be considered as constant for a given crystal. Assuming (2) and (3), simple mathematics leads to:

$$k_{ind} \times L_{mean} = \ln(N_0/N) - \ln(I_0/I). \qquad (4)$$

The evolution of k_{ind} vs $\ln(N_0/N)$ during recovery after irradiation is shown in Fig. 1 for a large number of crystals of different initial transmission. Each crystal has a different slope which depends on the value of L_{mean}. However, all the lines point to the origin within the measurement and fitting errors, which proves that the scintillation yield did not change within the errors (about 1%) under irradiation for all these crystals. It indicates that at
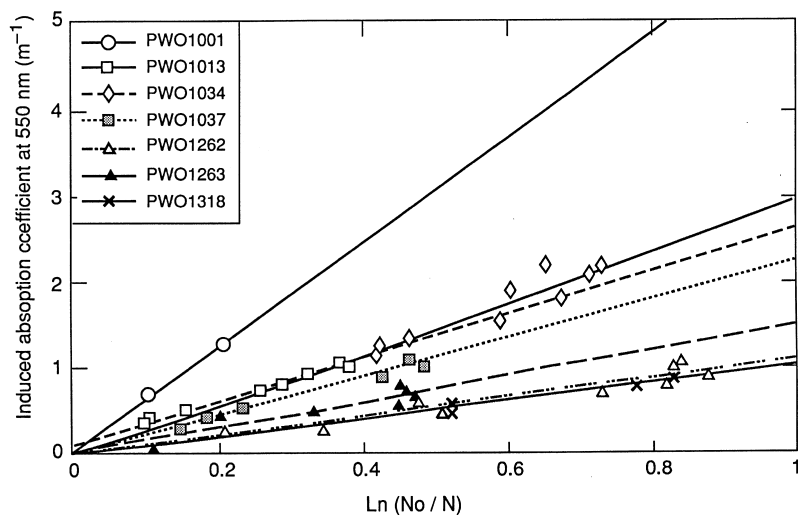

Fig. 1. Induced absorption coefficient at 550 nm vs ln (N_0/N). Crystal numbers refer to the CMS database.

least the fundamental properties of the radiating centers in PWO are not influenced by irradiation.

To clarify the features of the damage origin of the scintillating crystal under irradiation, as many parameters as possible have to be measured in an irradiation environment. But practically, only just the optical transmission of PWO crystals shows a detectable change under irradiation and is sufficient to explain the loss of the collected light. Such a change of the transmission in a spectral region is measured directly by a single- or double-beam spectrophotometer after the irradiation. Also, its relative change can be determined by recording the intensity of a monitoring light injected through the wrapped crystal equipped with a properly protected photodetector during the irradiation. The relative change of the monitor signal from the initial value is then proportional to the transmission change. Depending on the absorption spectrum induced by the irradiation, the monitoring signal variation at some wavelengths is correlated with the decrease of the particle signal detected in the scintillator. The best combination for this study is the measurement of the transmission, the monitoring, and the particle signals in the same experimental set-up implemented in beam facilities, but accessible only for a limited time each year. So independent investigation of the crystal transmission or monitor signal changes is implemented at irradiation by the widely used ^{60}Co source.

Keeping in mind that under LHC irradiation PWO will suffer a dose rate of 15–20 rad/h, the following irradiation facilities have been used both for very fast and detailed study of the crystals under irradiation:

2.1. COCASE facility, at Saclay, Dapnia

It consists of the ^{60}Co (1.25 MeV, 14 Ci) source with geometrical tuning of the dose rate in the region below 2 rad/min. Relative change of the monitoring signals in the spectral region 380–800 nm is measured. During the irradiation the monitoring light pulses are generated by a spectrometer made of a computer-driven fast-tuning monochromator, a Xe pulse lamp, fiber optics feeding light to the crystals under test, and electronics for recording the short- and long-term instability of the light pulses. Such a system provides registration of the monitor signal changes at specific wavelengths in the range mentioned above. The minimal available wavelength step is 5 nm. Also, longitudinal transmission is measured by a Perkin-Elmer spectrophotometer in the region 300–850 nm for the crystal before and after its irradiation (Chipaux and Toson, 1995).

2.2. ^{60}Co therapy unit of the Geneva Hospital

This provides the irradiation of the crystals with an irradiation rate of 420 rad/min. Change of the crystal transversal and longitudinal transmission, light yield, and scintillation kinetics are measured 40 min after the irradiation by a set of spectrometers located at CERN.

2.3. INP ^{60}Co source facility

It consists of the ^{60}Co well-shaped source with fixed irradiation rate of 14,000 rad/min. Change of the crystal transmission is measured 60 min after irradiation by a Varian 'Cary1E' spectrophotometer
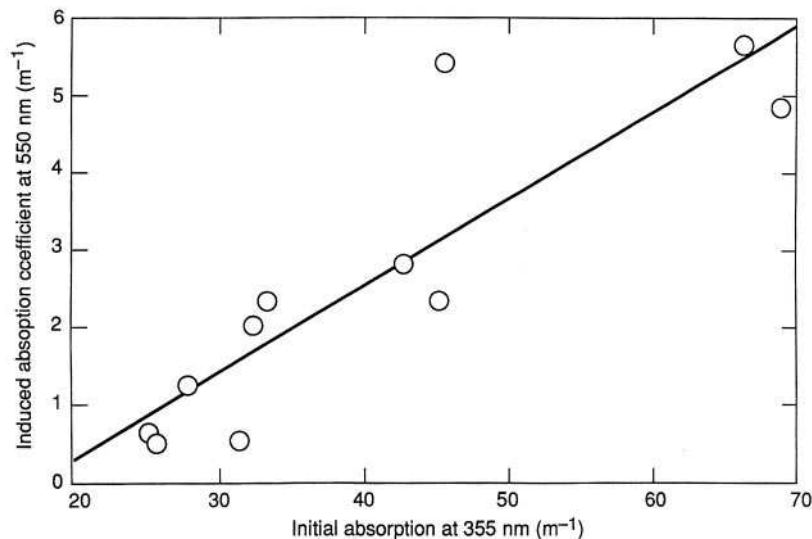

Fig. 2. Induced absorption coefficient of 550 nm vs initial absorption at 355 nm.

Defects creation in PWO
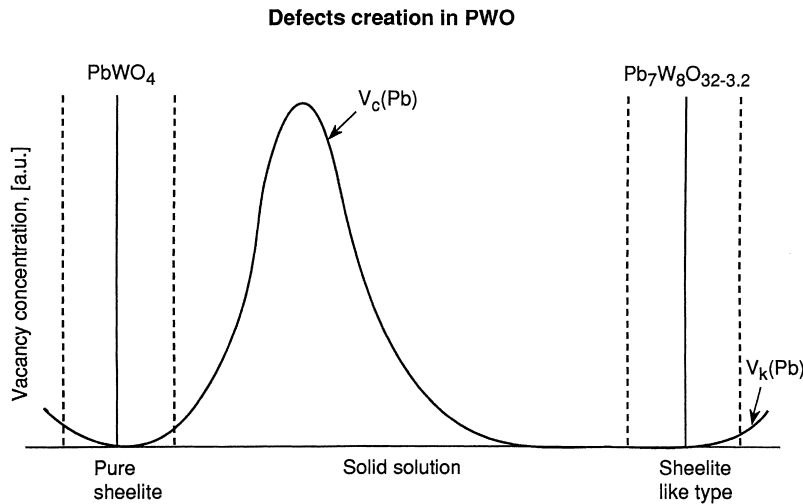
Fig. 3. Qualitative distribution of the cation vacancy V_c defects in PWO crystals with its structure.

in the range 300–900 nm. Control of other scintillation parameters is also carried out.

2.4. *INR irradiation facility*

A microtron MK-25 and linear electron accelerator (both of 25 MeV electron energy) are used as γ sources. Irradiation rates are tuned from 0.1 to 3000 rad/min. Longitudinal transmission is measured in the range 390–650 nm during the irradiation by a specially developed spectrophotometer based on a transparent grating.

2.5. *CERN H4 beam*

The CERN H4 beam (CERN, 1996) is also sometimes used as an irradiation facility. It includes specially constructed thermostabilized equipment for the simultaneous measurement of the time dependence of the particle signal and monitor signal in PWO scintillators. Light monitoring signals are generated by the same type of spectrometer as the one which is used in the COCASE facility.

2.6. *CERN X5 beam facilities*

These are under development. With a ^{137}Cs source and the possibility to probe the crystal in parallel with a muon or an electron beam, they will be equipped as far as possible with the best measuring systems tested in the above-mentioned facilities. They should become the main facilities for crystal tests at the CMS mass production stage.

3. RECHARGEABLE DEFECTS IN PWO CRYSTALS

Radiation damage in the crystal appears to be due to the charge-state change of the existing point defects. They are divided into two groups: the substitution defects and the point-structure defects. The radiation damage process is therefore driven by the change of the defects' electronic states which provides recharged ions and color centers and the creation or suppression of their associated absorption bands.

The data obtained to date for the radiation-induced effects in PWO crystals are summarized as follows:

(i) Irradiation of PWO crystals grown without specific tuning generates two absorption bands with maxima around 360 nm and 620 nm. Usually, induced absorption in such crystals reaches a value of about $10\ m^{-1}$ in the region 400–600 nm.

(ii) There is a correlation between the initial absorption of crystals at the wavelength near 360 nm and the absorption induced by irradiation in the green-red region as shown in Fig. 2.

(iii) The value of the absorption induced by radiation in the green-red region is correlated with the presence of red luminescence emitting centers, however, the blue and green luminescence radiating centers themselves are not damaged by irradiation.

(iv) The concentration of the defects able to create metastable color centers under irradiation does not depend on the atmosphere of the crystal growth, but is influenced by the purity of the raw material.

(v) In conclusion, only some impurities and point-structure defects contribute to the induced absorption in PWO crystals.

The point-structure defects in PWO crystals appear to be due to stoichiometric violation in the melt. This change may be casual in some fragments of the crystal or systematic if, for instance, the de-
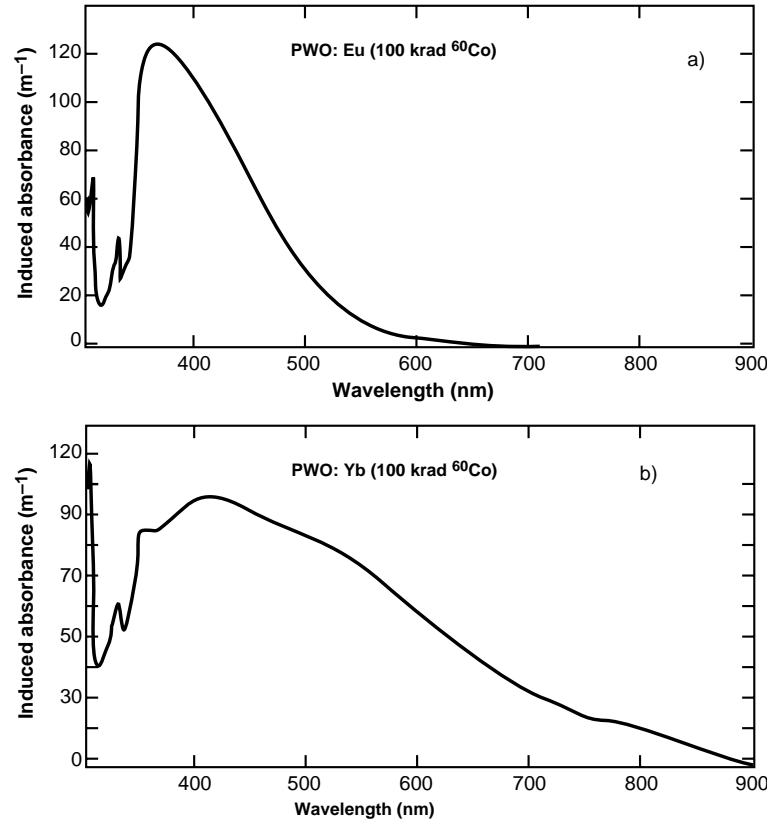
Fig. 4. Absorption of PWO:Eu (a) and PWO:Yb (b) crystals induced by irradiation. ^{60}Co source, 14,000 rad/min irradiation rate, accumulated dose 100 krad.

ficiency of one sort of atom becomes dominant. The dominating defects in the grown PWO crystal are due to lead leakage from the melt; however, two phases—pure sheelite and sheelite-like type crystals (Galez *et al.*, 1996) or their solid solution appear at the lead tungstate crystallization. Contrary to pure sheelite, sheelite-like crystals have already some deficiency of lead, but organized in a superstructure with a large range charge compensation. One can expect that lead leakage creates cat-
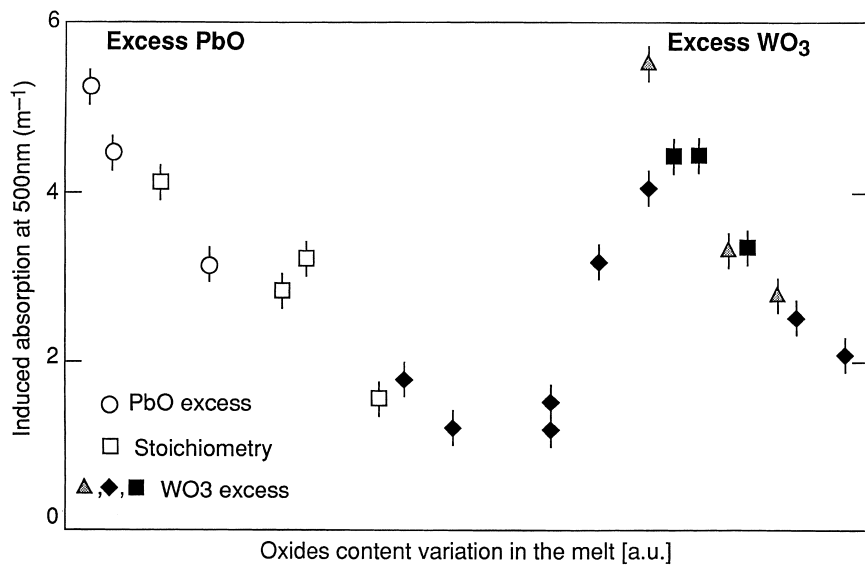

Fig. 5. Influence of the melt stoichiometry tuning on the induced absorption value at 500 nm. ^{60}Co source, 300 rad/min irradiation rate, accumulated dose 50 krad.

ion vacancies $V_{c(Pb)}$ whose concentration has three extremes in the system "pure sheelite–sheelite-like type" and depends on the portion of the pure sheelite in the solid solution (Fig. 3). In the crystals grown from purified raw materials, such vacancies are compensated by anion vacancies V_0 or different F-centers (Lecoq *et al.*, 1995). A cation vacancy locally generates O^- hole centers which may be separated or associated to form $(2O)^{2-}$ centers with antiparallel spins of electrons rotating around two oxygen atoms and the cation vacancy. These hole centers being recharged under irradiation create metastable color centers with associated absorption bands. As we observed that radiation-induced effects in PWO crystals do not depend on the atmosphere of the crystal growth, we concluded that anion vacancies V_0 do not contribute significantly to the discussed phenomena.

Among the impurities, even if they are present in small amounts, those which have charge transfer or interconfiguration transitions cause a detectable change of the crystal transmission. Let us consider some ions with charge transfer (CT) metal–ligand transition. Although the majority of the $3d$ elements are involved in such transitions, only different Fe ions produce detrimental effects in $PbWO_4$ crystals. In wide-gap oxide crystals, Fe^{3+} ions in tetrahedral coordination have O^{2-}–Fe^{3+} transitions in the region above $35,000\ cm^{-1}$ (280 nm) (Korzhik, 1990). In PWO they contribute to edge absorption or generate O^- centers with an absorption band around 350 nm (Korzhik, 1990). The Fe^{2+} ions being reduced from trivalent state under the irradiation also have CT bands in the region above $28,000\ cm^{-1}$ (350 nm). Both ions have relatively low intensity of the intraconfiguration d–d transitions in the visible and infrared region, but decrease the total PWO light yield due to overlapping of the CT levels and the radiating levels of the regular and irregular tungsten groups. An acceptable concen-
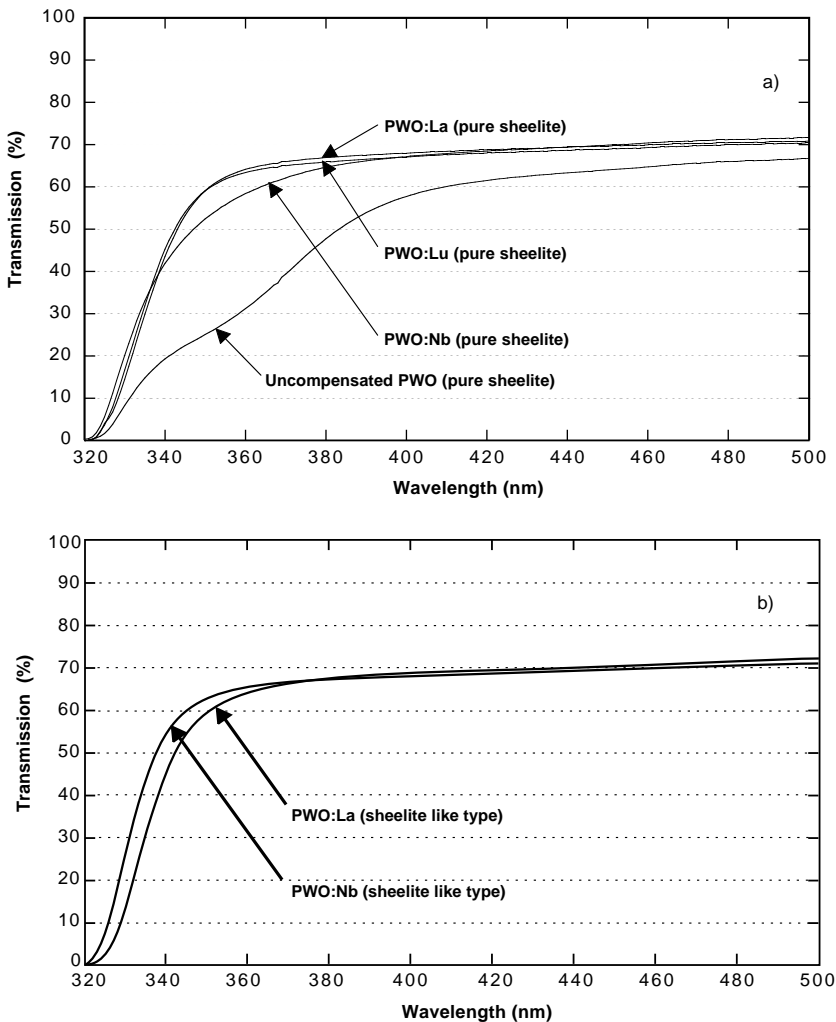

Fig. 6. Initial transmission of lead tungstate samples of 1 cm lengths of pure sheelite type (a) and sheelite-like type (b) doped with different activators. $T = 300\ K$.

tration of Fe in PWO crystals was already specified in raw materials during the PWO scintillation kinetics optimization (Annenkov *et al.*, 1996).

Among the ions having interconfiguration transitions, the most important class is made of lanthanoids or rare-earth elements, replacing divalent Pb ions in the host. Trivalent ions Ce^{3+}, Pr^{3+} and Nd^{3+} have 4f–5d interconfiguration transitions. However, such ions are not converted in the reduced valent state under irradiation. Their absorption bands related to the 4f–5d transitions are in the UV region and do not influence the radiating properties of PWO. The Eu and Yb ions are easily reduced from a trivalent to a divalent stable state under irradiation by the capture of electrons created under irradiation. In the trivalent state they have just f–f transitions exhibiting weak narrow absorption bands in the visible and infrared regions. However, Eu^{2+} have $4f^75d^0$–$4f^65d^1$ transitions, which generate a wide absorption band in the region below 400 nm in oxide crystals (Ellence, 1994). The Yb^{2+} ion has three interconfiguration

transitions $4f^{14}5d^0$–$4f^{13}5d^1$ and its associated absorption bands overlap all visible regions (Korzhik *et al.*, 1996) in oxide crystals. Both divalent ions have no interconfiguration luminescence at room temperature in PWO. The absorption spectra in Eu and Yb doped crystals induced by irradiation are shown in Fig. 4. They indicate that the presence of such heterovalent ions has to be carefully specified in the raw materials at a level below several ppm.

4. SUPPRESSION OF THE RECHARGEABLE DEFECTS IN PWO CRYSTALS

As previously noted (Annenkov *et al.*, 1997), the radiation induced absorption k in the crystal is described by the following equation:

$$k = \sum_i \frac{k_i^{\text{sat}}S}{S + \omega_i d_i}\left\{1 - \exp\left[-\left(\omega_i + \frac{S}{d_i}\right)t\right]\right\}. \quad (5)$$

At fixed dose rate S, it depends with time t on the
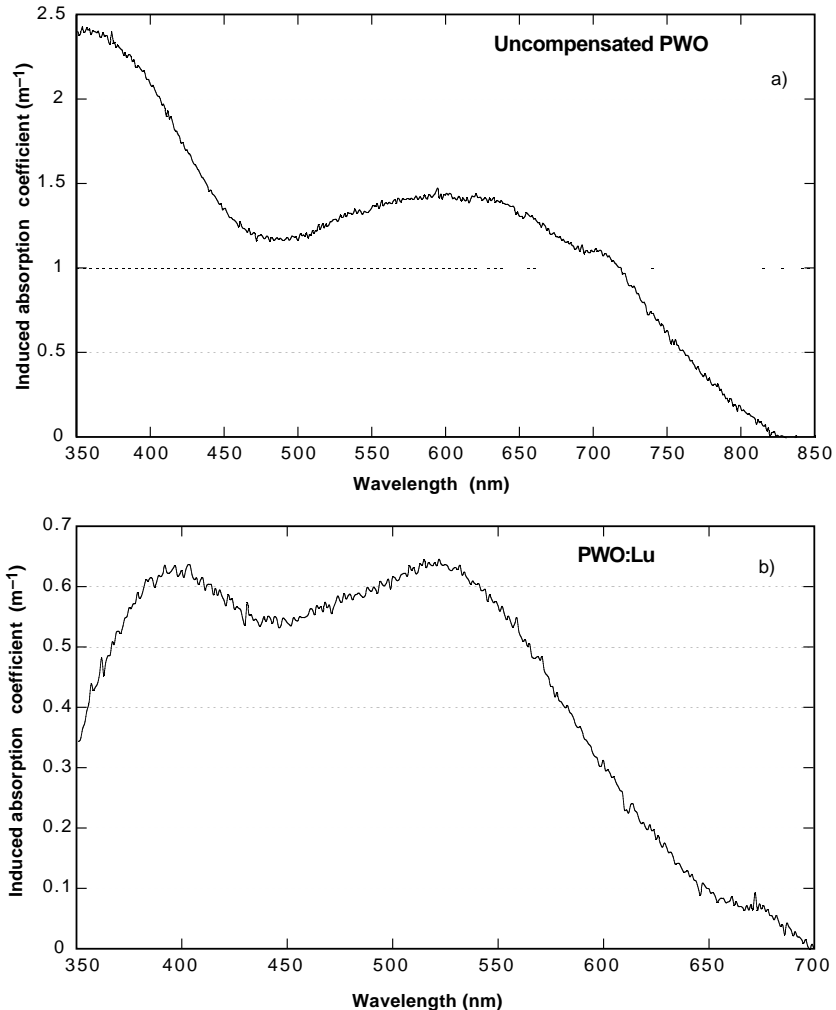

Fig. 7(a–b). *Caption overleaf.*
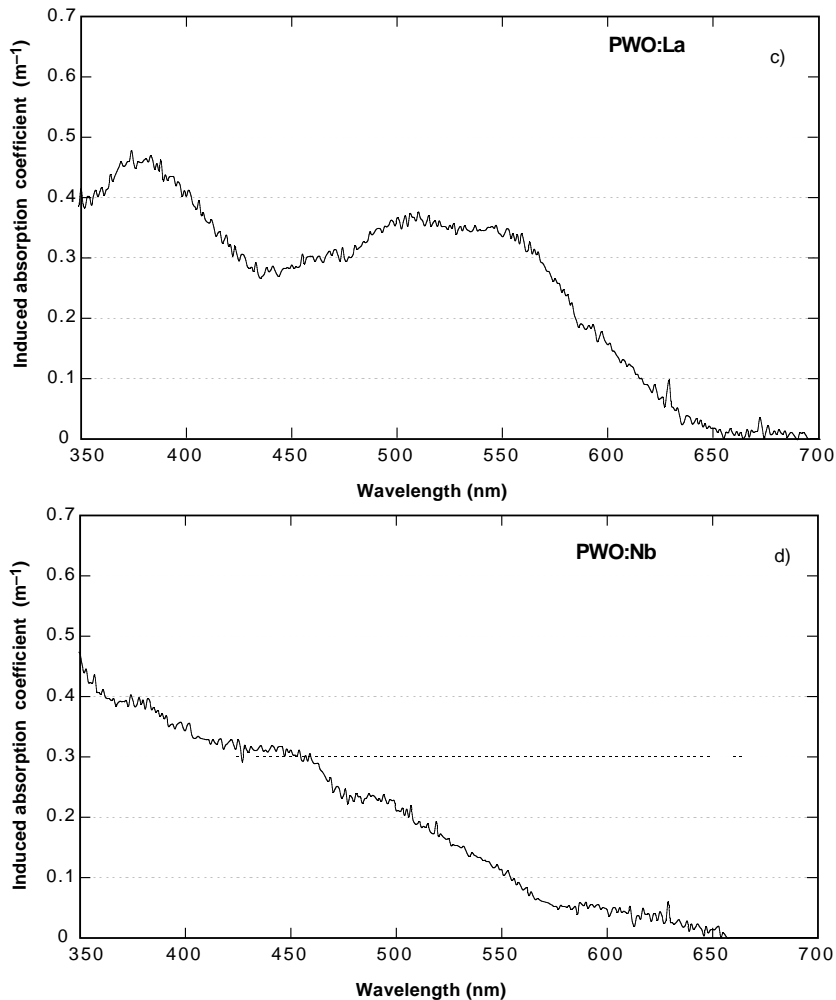
Fig. 7. Induced by irradiation absorption spectra in different PWO crystals: (a) grown in the conditions optimized by stoichiometry scan; (b) grown in the conditions optimized by stoichiometry scan and doped with Lu; (c) grown in the conditions optimized by stoichiometry scan and doped with La; (d) grown in the conditions optimized by stoichiometry scan and doped with Nb. [60]Co source, 14,000 rad/min irradiation rate, 1000 Gy accumulated dose.

amount N_i of the defects of kind i to be recharged, $k_i^{sat} = N_i \sigma_i$ with σ_i the absorbing cross section of the center i, the recovery probability ω_i and damage constant d_i.

Thus, the minimization of the observed transmission damage for a given dose rate S is achieved by the decrease of the total amount of slowly decaying color centers N_i or by the increase of their recovery probability ω_i. As it was determined at a dose rate of 5 rad/min and with a reasonable damage constant value, the defects with recovery times of less than a few minutes do not provide a significant contribution to the transmission damage of full-sized PWO crystals.

Specified impurity ions are extracted from the raw materials by chemical purification, so their contribution to the creation of rechargeable defects in PWO crystals can be easily minimized before crystal growth. To prevent the appearance of rechargeable point-structure defects in the crystal,

it is important to control the perfection of the crystal host structure. In the PWO case, it is realized by the choice of the crystal structure to a pure sheelite or a sheelite-like crystal type by a precise tuning of the oxide content in the melt. Figure 5 shows the results of the influence of the stoichiometric variation on the value of the absorption induced by irradiation in full-sized PWO scintillators. Such variation has been achieved by the addition of an appropriate oxide excess in the melt. Qualitatively, the stoichiometric scan results agree quite well with the expectations as shown in Fig. 3. The stoichiometric scan has given the possibility to reach an optimal combination of the oxides in the raw material and to minimize the induced damage in full-size elements. However, it has not led to a complete suppression of the damaged defects. This is due to the difficulty to control the stoichiometry when a considerable part of the melt is pulled into the crystal
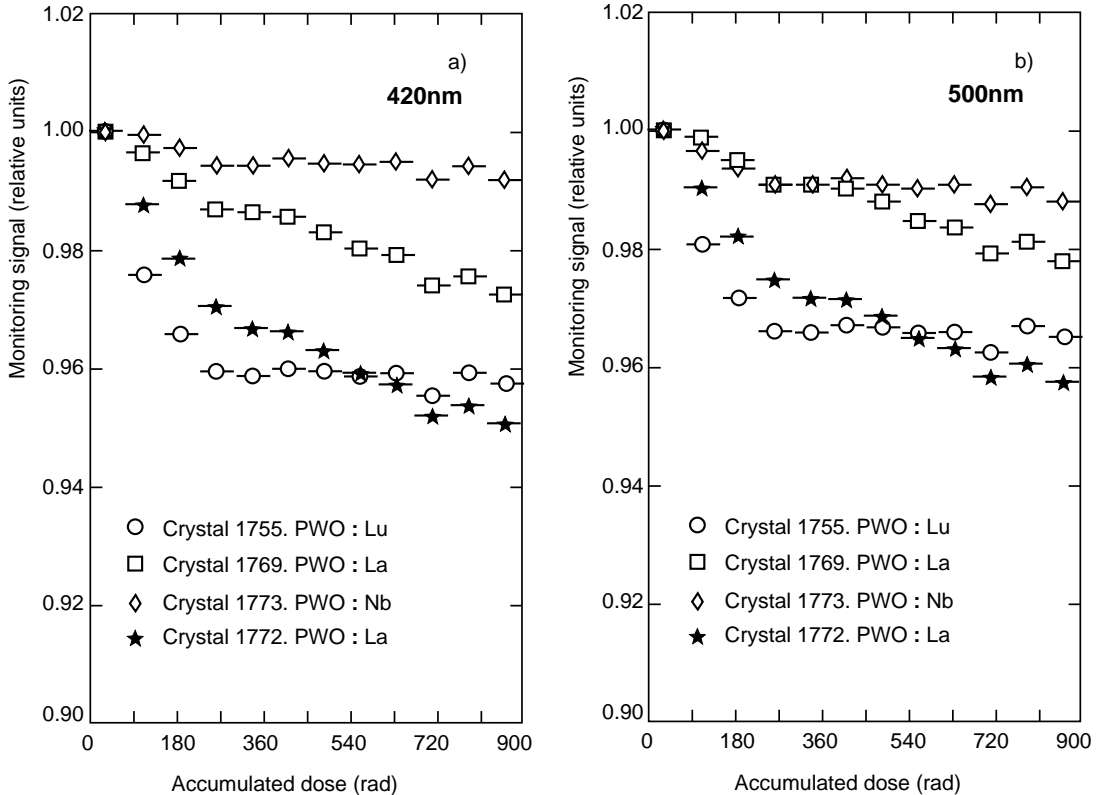
Fig. 8. Relative change of the monitoring signal at 420 nm (a) and 500 nm (b) obtained with crystals grown with stoichiometry tuning and additional doping with La, Lu and Nb. COCASE facilities, rate of dose accumulation 17 rad/h.

causing a significant gradient of defects from the seed to the tail part. It cannot be fully compensated by the tuning of the melt at the beginning of the crystallization. Thus, in addition to the structure tuning, an additional compensation or destruction of the defects is required. These phenomena have been investigated in the pure sheelite crystals and will be studied soon in the sheelite-like structure as well.

The destruction of the defects is achieved by the doping of PWO crystals by pentavalent Nb metal ion as described in Lecoq *et al.* (1995) and Fyodorov *et al.* (1996). The pentavalent Nb doping ion creates its own stable hole center when substituting to the W ion. The creation in the crystal of an additional amount of such stable hole centers decreases the amount of the unstable O$^-$ hole centers needed for cation vacancy compensation. Hole centers generated by Nb can also take part in the recharging processes under irradiation. However, owing to the stability of the valence state of the Nb^{5+} ions, such a reduced hole center has a short decay time. Therefore it does not contribute to the generation of a stable color center, but rather favors the fast recombination of free carriers created by irradiation. As the Nb concentration in the PWO crystal becomes similar or higher than the V$_c$ one, such a fast channel of electron-hole recombina-

tion does not leave any chance for a slow recharge process of O$^-$ hole centers near cation vacancies. With a further increase of Nb doping concentration, the probability of a local V$_c$ compensation is increased by the destruction of hole centers near cation vacancy. Most probably they create well-compensated and therefore stable associated defects like Nb^{5+}V$_0$V$_c$O$^-$. However, a practical concentration of the Nb doping is limited to some hundreds of ppm as described in Annenkov *et al.* (1996). Hole centers near cation vacancies may be compensated by the injection of stable trivalent ions replacing divalent lead ions in the crystal. The most convenient ions for such an application are Y, La and Lu which have no intracenter optical transitions and ionic radii compatible with the PWO structure.

5. EXPERIMENTAL RESULTS AND DISCUSSION

A large number of full-size doped and undoped crystals obtained after the optimization of the melt of stoichiometric scan have been investigated. Reference samples and full-sized elements obtained from crystals doped with La, Lu, Nb with concentration of the activator close to the optimum have been irradiated.
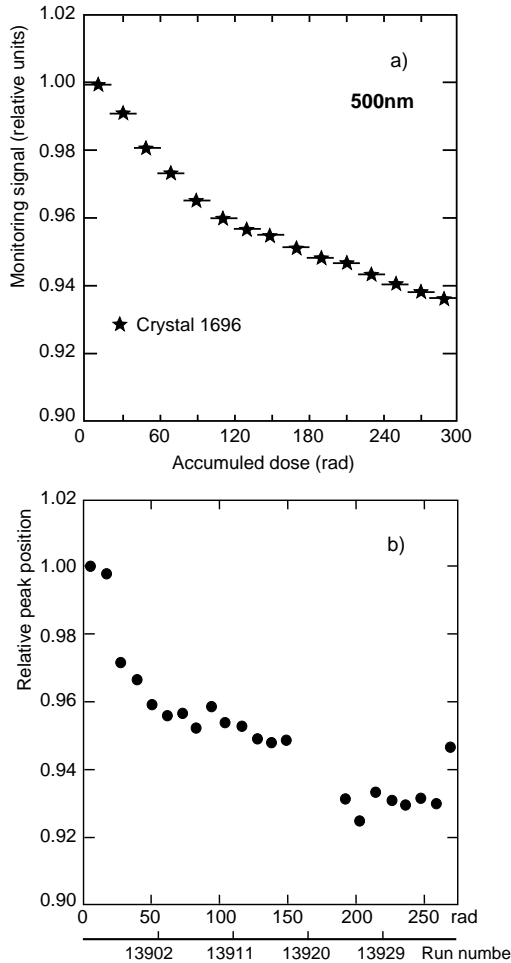
Fig. 9. The relative changes of monitor signal vs accumulated dose for the same crystal irradiated in the COCASE facilities (a) and relative peak position of the electron signal of energy 120 GeV/c irradiated at H4 (b). Corresponding run numbers are plotted at the bottom of the horizontal scale.

Figure 6 shows the initial transmission of crystals of the two sheelite types. A pure sheelite crystal grown without melt correction or any kind of compensation [Fig. 6(a)] has a clearly detectable absorption band with a maximum near 360 nm. As mentioned above, such crystals have shown a rather large radiation transmission damage in the spectral region 400–600 nm. A good correlation between the presence of this band in the crystal absorption spectrum and the value of the induced absorption has been observed (Auffray *et al.*, 1996) and confirmed

by our research. The Nb doping at the level of some tens of ppm suppresses this absorption band, but not completely. La or Lu doping with a concentration of about 100 ppm completely suppresses the absorption band and the transmission spectrum is not too far from ideal, as expected from Fresnel reflection losses. Both types of activators decrease the amount of O^- centers near cation vacancies and suppress the 360 nm absorption band associated with them.

In sheelite-like crystals, the concentration of the V_c is considerably reduced and both Nb and La provide complete suppression of the O^- centers with a slightly better transmission cut-off for Nb. The transmission spectra of such crystals are shown in Fig. 6(b).

In Fig. 7 the influence of suppression and compensation of the point-structure defects in the lead tungstate crystals is presented for pure sheelite crystals. Crystals grown from corrected melt, but without doping, show the appearance of two color centers with wide absorption bands maxima around 360 and 620 nm as indicated in Fig. 7(a). The first band is due to the additional creation of O^- centers in the irradiated crystal. Such metastable centers are probably stabilized around other macro defects or impurity traces in the host. The second absorption band is connected to the creation of the metastable color center $O^-V_cO^- + e^- \rightarrow O^{2-}V_cO^-$ due to the capture of one electron e^-. In the crystals obtained without tuning of the melt, the intensity of these absorption bands induced by the same irradiation conditions are 4–5 times larger than for crystals grown from optimized melt.

Figure 7(b, c) shows induced absorption of the crystals doped by trivalent Lu and La ions. The absorption band with maximum at 620 nm is suppressed in these samples, but a new band with maxima at 520 nm appears under irradiation. If the amount of the activator is too small, a partly compensated center $O^{2-}V_cO^- + La(Lu)^{3+}$ appears, jointly with the completely compensated centers $O^{2-}V_cO^{2-} + La(Lu)^{3+}$. Such a center capturing an electron gives a metastable color center $O^{2-}V_cO^{2-} + La(Lu)^{3+}$ which causes the 520 nm absorption band. When the activator concentration is increased, the concentration of partially compensated centers is reduced producing a decrease of the 520 nm induced absorption band. La doping has a positive influence on the PWO radiation hardness

Table 1. Crystal irradiation at the COCASE and H4 facilities for an accumulated dose of 200 rad

Scintillation element number*	1552	1557	1554	1474	1283	1564	1696	1694
Relative fall of the monitor signal at 500 nm in COCASE facilities (%)	25	18	21	9	8	4	5	30
Relative electron peak position shift (%) (Seez and Dobrzynski, personal communication)	22	17	21	3	5	4	7	22

    * Crystal numbers refer to the CMS database.

of small PWO crystals grown without additional tuning of the crystal to stoichiometry as described in Kobayashi *et al.* (1998). Thus, the activation by trivalent ions may be used as an additive to stoichiometric tuning to compensate rechargeable hole centers near the cation vacancy.

Figure 7(d) shows an absorption spectrum of PWO:Nb crystal induced by irradiation. Owing to the destruction of the complex defects $O^-V_cO^-$ for an activator concentration close to the optimal value, the 620 nm band in the induced absorption spectrum disappears. Also the 360 nm band is significantly suppressed due to the reasons described above. Thus, the Nb activation can be used as an additive to stoichiometric tuning in order to destroy rechargeable hole centers near the cation vacancy.

The data of the transmission loss at 420 and 500 nm for the full-sized elements irradiated at the COCASE facility are shown in Fig. 8(a, b). Crystal 1769 was obtained at the beginning of the series of crystallizations with stoichiometric tuning of the melt and defects compensation by La doping. Crystal 1772 is the last crystal from this series. Crystal 1755 was obtained at the end of a series of crystallizations with stoichiometric tuning of the melt and defect compensation by Lu doping. Crystal 1773 was obtained at the beginning of a series of crystallizations with stoichiometric tuning of the melt and defects destruction by Nb doping. The results show that for crystals grown from the tuned melt with additional compensation of the defects or their destruction by appropriate doping, the relative fall of the monitor signal in the relevant spectral region is below 5% for a dose rate similar to the one expected at LHC for the CMS electromagnetic calorimeter.

The results of a full-size scintillation element study in the COCASE and H4 facilities with the same type of light readout (PMT XP1921) are shown in Fig. 9(a, b). The element was produced from an ingot grown with tuned stoichiometry and doped with La with a concentration at half of the optimal value. The crystal was irradiated laterally uniformly along 18 cm by a ^{60}Co source for the COCASE test and longitudinally by a 120 GeV/c electron in the CERN H4 beam line with a similar dose rate of about 17 rad/h. In our study, some crystals were also tested in the COCASE facilities with PMT and in the H4 beam with APD readout. These data are presented in Table 1. They indicate that, at least to a first approximation, the source irradiation data correlate with the particle signal change under the beam irradiation. The model of the transmission damage kinetics quoted above (Annenkov *et al.*, 1997) allows to estimate the level of the induced absorption with a source which should correspond to a relative stability of the electron signal in a PWO calorimeter. A 5% electron peak position fall should correspond to an induced

absorption less than 0.5 m^{-1} at 500 nm with an irradiation rate above 100 rad/min.

6. CONCLUSIONS

Data from the irradiation of doped crystals allowed us to specify the raw material needed to grow crystals exhibiting low damage under irradiation. The specification is complemented by the requirements for impurities having charge transfer and interconfiguration transitions.

The transmission damage of PWO scintillating crystals under irradiation is suppressed by the simultaneous use of a combination of crystal host structure control due to stoichiometric tuning and compensation or destruction of the remaining defects.

The damaged defects in PWO crystals are destroyed by Nb doping at a level of several tens of ppm.

The compensation of the damaged defects in crystals is achieved by trivalent ion compensation like La, Lu at the level of some tens of ppm.

Crystals which show an induced absorption of less than 0.5 m^{-1} at 500 nm at a dose rate of more than 100 rad/min in source irradiation conditions will give an acceptable level of the loss of light signal induced by electrons in the irradiation conditions of the CMS electromagnetic calorimeter.

REFERENCES

Annenkov, A. N., Fyodorov, A., Galez, Ph. , Kachanov, V., Korzhik, M. V., Ligun, V. D., Moreau, J. M., Nephedov, V. N., Pavlenko, V. B., Peigneux, J-P., Timoschenko, T. N. and Zadneprovski, B. A. (1996) The influence of additional doping on the spectroscopic and scintillation parameters of PbWO₄ crystals. *Physica Status Solidi (a)* **156,** 493–504.

Annenkov, A., Auffray, E., Fedorov, A., Gninenko, S., Golubev, N., Korzhik, M. V., Lecoq, P., Ligun, V., Lobko, A., Missevitch, O., Peigneux, J-P., Prokoshkin, Yu D. and Singovski, A. (1997) Radiation damage kinetics in PWO crystals. CERN, Geneva, CMS Note 1997/008.

Annenkov, A., Auffray, E., Baccaro, S., Cecilia, A., Dafinei, I., Diemoz, M., Jarolimek, O., Korzhik, M. V., Lecoq, P. and Nikl, M. (1998) Improvement of several properties of lead tungstate crystals with different doping ions. CERN, Geneva, CMS Note 1997/054. Submitted to *Nuclear Instrument Methods.* In press.

Auffray, E., Dafinei, I., Gautheron, F., Lafont-Puyet, O., Lecoq, P. and Schneegans, M. 1996. Scintillation characteristics and radiation hardness of PWO scintillators to be used at the CMS electromagnetic calorimeter at CERN. Proc. Int. Conf. on Inorganic Scintillators and Their Applications, SCINT'95. Eds. Dorenbos P and van Eijk C. p. 282. Delft University Press, Delft.

Besson, P., Bonamy, P., Bougamont, E., Chipaux, R., Géléoc, M., Gentit, F-X., Pansart, J-P., Rander, J., Rebourgeard, P. and Villet, G. 1997. How to rely the variations of calibration and transmission parameters in ageing scintillating crystals. Presented at SCINT'97 Int. Conf. on Inorganic Scintillators and Their Applications. 22–25 September. Shanghai, China.

CERN Report (1996) Experiments at CERN. CERN, Geneva (November 1996), p. 6.

Chipaux, R. and Toson, O. (1995) Resistance of lead tungstate and cerium fluoride to low rate gamma irradiation or fast neutrons exposure. CERN, Geneva, CMS Technical Note TN/95-126.

CMS (1994) CMS Technical Proposal. CERN/LHCC 94-38.

Ellens, A., Meijerink and G. Blasse (1994) The first observation of ^6I, ^8S emission from Eu^{2+} in $KMgF_3$. *Journal of Luminescence* **60/61,** 70–73.

Fyodorov, A., Korzhik, M. V., Missevitch, O., Pavlenko, V., Kachanov, V., Singovski, A., Annenkov, A. N., Ligun, V. A., Peigneux, J-P., Vialles, J-P., Faure, J. L. and Binon, F. (1996) Progress in $PbWO_4$ scintillating crystal. *Radiation Measurements* **26,** 107–115.

Galez, Ph. , Moreau, J. M., Peigneux, J-P. and Korzhik, M. V. (1996) Structural characterization of $PbWO_4$ and related new phase $Pb_7W_8O_{(32-x)}$. *Journal of Alloys and Compounds* **238,** 46–48.

Kobayshi, M., Usuki, Y., Ishii, M., Yazawa, T., Hara, K., Tanaka, M., Nikl, M., Baccaro, S., Cecilia, A., Diemoz, M. and Dafinei, I. (1998) KEK Preprint 97-12, May 1997. Improvement of radiation hardness of $PbWO_4$ scintillating crystals by ta doping. Submitted to *Nucl. Instr. Meth. A*.

Korzhik, M. V. (1990) Influence of the iron ions doping on the spectroscopic and laser properties of the crystals and glasses activated by rare-earth ions. Thesis, Minsk.

Korzhik, M. V., Drobyshev, G. Yu, Kondratiev, D. M., Borisevich, A. E., Pavlenko, V. B. and Timoschenko, T. N. (1996) Scintillation quenching in cerium-doped ytterbium based crystals. *Physica Status Solidi (b)* **197,** .

Lecoq, P., Dafinei, I., Auffray, E., Schneegans, M., Korzhik, M. V., Missevitch, O. V., Pavlenko, V. B., Fedorov, A. A., Annenkov, A. N., Kostylev, V. L. and Ligun, V. D. (1995) Nuclear Instruments and Methods in Physics Research **A365,** .

Saclay, Group (1996) The ECAL calibration: use of the light monitoring system. CERN, Geneva CMS Technical Note TN/96-036.

Ytterbium-based scintillators, a new class of inorganic scintillators for solar neutrino spectroscopy

R. Chipaux[a,*], M. Cribier[a], C. Dujardin[b], N. Garnier, N. Guerassimova[c,b], J. Mallet[a], J.-P. Meyer[a], C. Pédrini[b], A.G. Petrosyan[d,b]

[a] DAPNIA/SED, CEA-Saclay, F-91191 Gif sur Yvette Cedex, France
[b] LPCML, UCB Lyon 1, UMR 5620 CNRS, Domaine scientifique de La Doua, 69622 Villeurbanne, France
[c] Synchrotron Radiation Laboratory, Faculty of Physics, Moscow State University, Moscow 119899, Russia
[d] Institute for Physical Research, Armenian National Academy of Science, Ashtarak-2 378410, Armenia

Abstract

The observed deficit of the solar neutrino flux is now well established. This puzzling problem of today's particle physics could be resolved soon. The most likely explanation would be the vacuum neutrino oscillation phenomenon, indirectly proving the non-zero mass of these fleeting particles. Following the proposition of Raghavan of using ^{176}Yb as a target for low-energy solar neutrino spectroscopy, an intense R&D work has started a few years ago to define a suitable scintillator incorporating a large amount of ytterbium. Recently, the observation of UV scintillation in mixed yttrium/ytterbium aluminium garnets opened the field of investigation to a new class of scintillating crystals with interesting luminescence properties, very attractive not only for neutrino physics but also for radiation detection, in general. Their luminescence properties present some peculiarities that make them interesting by themselves. © 2002 Elsevier Science B.V. All rights reserved.

PACS: 78.60.−b; 29.40.Mc; 95.55.Vj

Keywords: Scintillators; Neutrino spectroscopy; Ytterbium garnets

1. Introduction

All present solar neutrino experiments confirm without doubt that the flux of electron neutrinos coming from the sun is very significantly lower than the predicted flux [1]. This is attributed to the change of flavour (i.e. an electron neutrino transforms itself into a muon neutrino or a tau neutrino during its way from Sun to Earth). The explanation of such effect, also called neutrino oscillations, implies a non-zero mass for these particles [2].

Large statistic experiments, like SuperKamiokande [3] and SNO [4], begin to give information on the parameters of neutrino oscillations in the high-energy part ($> 5\,MeV$). However, the low-energy part ($< 1\,MeV$) of the solar neutrino spectrum, which is also the most reliably predicted, should be more sensitive to these parameters. Fig. 1 shows, for example, how the different oscillation-allowed scenarios would be discriminated in a Yb-LENS potential experiment.

*Corresponding author. Tel.: +33-1-69-08-21-79; fax: +33-1-69-08-30-24.

E-mail address: chipaux@hep.saclay.cea.fr (R. Chipaux).
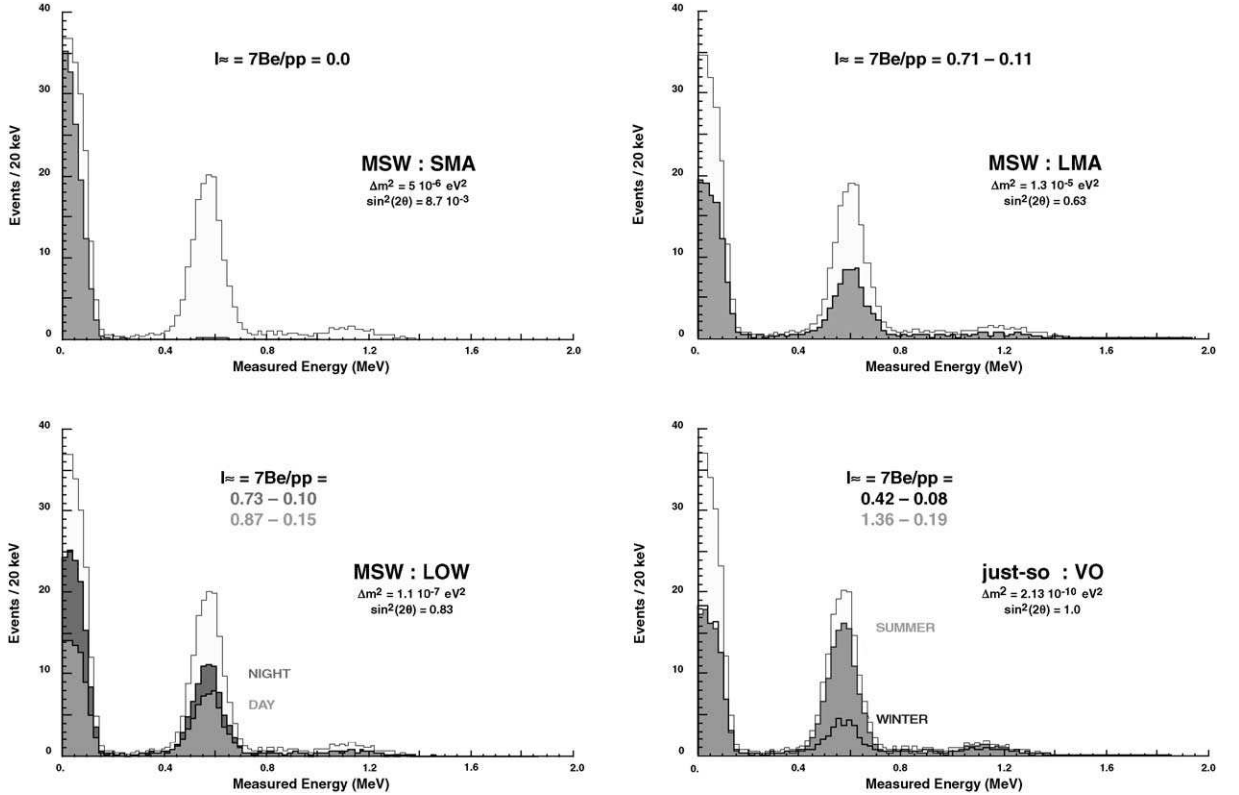
Fig. 1. Response of a potential Yb-LENS experiment to different solar neutrino oscillation scenarios.

The proposition of studying the low-energy part of the solar neutrino spectra by using specific interactions on selected nuclei [5] has received great interest and has given rise to the Low-Energy Neutrino Spectroscopy (LENS) collaboration [6].

2. LENS basis

2.1. Principle

The LENS detection principle is based on the detection of the neutrino interaction with a target nucleus that produces delayed nuclear decays, which can be used as a specific signature. As proposed by Raghavan [5], a few nuclei, namely ^{176}Yb, ^{160}Gd and ^{85}Se, meet the requirements: stable initial 0^+ state, neutrino capture producing $0^+ \rightarrow 1^+$ transitions to an excited state in the final nucleus with a low energy threshold. Excited

isomeric state decays to ground state in the 100 keV range with lifetimes within 100 ns. Fig. 2 shows the interaction scheme for ^{176}Yb. Interaction of an electron neutrino with this nucleus gives a prompt electron (or an electron immediately followed by a γ of 144 keV). The resulting nucleus, ^{176}Lu, is in an excited nuclear state, which emit a 72 keV γ in a mean lifetime of 50 ns. The energy of the neutrino is equal to the prompt electron energy plus the threshold (301 keV).

The purpose of the LENS collaboration is to develop a scintillator containing a suitable amount of one of these nuclei, to be used as an active target for neutrino spectroscopy. Se compounds have been withdrawn in for the first time, owing to the short lifetime (10.4 ns) and low energy of the γ-decay (29 keV), which would have required detection sensitivity clearly beyond those needed for Gd and Yb. Compared to Yb, Gd has the disadvantage to have 4 accessible levels for the neutrino interaction, making cross-section
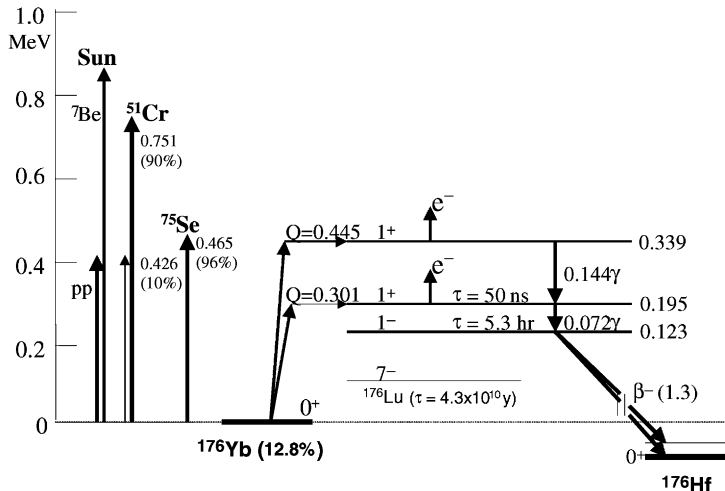
Fig. 2. $V_e - {}^{176}$Yb interaction scheme. Comparison with solar neutrino and ^{51}Cr/^{75}Se neutrino sources spectra (on left).

calibration much more complicated. It also includes a natural α-radioactive isotope, ^{152}Gd.

2.2. Constraints and specificity

One strong constraint is the low cross-section for the neutrino interaction. As estimated from Gamow–Teller matrix elements recent measurements [7], an overall mass of 20 tons of natural Yb (abundance of ^{176}Yb: 12.8%) is needed to obtain about one neutrino interaction per day.

Another constraint, deriving directly from this low event rate, is background. Considering neutrino signature, background is of three kinds.

2.2.1. Fortuitous coincidences

The rate depends on the contamination of the detector materials in radioactive elements, of the environment activity and is inversely proportional to the spatial resolution of the detector. It is lowered by purification of the materials, shielding and spatial resolution of the detector.

2.2.2. Correlated background

Nuclear decay cascades may have similar decay kinetics. This includes long-lived isotope like ^{235}U. Other nuclei can be produced by cosmogenic nuclear interactions. This is the case for ^{169}Yb, which will imply an underground cooling of about

2 years before use. A specific contaminant of Yb is Lu. ^{176}Lu, (2.6% of natural Lu), gives β decays followed by an 88 keV γ-emission of 2 ns mean lifetime.

2.2.3. False signature

A last background is due to statistical fluctuations of light pulses, which can, especially for low energy signals, mimic the signature. Discrimination algorithms are developed to recognize and exclude this false signature. However, considering the range of energy and the time characteristics addressed (below 1 MeV and 100 ns), this implies the use of a fast and efficient scintillator. This problem, added to the ^{152}Gd background, was the major reason for the withdrawal of GSO scintillator [8].

2.3. Developments

Beside the main LENS development of organic liquid scintillators charged in rare earth (Gd and Yb) [9], scintillating crystals are also considered. As mentioned above, GSO was studied for the first time and recently Yb-based scintillating crystals came on the stage.

3. Ytterbium inorganic scintillators

Until recently, it was considered that Yb was very unlikely to form inorganic fast scintillators (understood with Ce doping), because of charge transfer between Yb and Ce ($Yb^{3+} + Ce^{3+} \rightarrow Yb^{2+} + Ce^{4+}$).

The recent discovery of UV fast scintillation in yttrium–ytterbium aluminium garnets by Carugno et al. [10] reintroduced Yb-based crystals as potential scintillators for neutrino detection.

3.1. Aluminium garnets

We have undertaken investigation on the $(Y-Yb)_3Al_5O_{12}$ system. Detailed results are reported in Ref. [11]. These crystals exhibit a fast emission with a main peak at 330 nm and a less intense one at 500 nm. They have been attributed to transition from oxygen charge transfer state to, respectively, $^2F_{7/2}$ and $^2F_{5/2}$ Yb^{3+} states. The main feature of this emission is its variation of intensity with the temperature. As shown in Fig. 3, the UV-excited emission follows a classical temperature-quenched behaviour, whereas the X-ray-excited emission
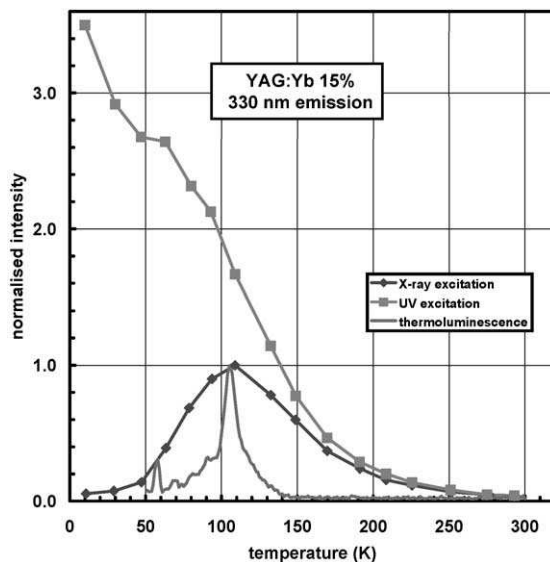

Fig. 3. 330 nm emission under UV (squares) and X-ray (diamonds) excitation and thermo-luminescence spectrum (line) of $Y_{2.75}Yb_{0.45}Al_5O_{12}$ as function of temperature (see Ref. [11]).
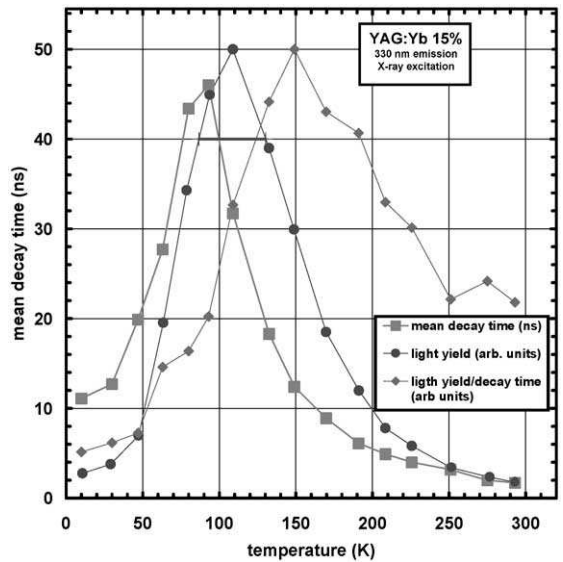
Fig. 4. Mean decay time (squares), intensity (circles) and ratio intensity/decay time (diamonds) of the 330 nm emission under X-ray excitation of $Y_{2.75}Yb_{0.45}Al_5O_{12}$ as function of temperature (see Ref. [11]).

goes through a maximum around 100 K. This maximum is correlated with thermoluminescence peak, leading to assume a trapping mechanism to explain the different variations with temperature.

As shown in Fig. 4, a maximum is correlatively observed in decay time. One should notice that the maxima of yield and decay time do not coincide. Taking the ratio of light yield versus decay time as a criterion, the optimal temperature would be around 150 K. However, a more detailed analysis of the decay components is needed.

The maximum of light emission is found for ytterbium concentration around 15% (i.e. $Y_{2.55}Yb_{0.45}Al_5O_{12}$) and is equivalent to almost four times the emission of bismuth germanate (BGO) (measured at room temperature) (Figs. 5 and 6). Crystals with ytterbium concentrations between 15% and 50% should be studied to be more conclusive.

The light decay properties seem to be less sensitive to the ytterbium concentration, as shown in Table 1. More detailed analysis of the decays as function of concentration and temperature are in progress.
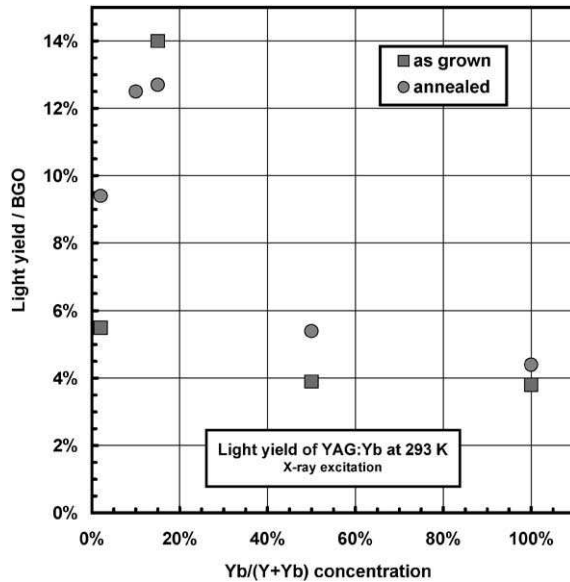
Fig. 5. Light yield of yttrium–ytterbium aluminium garnets at room temperature as function of ytterbium concentration, for single crystals as-grown and after annealing in air.
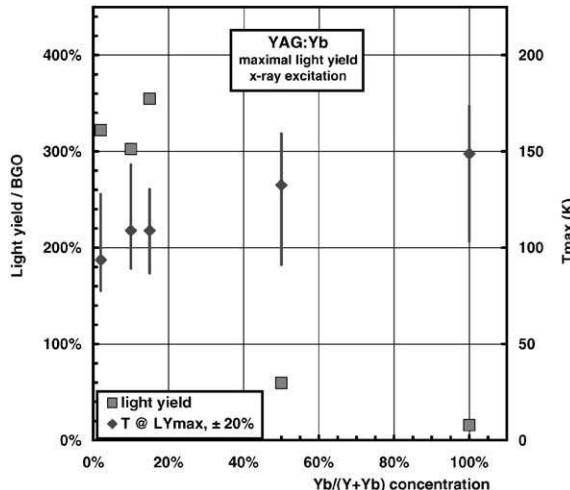

Fig. 6. Light yield of yttrium–ytterbium aluminium garnets at the temperature of maximal emission (squares) and temperature of maximal emission (diamonds) as function of ytterbium concentration, for single crystals after annealing in air. The vertical lines indicate the width at 80% of the maximum of the light emission as function of temperature.

Table 1
Light yield (Ly) and decay parameters of yttrium–ytterbium aluminium garnet single crystals after air annealing, at room temperature (fit by $I = I_1/\tau_1 \exp(\tau_1) + I_2/\tau_2 \exp(\tau_2)$)

| Crystal	Ly (%BGO)	I_1 (%)	τ_1 (ns)	I_2 (%)	τ_2 (ns)
YAG:Yb (2%)	9.4	74	1.8	26	15.5
YAG:Yb (10%)	12.5	71	1.7	29	19.0
YAG:Yb (15%)	12.7	67	1.6	33	17.0
YAG:Yb (50%)	5.4	71	1.5	29	13.0
YbAG	4.4	66	1.0	34	15.0
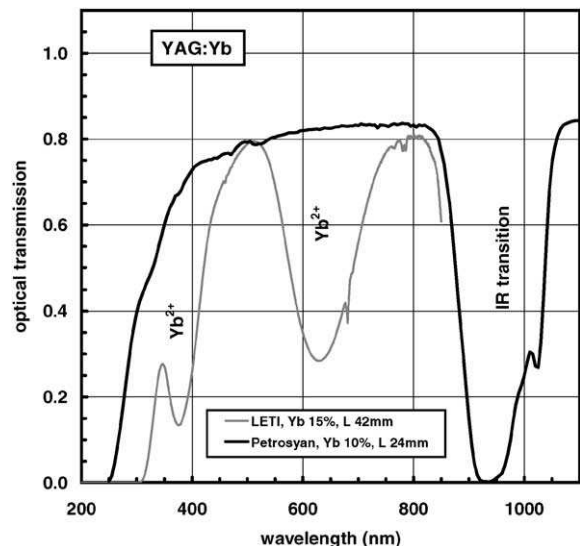
Fig. 7. Optical transmission of a 42 mm long YAG:Yb 15% crystal, as grown, and of a 24 mm long YAG:Yb 10% as function of wavelength, not corrected for surface reflections.

grown without special precaution (see Fig. 7) exhibit broad absorption bands at 280, 400 and 660 nm, which can be unambiguously attributed to Yb^{2+} [12]. Post-growth annealing in air improves the transparence properties of the materials, thus the light yield. However, an important absorption remains in the UV emission region, which should be reduced if one intends to use long crystals.

Further investigations are needed to determine if these crystals could satisfy the criteria for neutrino detection, and in that case what are the optimal Yb concentration and temperature. Other parameters could influence, notably the eventual $\alpha/e^-/\gamma$ pulse shape differences and the possibility to use the infrared emission for $\alpha/e^-/\gamma$ discrimi-

Growth and post-growth conditions appear to be crucial. The optical absorption in crystals is strongly influenced by the Yb^{2+} content. Crystals

Table 2
Light yield (Ly) (in % of BGO) and decay parameters (fit by $I = I_1/\tau_1 \exp(\tau_i) + I_2/\tau_2 \exp(\tau_2) + I_3/\tau_3 \exp(\tau_3)$, I_i in % and τ_i in ns) of ytterbium-containing compounds (in powder form)

	Ly	I_1	τ_1	I_2	τ_2	I_3	τ_3
$YAlO_3$:Yb (8%)	7.3						
$LaYbO_3$	1.6	62	0.53	38	16		
$Y_3Ga_5O_{12}$:Yb (2%)	24.8	9	1.1	41	7.8	50	50.4
$Y_3Ga_5O_{12}$:Yb (15%)	4.5	10	1.0	31	9.9	59	53.6
$Yb_3Ga_5O_{12}$	5.5	15	1.0	34	9.7	53	47.8

Table 3
Theoretical density (in g/cm^3) and radiation length (in cm) of some of the ytterbium compounds studied

	Density	Radiation length
YAG:Yb (15%)	4.86	2.57
YAG:Yb (50%)	5.57	2.12
$Yb_3Al_5O_{12}$ (YbAG)	6.62	1.50
$Yb_3Ga_5O_{12}$ (YbGG)	7.74	1.27
$Y_{0.85}Yb_{0.15}AlO_3$	5.78	2.27
$YbAlO_3$ (YbAP)	8.24	1.11
$LaYbO_3$	8.16	1.02

nation or to improve the energy resolution. This could obviously influence the radioactive purity constraints in an easier way.

3.2. Other ytterbium-based scintillators

Preliminary investigations on powder compounds have shown that Yb scintillation can also be found in other materials, such as the perovskites (Y–Yb)AlO_3 and $LaYbO_3$, or the garnets (Y–Yb)$_3Ga_5O_{12}$ [11]. Table 2 resumes the light yield and timing properties at room temperature of the studied compounds.

On the contrary, we did not observe any X-ray luminescence at room temperature nor at 77 K in Y_2SiO_5 doped with 10% Yb (single crystal).

4. Conclusion

The observation of UV scintillation in the ytterbium–yttrium aluminium garnet system has opened the field of a new class of inorganic scintillators based on ytterbium. They present interesting features, unusual dependency of luminescence on temperature and Yb-concentration. For particle detection they may be attractive, as fast and dense (see Table 3) scintillators with light yield competing with BGO – at least at low temperature – , and decay time in the range of 10 ns if not less. They may present an interesting alternative to organic scintillating liquids for the LENS detector, provided their properties could be optimized and purity requirements could be achieved.

References

[1] M.C. Gonzalez-Garcia, C. Peña-Garay, Nucl. Phys. B 91 (2001) 80.
[2] J.N. Bahcall, P.I. Krastev, A.Yu. Smirnov, Phys. Rev. D 58 (1998) 096016.
[3] S. Fukuda, et al., Phys. Rev. Lett. 86 (2001) 5651;
    S. Fukuda, et al., Phys. Rev. Lett. 86 (2001) 5656.
[4] A. McDonald, Nucl. Phys. B 77 (1999) 43;
    J. Boger, et al., Nucl. Instr. and Methods A 449 (2000) 172.
[5] R.S. Raghavan, Phys. Rev. Lett. 78 (1997) 3618.
[6] M. Cribier, Nucl. Phys. B 87 (2000) 195.
[7] M. Fujiwara, et al., Phys. Rev. Lett. 85 (2000) 4442;
    M. Bhattacharya, et al., Phys. Rev. Lett. 85 (2000) 4446.
[8] J. Lamblin, Reports ISN 99-105 and 99-108, unpublished.
[9] R.S. Raghavan, for the Lens Collaboration, Low energy neutrino spectroscopy (LENS), status and outlook, Report to the Scientific Committee, Gran Sasso National Laboratory, March 12, 2001, unpublished.
[10] G. Bressi, et al., Nucl. Instr. and Methods A 461 (2001) 361;
    P. Antonini, et al., Nucl. Instr. and Methods A 460 (2001) 469.
[11] N. Guerassimova, et al., Chem. Phys. Lett. 339 (2001) 197;
    N. Guerassimova, et al., Nucl. Instr. and Meth. A 486 (2002) 278, these proceedings.
[12] M. Henke, J. Persson, S. Kück, J. Lumin. 87–89 (2000) 1049.

Radiation hardness qualification of $PbWO_4$ scintillation crystals for the CMS Electromagnetic Calorimeter

Radiation hardness qualification of PbWO$_4$ scintillation crystals for the CMS Electromagnetic Calorimeter

The CMS Electromagnetic Calorimeter Group

P. Adzic,[v] N. Almeida,[r] D. Andelin,[ag] I. Anicin,[v,1] Z. Antunovic,[d] R. Arcidiacono,[p]
M.W. Arenton,[ag] E. Auffray,[w] S. Argiro,[p] A. Askew,[an] S. Baccaro,[o] S. Baffioni,[h]
M. Balazs,[ag] D. Bandurin,[ai] D. Barney,[w] L.M. Barone,[o] A. Bartoloni,[o] C. Baty,[i]
S. Beauceron,[w] K.W. Bell,[ac] C. Bernet,[h] M. Besancon,[g] B. Betev,[y] R. Beuselinck,[ad]
C. Biino,[p] J. Blaha,[i] P. Bloch,[w] A. Borisevitch,[b] A. Bornheim,[al] J. Bourotte,[h]
R.M. Brown,[ac] M. Buehler,[ag] P. Busson,[h] B. Camanzi,[ac] T. Camporesi,[ad] N. Cartiglia,[p]
F. Cavallari,[o] A. Cecilia,[o,2] P. Chang,[aa] Y.H. Chang,[z] C. Charlot,[h] E.A. Chen,[z]
W.T. Chen,[z] Z. Chen,[y] R. Chipaux,[g] B.C. Choudhary,[l] R.K. Choudhury,[m]
D.J.A. Cockerill,[ac] S. Conetti,[ag] S. Cooper,[aj] F. Cossutti,[q] B. Cox,[ag] D.G. Cussans,[ab]
I. Dafinei,[o,3] D.R. Da Silva Di Calafiori,[y] G. Daskalakis,[j] A. David,[r] K. Deiters,[x]
M. Dejardin,[g] A. De Benedetti,[aj] G. Della Ricca,[q] D. Del Re,[o] D. Denegri,[g]
P. Depasse,[i] J. Descamps,[g] M. Diemoz,[o] E. Di Marco,[o] G. Dissertori,[y] M. Dittmar,[y]
L. Djambazov,[y] M. Djordjevic,[v] L. Dobrzynski,[h] A. Dolgopolov,[aj] S. Drndarevic,[v,1]
G. Drobychev,[b] D. Dutta,[m] M. Dzelalija,[d] A. Elliott-Peisert,[w] H. El Mamouni,[i]
I. Evangelou,[k] B. Fabbro,[g] J.L. Faure,[g] J. Fay,[i] A. Fedorov,[b] F. Ferri,[g] D. Franci,[o]
G. Franzoni,[aj] K. Freudenreich,[y] W. Funk,[w] S. Ganjour,[g] S. Gascon,[i] M. Gataullin,[al]
F.X. Gentit,[g] A. Ghezzi,[n,w] A. Givernaud,[g] S. Gninenko,[s] A. Go,[z] B. Gobbo,[q]
N. Godinovic,[c] N. Golubev,[s] P. Govoni,[n] N. Grant,[ab] P. Gras,[g] M. Haguenauer,[h]
G. Hamel de Monchenault,[g] M. Hansen,[w] J. Haupt,[aj] H.F. Heath,[ab] B. Heltsley,[ah]
W. Hintz,[y] R. Hirosky,[ag] P.R. Hobson,[ae] A. Honma,[w] G.W.S. Hou,[aa] Y. Hsiung,[aa]
M. Huhtinen,[w] B. Ille,[i] Q. Ingram,[x] A. Inyakin,[aj] P. Jarry,[g] C. Jessop,[ak]
D. Jovanovic,[v,1] K. Kaadze,[ai] V. Kachanov,[u] S. Kailas,[m] S.K. Kataria,[m]
B.W. Kennedy,[ac] P. Kokkas,[k] T. Kolberg,[ak] M. Korjik,[b] N. Krasnikov,[s] D. Krpic,[v,1]

[1]Also at: Faculty of Physics of University of Belgrade, Belgrade, Serbia

[2]Now at: the Institut für Synchrotronstrahlung - ANKA, Forschungszentrum Karlsruhe, Germany

[3]Corresponding author.

Y. Kubota,^{aj} **C.M. Kuo,**^{z} **P. Kyberd,**^{ae} **A. Kyriakis,**^{j} **M. Lebeau,**^{w} **P. Lecomte,**^{y}
P. Lecoq,^{w} **A. Ledovskoy,**^{ag} **M. Lethuillier,**^{i} **S.W. Lin,**^{aa} **W. Lin,**^{z} **V. Litvine,**^{al} **E. Locci,**^{g}
E. Longo,^{o} **D. Loukas,**^{j} **P.D. Luckey,**^{y} **W. Lustermann,**^{y} **Y. Ma,**^{al} **M. Malberti,**^{n}
J. Malclès,^{g} **D. Maletic,**^{v} **N. Manthos,**^{k} **Y. Maravin,**^{ai} **C. Marchica,**^{x,y} **N. Marinelli,**^{ak}
A. Markou,^{j} **C. Markou,**^{j} **M. Marone,**^{p} **V. Matveev,**^{s} **C. Mavrommatis,**^{j} **P. Meridiani,**^{w}
P. Milenovic,^{v,y} **P. Miné,**^{h} **O. Missevitch,**^{b} **A.K. Mohanty,**^{m} **F. Moortgat,**^{y} **P. Musella,**^{r}
Y. Musienko,^{s,af} **A. Nardulli,**^{y} **J. Nash,**^{ad} **P. Nedelec,**^{f} **P. Negri,**^{n} **H.B. Newman,**^{al}
A. Nikitenko,^{ad} **F. Nessi-Tedaldi,**^{y} **M.M. Obertino,**^{p} **G. Organtini,**^{o} **T. Orimoto,**^{al}
M. Paganoni,^{n} **P. Paganini,**^{h} **A. Palma,**^{o} **L. Pant,**^{m} **A. Papadakis,**^{e} **I. Papadakis,**^{j}
I. Papadopoulos,^{k} **R. Paramatti,**^{o} **P. Parracho,**^{r} **N. Pastrone,**^{p} **J.R. Patterson,**^{ah}
F. Pauss,^{y} **J-P. Peigneux,**^{f} **E. Petrakou,**^{j} **D.G. Phillips II,**^{ag} **P. Piroué,**^{am} **F. Ptochos,**^{e}
I. Puljak,^{c} **A. Pullia,**^{n} **T. Punz,**^{y} **J. Puzovic,**^{v,1} **S. Ragazzi,**^{n} **S. Rahatlou,**^{o} **J. Rander,**^{g}
P.A. Razis,^{e} **N. Redaelli,**^{n} **D. Renker,**^{x} **S. Reucroft,**^{af} **P. Ribeiro,**^{r} **C. Rogan,**^{al}
M. Ronquest,^{ag} **A. Rosowsky,**^{g} **C. Rovelli,**^{o} **P. Rumerio,**^{w} **R. Rusack,**^{aj} **S.V. Rusakov,**^{t}
M.J. Ryan,^{ad} **L. Sala,**^{y} **R. Salerno,**^{n} **M. Schneegans,**^{f} **C. Seez,**^{ad} **P. Sharp,**^{w,ad}
C.H. Shepherd-Themistocleous,^{ac} **J.G. Shiu,**^{aa} **R.K. Shivpuri,**^{l} **P. Shukla,**^{m}
C. Siamitros,^{ae} **D. Sillou,**^{f} **J. Silva,**^{r} **P. Silva,**^{r} **A. Singovsky,**^{aj} **Y. Sirois,**^{h} **A. Sirunyan,**^{a}
V.J. Smith,^{ab} **F. Stöckli,**^{y} **J. Swain,**^{af} **T. Tabarelli de Fatis,**^{n} **M. Takahashi,**^{ad}
V. Tancini,^{n} **O. Teller,**^{w} **K. Theofilatos,**^{y} **C. Thiebaux,**^{h} **V. Timciuc,**^{al} **C. Timlin,**^{ad}
M. Titov,^{g} **A. Topkar,**^{m} **F.A. Triantis,**^{k} **S. Troshin,**^{u} **N. Tyurin,**^{u} **K. Ueno,**^{aa} **A. Uzunian,**^{u}
J. Varela,^{r,w} **P. Verrecchia,**^{g} **J. Veverka,**^{al} **T. Virdee,**^{w,ad} **M. Wang,**^{aa} **D. Wardrope,**^{ad}
M. Weber,^{y} **J. Weng,**^{y} **J.H. Williams,**^{ac,4} **Y. Yang,**^{al} **I. Yaselli,**^{ae} **R. Yohay,**^{ag} **A. Zabi,**^{h}
S. Zelepoukine,^{u,y} **J. Zhang,**^{aj} **L.Y. Zhang,**^{al} **K. Zhu**^{al} **and R.Y. Zhu**^{al}

^{a}*Yerevan Physics Institute, Yerevan, Armenia*

^{b}*Research Institute for Nuclear Problems, Minsk, Belarus*

^{c}*Technical University of Split, Split, Croatia*

^{d}*University of Split, Split, Croatia*

^{e}*University of Cyprus, Nicosia, Cyprus*

^{f}*Laboratoire d'Annecy-le-Vieux de Physique des Particules, IN2P3-CNRS, Annecy-le-Vieux, France*

^{g}*DSM/DAPNIA, CEA/Saclay, Gif-sur-Yvette, France*

^{h}*Laboratoire Leprince-Ringuet, Ecole Polytechnique, IN2P3-CNRS, Palaiseau, France*

^{i}*Institut de Physique Nucléaire de Lyon, Université Lyon 1, CNRS/IN2P3, Villeurbanne, France*

^{j}*Institute of Nuclear Physics "Demokritos", Aghia Paraskevi, Greece*

^{k}*University of Ioánnina, Ioánnina, Greece*

^{l}*University of Delhi, Delhi, India*

^{m}*Bhabha Atomic Research Centre, Mumbai, India*

^{n}*Istituto Nazionale di Fisica Nucleare e Università degli Studi di Milano Bicocca, Milano, Italy*

^{o}*Sapienza Università di Roma e Sezione dell'INFN, Roma, Italy*

^{p}*Università di Torino e Sezione dell'INFN, Torino, Italy*

---

^{4}Deceased

^{q}*Università di Trieste e Sezione dell'INFN, Trieste, Italy*

^{r}*Laboratório de Instrumentação e Física Experimental de Partículas, Lisboa, Portugal*

^{s}*Institute for Nuclear Research, Moscow, Russia*

^{t}*Lebedev Physical Institute, Moscow, Russia*

^{u}*IHEP, Protvino, Russia*

^{v}*Vinca Institute of Nuclear Sciences, Belgrade, Serbia*

^{w}*CERN, European Organisation for Nuclear Research, Geneva, Switzerland*

^{x}*Paul Scherrer Institut, Villigen, Switzerland*

^{y}*Institute for Particle Physics, ETH Zurich, Zurich, Switzerland*

^{z}*National Central University, Chung-Li, Taiwan*

^{aa}*National Taiwan University (NTU), Taipei, Taiwan*

^{ab}*University of Bristol, Bristol, United Kingdom*

^{ac}*Rutherford Appleton Laboratory, Didcot, United Kingdom*

^{ad}*Imperial College, University of London, London, United Kingdom*

^{ae}*Brunel University, Uxbridge, United Kingdom*

^{af}*Northeastern University, Boston, Massachusetts, U.S.A.*

^{ag}*University of Virginia, Charlottesville, Virginia, U.S.A.*

^{ah}*Cornell University, Ithaca, New York, U.S.A.*

^{ai}*Kansas State University, Manhattan, Kansas, U.S.A.*

^{aj}*University of Minnesota, Minneapolis, MN, U.S.A.*

^{ak}*University of Notre Dame, Notre Dame, IN, U.S.A.*

^{al}*California Institute of Technology, Pasadena, California, U.S.A.*

^{am}*Princeton University, Princeton, NJ, U.S.A.*

^{an}*Florida State University, Tallahassee, FL, U.S.A.*

E-mail: ioan.dafinei@roma1.infn.it

ABSTRACT: Ensuring the radiation hardness of $PbWO_4$ crystals was one of the main priorities during the construction of the electromagnetic calorimeter of the CMS experiment at CERN. The production on an industrial scale of radiation hard crystals and their certification over a period of several years represented a difficult challenge both for CMS and for the crystal suppliers. The present article reviews the related scientific and technological problems encountered.

Contents

Figure 1. ECAL layout.

1 Introduction

The Compact Muon Solenoid (CMS) [1] is a general purpose detector installed at the Large Hadron Collider (LHC) at CERN, Geneva. Detection and precise energy measurement of photons and electrons is a key to new physics that is expected at the 100 GeV-TeV scale. The discovery of the postulated Higgs boson is a primary goal at LHC and H → γγ is the most promising discovery channel if the mass is between 114 and 130 GeV. In this mass range the Higgs decay width is very narrow, but the signal will lie above an irreducible background and so good energy resolution is crucial. A photon energy resolution of 0.5% above 100 GeV has therefore been set as a requirement for the CMS performance.

The CMS experiment has opted [2] for a hermetic homogeneous electromagnetic calorimeter (ECAL), made of lead tungstate (PbWO$_4$) crystals. The choice of lead tungstate has been driven by operating conditions which require that the ECAL be fast and highly granular and be able to withstand radiation doses of up to 4 kGy and 4·10^{13} n/cm^2 in the Barrel and 25 times more in the Endcaps. These doses correspond to an integrated luminosity of 500 fb^{-1} expected to be accumulated over 10 years.

The ECAL layout is shown in figure 1. The high density of lead tungstate allows the design of a very compact detector. The region in space covered by a particle detector is usually described by pseudorapidity η, which is a spatial coordinate related to the angle of a particle relative to the beam axis. It is defined as:

$$\eta = -\ln\left[\tan\left(\frac{\Theta}{2}\right)\right] \tag{1.1}$$

where θ is the angle between the particle momentum and the beam axis. The ECAL consists of a Barrel, covering the pseudorapidity range $|\eta| < 1.479$, and two Endcaps which extend the coverage up to $|\eta| = 3$. There are 61200 crystals in the Barrel and 7324 crystals in each of two Endcaps, amounting to more than 91 metric tons of PbWO$_4$ crystals, with a total volume of approximately 11 m^3. The Barrel crystals are slightly tapered with dimensions about $24 \times 24 \times 230$ mm^3. The exact shape varies with the pseudorapidity, requiring 17 different geometrical types each one having two symmetries (left and right). Following dedicated studies aimed at optimizing the uniformity of the

light yield, one of the lateral faces of the Barrel crystals is semi-polished (roughness Ra $\sim$ 0.25 μm) while all other faces are optically polished (roughness Ra $<$ 0.02 μm). The Endcap crystals are less tapered, all identical in shape and have dimensions of about $30 \times 30 \times 220$ mm^3. All faces of Endcap crystals are optically polished (roughness Ra $<$ 0.02 μm).

The design energy resolution of CMS requires important properties of the PbWO$_4$ crystals, in particular:

- a large enough light yield (LY) to keep the stochastic contribution to the energy resolution small,

- a uniform longitudinal response to avoid a large constant term in the energy resolution at high energy, induced by the longitudinal fluctuations of electromagnetic showers.

These properties must be maintained in the high radiation field mentioned above. Furthermore, one should be able to track and correct for any radiation-induced changes in the light yield at the level of a few tenths of a percent. The aim of this paper is to present how these issues have been studied and solved by the CMS ECAL group in a way compatible with an unprecedentedly large industrial production. The paper is organized as follows: section 2 describes the radiation environment of ECAL. Section 3 presents the general properties of the lead tungstate scintillator with particular emphasis on its radiation hardness related properties. The experimental methods and tools used to characterize PbWO$_4$ crystals for CMS and related experimental results are presented in sections 4 and 5 respectively. Section 6 is dedicated to the monitoring of the light yield variation under irradiation conditions. Finally, section 7 describes the practical implementation of the quality assurance for the mass production for the two producers, Bogoroditsk Technochemical Plant (BTCP) in Russia and Shanghai Institute of Ceramics, Chinese Academy of Sciences (SICCAS) in China.

2 ECAL radiation environment

Operating at a peak luminosity of 10^{34} cm^{-2}s^{-1}, the LHC will produce a very harsh radiation environment for the detectors. The ECAL will be exposed to fast hadrons, mostly pions, which, in interactions with the ECAL itself, produce secondary hadrons, and build up a flux of low energy neutrons, with energies typically below 10 MeV. In addition, electromagnetic showers inside the crystals produce a significant dose.

No single quantity is sufficient to fully characterize this complex environment. A fairly complete picture can be obtained by looking at the absorbed gamma-irradiation dose, the neutron fluence and the charged hadron fluence. With respect to radiation damage, threshold behavior is often observed, i.e. only particles above a certain energy cause damage. These aspects will be discussed in detail in the sections 5.2 and 5.3 of this article, but it appears that low-energy ($<$ 20MeV) neutrons do not cause significant damage in the crystals. As for damage due to fast hadrons, it has been suggested [3] that it is better parametrized in terms of the density of their inelastic interactions than by the hadron fluence directly.

Therefore we introduce three quantities to characterize the environment:

- The absorbed dose
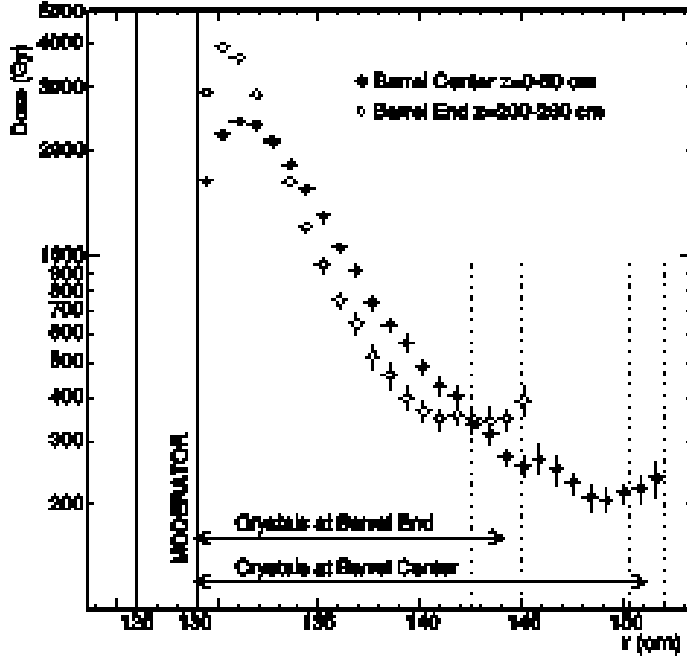
Figure 2. Absorbed dose as a function of radial distance from the beam axis in the center and at the ends of the Barrel ECAL [2]. Averaging has been performed over 60 cm in z, which causes the end of the crystal envelope to span the range indicated in the plot by the vertical dotted lines. Values are for $500\,\mathrm{fb}^{-1}$ integrated luminosity.

- The density of inelastic hadronic interactions (star density)

- The neutron fluence below 20 MeV

For consistency, the values are presented for an integrated luminosity of $500\,\mathrm{fb}^{-1}$, expected to be reached after 10 years, or $5\cdot10^7$ s operation at peak luminosity. Thus the average dose per hour at $10^{34}\,\mathrm{cm}^{-2}\mathrm{s}^{-1}$ will be $7.2\cdot10^{-5}$ of the 10-year integral. However, while the LHC is being filled and the beams accelerated there is no associated radiation, while during the subsequent collision period of typically 20 h duration, the luminosity will decrease by a factor of about 5 from its initial value. Thus there will be substantial short-term variations in the instantaneous dose rate.

Figure 2 shows the absorbed dose in the Barrel ECAL as a function of radial distance from the beam axis. It can be seen that the value varies by roughly an order of magnitude over the crystal length. Note that the data are plotted as a function of radius, not along the (tilted) crystal axis.

Figure 3 shows, as a function of pseudorapidity, the three radiation quantities we use to characterize the environment: absorbed dose, star density and neutron fluence. The solid symbols in figure 3 correspond to their average values along the crystal axis and the open symbols correspond to the maximum values. In the Barrel all three quantities are almost independent of η. Here the dose rate at shower maximum corresponds to 0.17–0.25 Gy/h at nominal LHC peak luminosity. However, in the Endcaps, the radiation levels increase rapidly with increasing η. The performance requirements are most stringent for the region below $|\eta| = 2.5$, which is the limit of coverage of the central tracking detector. This limit is indicated by the dotted vertical line in figure 3, where it can be seen that, at this value of η, the dose rate at shower maximum is 5 Gy/hr. An overall uncertainty
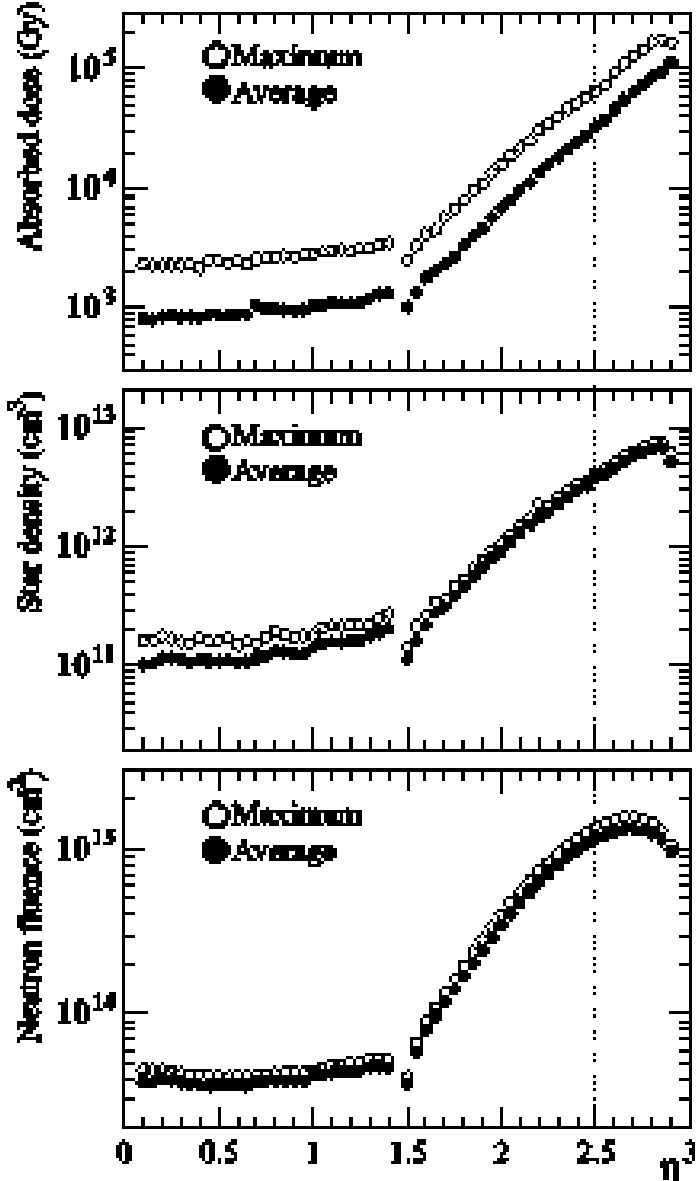
Figure 3. Radiation exposure of the ECAL as a function of η. The star densities are for interactions above 20 MeV hadron energy and neutron fluences comprise neutrons with energies between thermal and 20 MeV. The dotted vertical line indicates the limit of coverage of the CMS central tracker (see text). All values are for $500\,\text{fb}^{-1}$ integrated luminosity.

of about a factor of 2 should be assigned to the dose estimates, which are obtained from Monte Carlo simulations [2]. Such relatively large uncertainty is mainly linked to the approximate geometrical description of the detector and its component materials as well as to the limited precision of the physics simulation in FLUKA. The collision energy used in the simulation was 14 TeV and a cross-section of 80 mb, including diffractive events. The events were generated by DPMJET-II (FLUKA-2006) [2].

Table 1. Lead tungstate crystal properties.

ρ, g/cm^3	X$_0$, cm	Molière radius, cm	LY, ph/MeV	Temperature dependence of LY [11] %/$^\circ$K	τ_{sc}, ns (%)	λ_{em}, nm	Refractive indices [12] n$_o$/n$_e$
8.28	0.89	2.19	200	-1.98	5 (73%) 14 (23%) 110 (4%)	420	420nm: 2.360/2.240 600nm: 2.242/2.169

3 General properties of PbWO$_4$ scintillator

In order to meet the granularity and energy resolution requirements, CMS selected lead tungstate (PbWO$_4$) as the most suitable affordable scintillator for its electromagnetic calorimeter. This crystal combines a number of attractive properties, such as high density, fast luminescence, good radiation tolerance when properly optimized [4]–[10] and adequate light yield. Table 1 summarizes the main physical and optical properties of PbWO$_4$. The scintillation emission may be described as the sum of three exponential terms with the time constants (relative intensities) shown in column six of the table. Lead tungstate is bi-refringent; column eight gives values for the two refractive indices (ordinary, n$_o$ and extraordinary, n$_e$) at two wavelengths (420 nm and 600 nm).

Considerable efforts over many years were made to understand the properties and to optimize the performance of PbWO$_4$ for the demanding CMS specifications. The methods needed to grow large and colorless crystals, to suppress slow scintillation components and to reach good radiation tolerance levels were investigated. In addition the development of mass production technologies (crystal growth and mechanical processing) allowing this unprecedented production to be made with a high production yield was addressed with high priority. A review of this work and of PbWO$_4$ properties is given in [10]. A detailed description of the PbWO$_4$ growth method applied at SICCAS is given in [13].

3.1 Requirements of radiation resistance

All known crystal scintillators suffer from radiation damage. The most common damage is radiation-induced light absorption caused by the formation of color centers. The absorption coefficient is proportional to the density of color centers which in most cases is proportional to the concentration of defects and impurities pre-existent in the crystal. Radiation may also cause phosphorescence (afterglow), which leads to increased readout noise. Additional effects may include reduced scintillation light yield (damage to the scintillation mechanism) and a change in the light response uniformity (since the radiation dose profile is usually not uniform). Light output variation caused by radiation-induced absorption can be corrected by external light monitoring [1]. On the other hand, a variation of the scintillation mechanism or a strong non-uniformity of the light response cannot be monitored in situ. This sets therefore two major requirements for the CMS application:

the scintillation mechanism must not be affected by radiation and the density of radiation-induced color centers must be kept below a maximum level.

3.2 Nature of point defects and luminescence centers

The crystallographic structure of synthetic lead tungstate crystal has been determined by X-ray diffraction and identified as sheelite-type with tetragonal symmetry and space group $I4_1/a$. The parameters of the unit cell are $a = b = 5.456$, $c = 12.020$ Ångström. However a significant loss of lead during the crystal growth process is expected to induce a reorganization of the lattice with the majority of lead and oxygen related vacancies distributed in a sheelite-like superstructure with a slightly reduced symmetry (space group $P4^-$) and lattice constant values: a = b = 7.719, c = 12.018 Ångström [14]. In this structure the ordering of the vacancies is compensated by a distortion of the tungstate anionic polyhedra. However the existence of this superstructure has not been confirmed by neutron diffraction studies [15] nor by other dedicated X-ray diffraction studies [16]–[18]. Although the presence of an optimum of radiation resistance for crystals grown slightly off-stoechiometry seems to play in its favor, the cation vacancy ordering in a superstructure in $PbWO_4$ still remains a matter of discussion.

$PbWO_4$ crystals grown from purified raw materials (5N or 6N with Molybdenum contamination limited to a few ppm) have their scintillation and radiation damage properties completely dominated by cation and anion vacancies and not by impurities. The position of these vacancies, either as part of the scheelite-like structure or randomly distributed, may influence these properties.

It has been established in several studies (see [19] for detailed analysis and extended references) that the luminescence of $PbWO_4$ crystals is related to charge transfer transitions in the regular anionic molecular complex WO_4^{2-} and in similar tetrahedra but distorted by an oxygen vacancy WO_3. The charge state of these centers not being modified by gamma and charged particle irradiation (at least in the range of doses and dose rates expected at LHC) the scintillation properties of $PbWO_4$ (radio- and photo-luminescence spectra, decay time, intrinsic light yield) should remain unchanged in the LHC radiation environment.

3.3 Radiation damage mechanism and point-defect compensation by specific doping

When $PbWO_4$ crystals are exposed to ionizing radiation pre-existing point-structure defects may act as traps for electrons or holes. The resulting charged defects have discrete energy levels and optical transitions can be induced, absorbing part of the scintillation light during its transport to the photodetector. This is the well known mechanism of radiation-induced color centers, which is the main source of optical damage in lead tungstate at LHC. Ionizing radiation damage can be considered as a three step process consisting of:

- creation of hot electrons and holes from the interaction of high energy particles with the lattice

- free carrier separation during the thermalization (through strong coupling with lattice phonons) and diffusion process

- localisation of electrons and holes near lattice defects, to balance local charge

Up to five types of color centers have been identified in PbWO$_4$ with corresponding absorption bands at 350-400, 470, 520, 620 and 715 nm. Through detailed studies of EPR (electron paramagnetic resonance), TSL (thermo-stimulated luminescence), PSC (photo-stimulated conductivity) and TSC (thermo-stimulated conductivity) it was possible to identify the corresponding color centers as follows:

- 350–400 nm: WO$_3^{2-}$ di-electron center on a Frenkel defect resulting from an out-of-position oxygen atom

- 470 and 520 nm: several types of di-O$^-$ centers

- 620 nm: electron transfer from the valence band to the lead vacancy (V$_c$) related defect $O^-V_cO^-$ ground state

- 715nm: photo-ionization of the dimer center $(WO_3 + WO_3)^{2-}$

However, the induced absorption spectrum and relative intensity of these five bands strongly depend on the nature and density of pre-existing structural defects, which depend themselves on the crystal growth conditions. Undoped crystal grown from stoechiometric raw-material have an absorption spectrum with two dominating broad bands peaked near 380 and 620 nm.

The doping of PbWO$_4$ crystals by specified impurities such as La, Y, Nb at different stages of the growth process has been used for the production of CMS crystals to improve their radiation hardness. Indeed, pentavalent doping with niobium prevents the trapping of holes on oxygen near a lead vacancy by forcing oxygen leakage. Cation vacancies can be compensated by substituting stable trivalent ions for lead ions in the nearest co-ordination sphere around the defect. Different ions have been tried like Y^{3+}, La^{3+}, Lu^{3+}, Gd^{3+}, Al^{3+}. A very significant suppression of the electron/hole trapping processes is already observed for a doping concentration of the order of 100 ppm if the crystal stoechiometry is well controlled [5, 6, 10].

3.4 Kinetics of damage production and recovery

A parameter which characterises the change in optical properties induced by radiation exposure is the radiation-induced absorption coefficient (μ), defined as:

$$\mu = \frac{1}{L} \cdot \ln \frac{T_{init}}{T_{irr}} \tag{3.1}$$

where T$_{init}$ and T$_{irr}$ are respectively the values of the crystal transmission measured before and after irradiation and L is the length of the crystal along the measurement direction. For a given wavelength, the induced absorption coefficient is directly proportional to the total concentration of all color centers absorbing at this wavelength:

$$\mu \propto N = \sum_i N_i \tag{3.2}$$

At a given time, t, under continuous irradiation at a fixed dose rate S the radiation-induced absorption coefficient μ in the crystal results from the balance between the creation of color centers with damage constant d$_i$ (related to the cross section of free carrier capture by defects of type i) and

their destruction due to annealing at the detector operating temperature with a recovery rate ω_i. The process may be described by the following equation [20]:

$$\mu = \sum_i \frac{\mu_i^{sat} S}{S + \omega_i d_i} \left\{ 1 - \exp\left[-\left(\omega_i + \frac{S}{d_i} \right) t \right] \right\} \tag{3.3}$$

where μ_i^{sat} is the induced absorption coefficient at saturation due to defects of type i. After some time a dynamic equilibrium is reached, which is dose rate dependent as expressed by the first term of the equation (3.3). In general, it is less than the saturation level,

$$\mu^{sat} = \sum_i \mu_i^{sat} = \sum_i N_i \sigma_i \tag{3.4}$$

where N_i is the concentration of color centers of type i and σ_i is their photon absorption cross section.

In ECAL working conditions, each collision run will be followed by a refill period. Supposing a constant irradiation rate S for a time interval t_0 (during collision run), the recovery of the induced absorption during refill time will be described by the equation:

$$\mu = \sum_i \frac{\mu_i^{sat} S}{S + \omega_i d_i} \left\{ 1 - \exp\left[-\left(\omega_i + \frac{S}{d_i} \right) t_0 \right] \right\} \exp\left(-\omega_i (t - t_0) \right) \tag{3.5}$$

Under normal LHC operation conditions the dose rate will be such that the full defect saturation will never be reached, and the optical transmission of the crystals will oscillate around a point corresponding to a loss as compared to its initial value, which is less than a few percent except at large values of η in the Endcaps. In order for these oscillations to remain as small as possible so that one can monitor them at a reasonable frequency during the periods of beam and machine refill, crystals have been optimized for minimizing the contribution of fast recovery constants at room temperature (in the range of minutes). In some cases this has led to an increase of slow recovery centers (SICCAS crystals), in other cases to an increase of ultrafast recovering (microseconds) shallow traps (BTCP crystals), which are not harmful for the CMS detector operation. This optimization has been made for the centers absorbing in the domain of the scintillation emission spectrum, i.e. for the 350-400, 470, 520 nm centers and is not necessarily valid for red absorbing centers, which generally have a faster recovery constant. The 420 nm induced absorption recovery is well fitted with a double exponential with time constants of about 1 hour and 40 to 75 hours respectively. The infrared band however has a much faster recovery of about 8 minutes; this characteristic allows monitoring at long wavelengths to be used as a cross-check of the performance of the laser monitoring system.

4 Experimental methods, measurement equipment and parameters

The investigation of radiation damage mechanisms in PbWO$_4$ involved a large number of experts in different scientific domains and complex testing equipment in many locations. In order to build a complete picture of radiation effects in PbWO$_4$ it was necessary to study all possible sources of damage, namely electromagnetic (gammas and electrons), charged hadrons and neutrons. It was therefore mandatory to organize irradiation facilities able to cover a large range of doses and

dose rates for a detailed study of the crystal behavior in all possible conditions, even those with low probability, such as very high dose rates arising from accidental beam loss. Special care was taken to cross-check the dosimetry of irradiation facilities used for the certification of the mass production. The uniformity of dose through the volume of a crystal was of particular relevance. The irradiation facilities used by ECAL group are summarized in the appendix.

The crystal radiation damage behavior in ECAL CMS was assessed through a number of optical measurements, as described below.

4.1 Optical transmission and LY measurements

To compute the induced absorption parameter, μs one has to measure the optical transmission at different times during or after irradiation exposure. Standard optical transmission measurement of PbWO$_4$ crystals used in CMS comprised measurements made along the crystal length (longitudinal transmission, LT) and transversely (transverse transmission, TT) in the direction having both lateral faces optically polished. A number of purpose built or commercial spectrophotometers were used in different laboratories. In most of the cases these were double beam spectrophotometers with 2 nm wavelength resolution or better. Scans were usually performed with a step of 5 to 10 nm and the transmission measurement precision was typically about 1%. During the ECAL production, transmission and LY measurements were performed with automatic systems ACCOS [21] at CERN and ACCOR [22] at the Italian National Institute for Nuclear Physics (INFN). A second, simplified version of an ACCOR machine (only transmission measurements) was also used for the irradiation tests made at INFN. In addition, a dedicated spectrophotometer [23] was built at INFN for high precision measurements of the optical properties of PbWO$_4$ crystals (reflection, absorption, refractive index, surface quality and geometrical effects). The instrument was also used for high precision measurements of radiation-induced absorption coefficient in PbWO$_4$ crystals.

The LY is defined as the number of photoelectrons produced in a photomultiplier placed at the rear face of the crystal for 1 MeV of energy deposited (pe/MeV). A standard CMS measurement for crystals consisted of measuring the LY for 22 positions of the radioactive source along the crystal, starting 0.5 cm from the front face, in 1 cm steps. Measured LY values are the result of a fit procedures described in [21] and [24] for the two automatic machines ACCOS and ACCOR respectively. The LY value given in this work corresponds to the value calculated at 8 X_0 (7.5 cm from the front face) using the formula:

$$LY_{8X_0} = a + 7.5 \cdot b \tag{4.1}$$

where a and b are respectively the intercept and slope of the linear fit of 11 LY values starting from the front face of the crystal.

Studies of a number of PbWO$_4$ crystals have shown that LY and longitudinal transmission are strongly correlated [25]. As will be discussed in the next section, the scintillation mechanism is not affected by radiation. This characteristic implies a strong correlation between LY loss and the induced absorption coefficient at wavelengths close to the scintillation emission peak (400-450 nm), an essential condition for a reliable monitoring of the crystal yield with injected light pulses.

4.2 Scintillation spectrum analysis

Scintillation spectrum analysis allows investigation of the nature of light emission center(s) and the possible influence of radiation exposure [26]–[29]. In particular the photo-luminescence and radio-luminescence spectra were recorded over the whole temperature range from liquid helium temperature to 200°C, before and after irradiation with dedicated (purpose built) or commercial spectrofluorimeters such as the Perkin-ELMER LS 55 at CERN. In the case of radio-luminescence the crystal was excited by a pulsed X-ray source (Hitachi) or in a synchrotron radiation facility (Hasylab in Hamburg or LURE in Orsay).

4.3 Decay time measurement

Another technique used in the study of radiation-induced traps was investigation of the decay time of the different emission centers as a function of temperature before and at different times after irradiation. Usually these tests were performed in parallel with those mentioned in paragraph 4.1 above. The setup was based on the single delayed photon counting method originated by Bollinger and Thomas [30].

4.4 Other analytical methods

In addition to the optical characterization of crystal defects, which was done systematically in the early stage of the R&D, and also on a sampling basis during all the production period, a number of other analytical methods were used such as X-ray diffraction, GDMS (Glow Discharge Mass Spectroscopy), ENDOR (Electron-Nuclear Double Resonance) spectroscopy, SEM (Scanning Electron Microscopy), ESR (Electron Spin Resonance), EPR (Electron Paramagnetic Resonance), TSL (Thermo-Stimulated Luminescence), TSC (Thermo-stimulated Conductivity) and PSC (Photo-stimulated Conductivity).

5 Radiation damage effects in PbWO$_4$ crystals

5.1 Radiation damage effects under gamma irradiation

A key point in the studies of PbWO$_4$ radiation damage mechanisms is to verify that the scintillation mechanism is not modified by the radiation (see section 3.1). This was shown in early work on PbWO$_4$ [11, 26, 27] and further studied by detailed analysis of the light emission centers. Figure 4 shows a comparison of the radio-luminescence (X-ray excited) spectra measured before and after 1 kGy (350Gy/h) gamma irradiation for a PbWO$_4$ crystal of the standard ECAL production. The shape of the luminescence spectrum is not changed by the gamma irradiation, indicating no damage to the scintillation mechanism.

In order to study the nature and relative concentration of gamma radiation-induced color centers, three types of transmission spectra were found to be useful as a means of classification [27]. In addition research was carried out aimed at establishing the microscopic origin of radiation damage in PbWO$_4$ (nature and properties of related color centers) and finding ways to improve the crystals radiation hardness [31]–[41]. Reliable certification procedures for crystals produced on an industrial scale for ECAL were defined on the basis of this R&D activity.
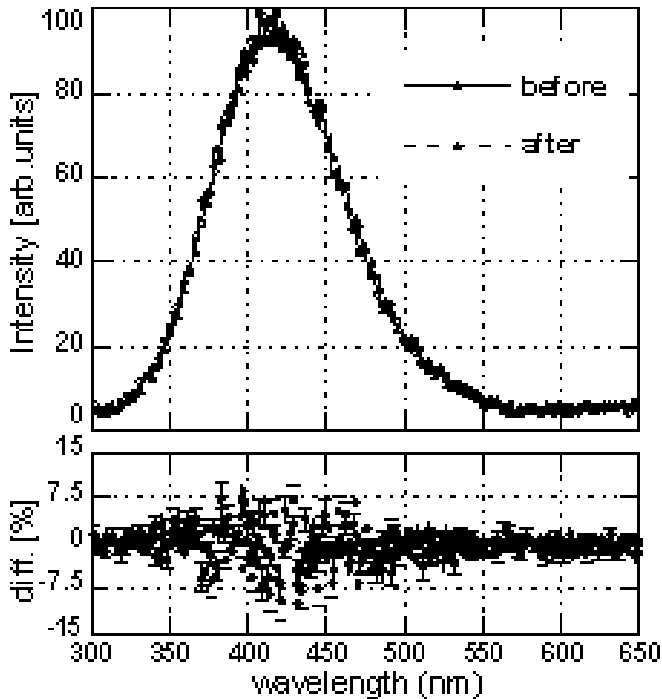
Figure 4. Above: radio-luminescence (X-ray excited) spectrum of PbWO$_4$ crystal before and after gamma radiation exposure (1 kGy at 350 Gy/h). Below: the difference between the two measurements.

A large number of radiation hardness tests were performed on different production crystals. Unless otherwise stated, the results reported here employed lateral irradiation (simultaneous irradiation of the full length of the crystal from the side) with a ^{60}Co source. These tests showed that radiation-induced color centers are always the same. Only their relative concentration and their distribution along the crystal growth axis may differ depending on the raw material characteristics (stoechiometry and possible doping), crystal growth conditions and post-growth thermal treatments. All these production parameters were different for the two crystal suppliers, BTCP and SICCAS. Nevertheless dedicated production protocols and certification procedures were defined at both producers in order to have similar radiation hardness characteristics of the crystals. Figure 5 shows typical absorption coefficient (μ_{LT}) induced by gamma radiation, measured along the length of the crystal, in randomly selected production crystals. The similar shape of the absorption spectra is an indication of the similar nature of the absorption centers, no matter the growth technology applied. The dispersion of absorption spectra is fully understandable given the industrial scale of the production and the relatively large size of the crystals.

Figure 6 shows the value of the induced absorption coefficient μ_{TT} at 420 nm measured transversely at different points along the growth axis of the crystals. The different variation of color centers along the crystal growth axis due to different growth technique (Czochralski at BTCP, Bridgman at SICCAS) may be noted. The increase in color centers in Bridgman-grown crystals along the axis is compensated by appropriate cutting of the ingot such that the front region of the crystal (most exposed to irradiation in LHC conditions) has the lowest concentration of color centers (highest radiation hardness).
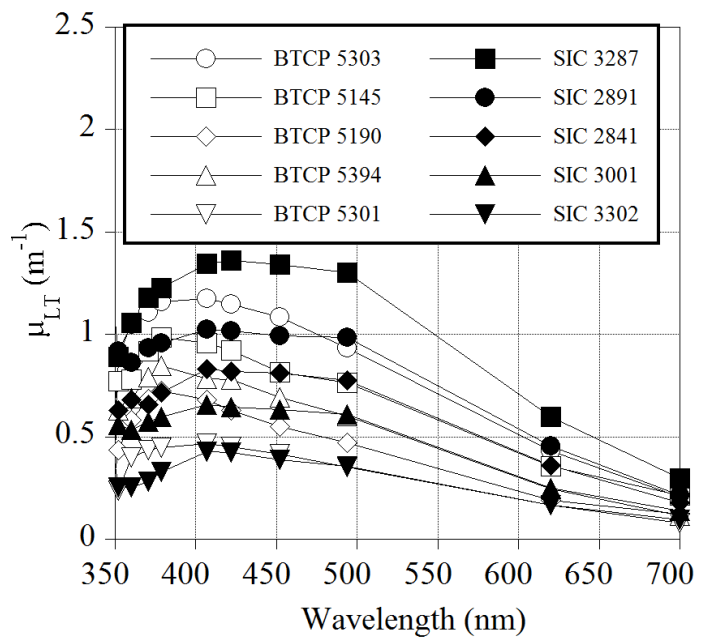
Figure 5. Radiation-induced absorption coefficient as a function of wavelength measured over the length of a crystal on randomly selected production crystals. Results were obtained after a total dose of 350 Gy, at a dose rate of 350 Gy/h. Open and solid symbols refer to BTCP and SICCAS crystals respectively.
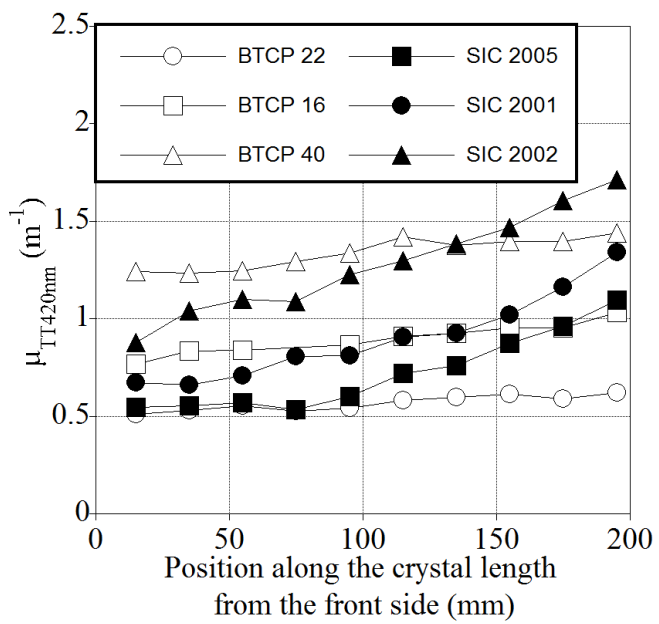
Figure 6. Radiation induced absorption coefficient at 420 nm measured transversely at different points along the growth axis of randomly selected production crystals. Results were obtained after a total dose of 350 Gy, at a dose rate of 350 Gy/h. Open and solid symbols refer to BTCP and SICCAS crystals respectively.
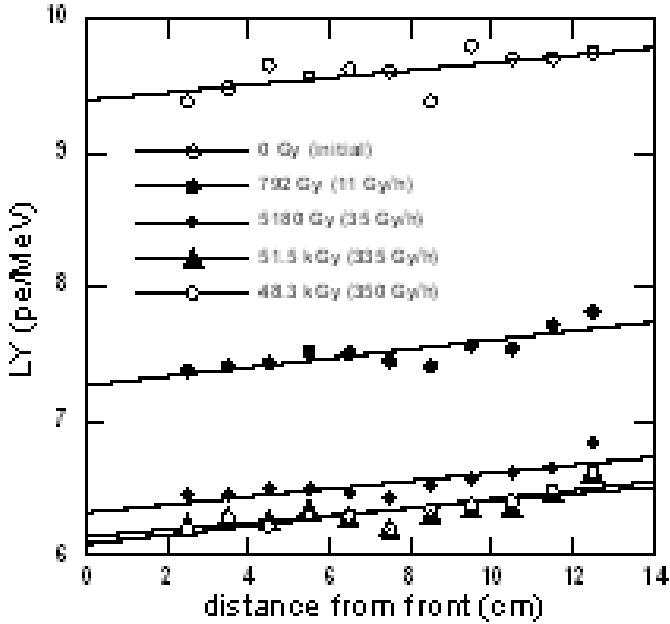
Figure 7. Light yield uniformity measured under equilibrium conditions for different gamma radiation doses for a randomly selected production crystal. The lines are linear fits to the data.

Studying the distribution of the damage along the growth axis may give valuable information to the crystal grower such as the distribution of defects responsible for color center production with respect to the seed position, stability of growth conditions and quality of the raw material.

Figure 7 shows the typical LY uniformity behavior under gamma irradiation of production crystals. The measurement was made using a collimated source positioned at different points along crystal. Measurement was made after reaching the equilibrium of induced absorption, with dose rates of 11 Gy/h, 35 Gy/h, 335 Gy/h and 350 Gy/h. Linear fits show that, within measurement errors, the slope of the LY uniformity, 0.03 pe/MeV/cm is not changed under gamma ray dose rates up to 350 Gy/h and integrated doses of several tens of kGy.

Based upon such studies and on Monte Carlo simulations of the effect of optical absorption on energy resolution, the maximum acceptable value of the induced absorption coefficient μ_{LT} at saturation was set at 1.5 m^{-1} for BTCP crystals and 1.6 m^{-1} for SICCAS crystals at the peak emission wavelength (420nm), which corresponds to a light yield loss of approximately 6% (see also section 6 and refs. [42, 43]).

Radiation-induced color centers anneal at room temperature, leading to spontaneous recovery of radiation damage. Figure 8 shows an example of spontaneous recovery at room temperature.

In common with other scintillating crystals, thermal annealing and optical bleaching were found effective in removing radiation-induced absorption in PbWO$_4$ crystals [28]. Thermal annealing at 200°C for two hours was found to be effective in removing all residual color centers, and was used as a standard procedure for restoring crystals to their initial condition following gamma irradiation.
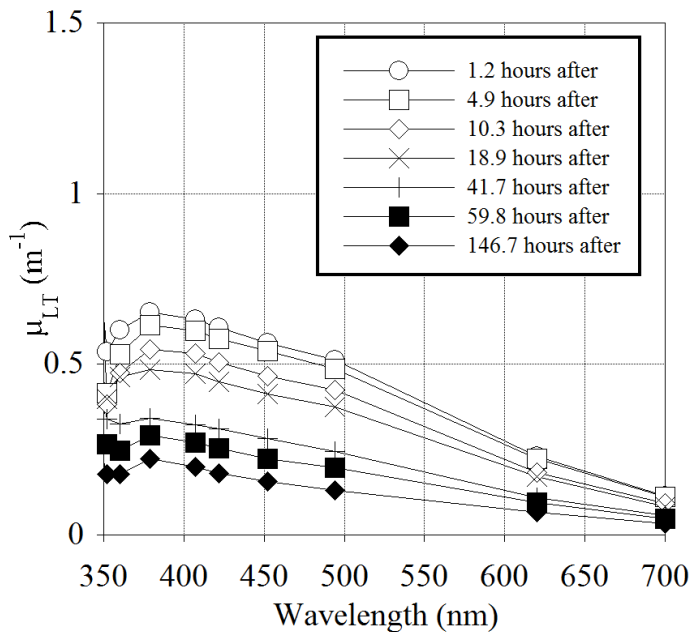
Figure 8. Induced absorption coefficient in a crystal measured at different time after gamma irradiation at a rate of 350 Gy/h for 1 h. Recovery in the dark at room temperature (20°C).

5.1.1 Dose rate dependence and low dose rate irradiation effects

The kinetics of color center creation under ionizing radiation and spontaneous annealing at room temperature may be described by simple models [19, 39], valid in the case of a low concentration of crystal defects. Such simple models lead to a two exponential time dependence of the concentration of color centers (i.e. of the induced absorption coefficient). Different studies on the interplay between gamma radiation damage and its recovery confirmed that the radiation-induced color center density depends on the dose rate. For a given dose a constant level is reached corresponding to the equilibrium between damage and recovery processes. Beyond a given dose rate and accumulated dose the induced absorption saturates corresponding to the full saturation of defects. Figure 9 shows degradation of the longitudinal transmission of a production crystal for different gamma dose rates. Longitudinal transmission spectra were measured when the radiation damage reached equilibrium for a given dose rate.

Using longitudinal transmission data, e.g. figure 9, numerical values of radiation-induced absorption coefficients (related to the radiation-induced color center density) can be calculated. The shape of the induced absorption as a function of wavelength is the same for all crystals, indicating an identical nature of the radiation damage as shown by several studies [4-10, 29, 44].

The radiation dose in CMS will not add significantly to the number of point defects acting as color centers [45]. The main source of deep traps in $PbWO_4$ crystals are pre-existing oxygen related Frenkel defects and cation vacancies. However, synthetic lead tungstate crystals also contain shallow electron traps associated with oxygen vacancies. The long duration of the crystal irradiation creates conditions for the diffusion of the neutral shallow electronic traps significantly increasing the probability of their coupling in pairs and more complex defects. Pairs have deeper
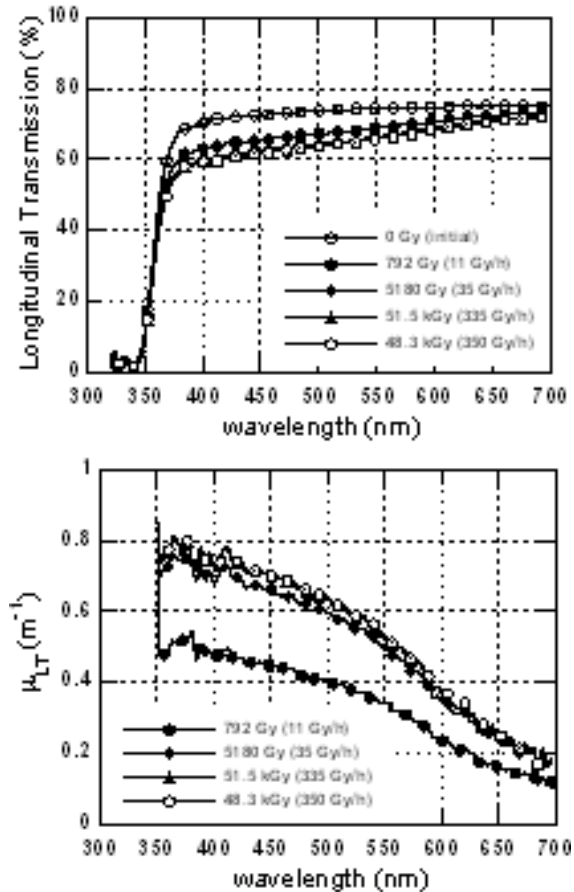
Figure 9. Longitudinal transmission and corresponding equilibrium values for the induced absorption coefficient for a production crystal exposed to gamma irradiation. The measured transmission is not corrected for reflection at crystal faces. The crystals were thermally annealed before each irradiation cycle.

capture levels compared to single vacancies and can create metastable color centers increasing the optical absorption in the visible spectral region under ionizing radiation. The presence of such metastable color centers may explain the slow decrease of the crystal transmission (and consequently of measured light yield) and the existence of a dynamic saturation (equilibrium between damage and recovery) whose level depends on the radiation dose rate.

The characteristics of point defects responsible for color centre creation are also discussed in [37]. The parameters of trap levels responsible for the thermal bleaching of color centers are measured and the kinetics of the bleaching process is explained in the frame of a model which takes into account the annihilation of electron and hole centers by tunneling. The model clarifies the existence of the very slow recovery component which cannot be explained by simple thermal annealing.

Figure 10 shows the measured relative LY (normalized to the initial value, $LY_{rel}=LY/LY_{init}$) as a function of time under lateral gamma irradiation for a production crystal subjected to increasing dose rates of 11 Gy/h, 35 Gy/h, 335 Gy/h and 350 Gy/h. The radiation exposure continued at a given dose rate till the equilibrium condition of the induced absorption coefficient was reached,
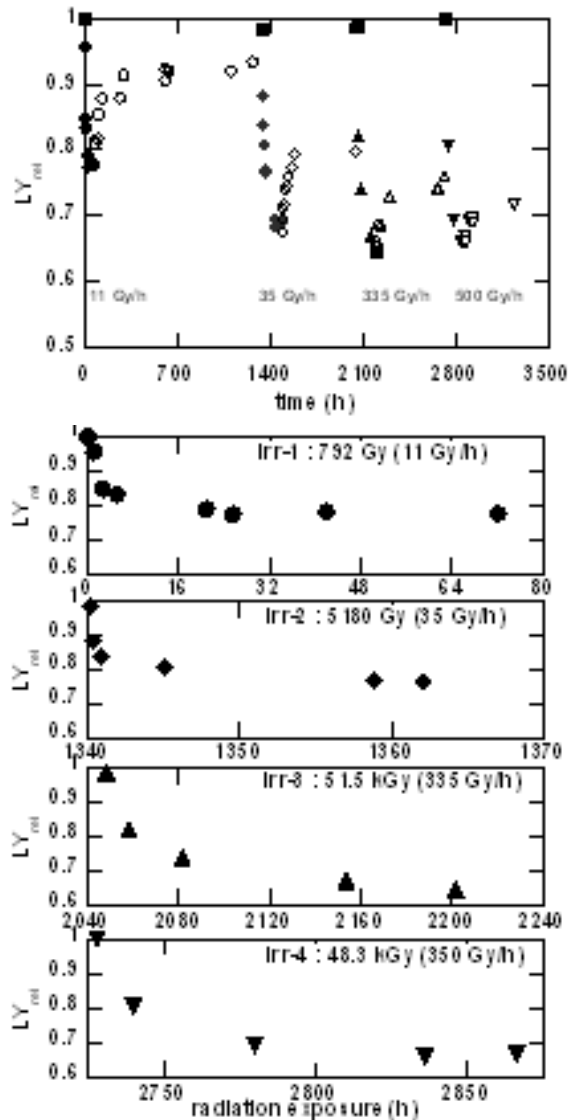
Figure 10. Variation of light yield during gamma irradiation (solid symbols) and successive room temperature recovery (open symbols) of a production crystal (note different time scales of zoomed plots). Solid black squares are the values measured after the thermal annealing made before each irradiation cycle.

after which the recovery of damage at room temperature was observed for several hours. The saturation effect is better seen on the right side of the figure where different time scales are used for each irradiation step. Crystals were thermally annealed before each irradiation cycle. As seen in the figure, the LY degradation shows a clear dose rate dependence and, as for the induced absorption coefficient, different equilibrium values are reached for each radiation dose. Similar tests made on production crystals exposed at the dose rate expected for the CMS Barrel calorimeter in situ at LHC (0.15 Gy/h) showed a loss of the LY of less than 6% (see also section 7). Series production crystals exposed to LHC-like radiation conditions (front irradiation) presented a light yield loss below the CMS specification limit of 6% [42, 43]. The light yield of crystals from both suppliers
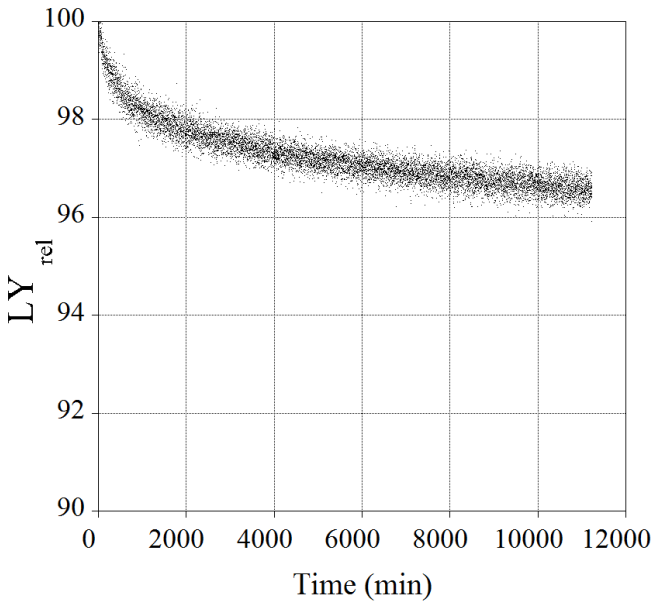
Figure 11. Relative LY (LY$_{rel}$) is shown as a function of time for a production crystal under front irradiation with a dose rate of 0.15 Gy/h. The spread of measured values indicates the reproducibility of the measurements, which is better than 1%.

shows similar dose rate dependent damage.

Figure 11 shows crystal light yield variation measured under front irradiation described in [46] at a dose rate of 0.15 Gy/h. Crystals were irradiated for more than one month ($5 \cdot 10^4$ min) and a correction of the data for the irradiation source decay has been applied. The continuing decrease in light yield at long irradiation times can be attributed to the formation of a second type of color center which reaches equilibrium more slowly, as mentioned above

5.2 Radiation damage effects under neutron irradiation

In view of the intense neutron flux expected in CMS (see section 2) the effects on lead tungstate of neutron exposure were studied in nuclear reactors [47, 48]. The neutron fluxes and energies in these exposures were comparable to those expected in CMS. However, in reactors there is a strong associated gamma dose. The effect arising from neutrons was estimated by comparing the reactor results with results obtained from pure gamma irradiations. This indicated that there was no specific effect due to neutrons on the optical and scintillating properties of lead tungstate, at least up to fluences of 10^{14} cm^{-2}. This was confirmed by later independent studies [49]. It is also to be mentioned that recent tests performed at a very high fluence, of the order of 10^{19} to 10^{20} n·cm^{-2} and 330 MGy (i.e. well above the level that will be ever achieved in any physics experiment) revealed the robustness of lead tungstate crystals which were not destroyed nor locally vitrified, and remained scintillating after such heavy irradiation [50].

5.3 Radiation damage effects due to fast hadrons

In CMS the flux of fast hadrons is dominated by charged pions with energies of order 1 GeV. The effect of charged hadrons on crystals has been the subject of an extensive series of measurements, whose results are presented in refs. [3, 51, 52]. Those studies show that hadrons cause a specific, cumulative loss of light transmission in the crystals [3]. The data for absorption induced by charged hadrons versus wavelength exhibit a λ^{-4} dependence, unlike those for damage from γ-irradiations. As explained in [3], this is an indication of Rayleigh scattering from small centers of severe damage, as might be caused by the high energy deposition, along their path, of heavily ionizing fragments, locally generating extended defects in the crystal. Since the crystal contains heavy elements, fast-hadron specific damage is in fact expected from the production, above a $\sim$20 MeV threshold, of heavy fragments with up to 10 μm range and energies up to $\sim$100 MeV, causing a displacement of lattice atoms and energy losses along their path, up to 50000 times that of minimum-ionizing particles.

Apart from the effect on light transmission, no fast-hadron specific damage to the scintillation mechanism was observed within the accuracy of the measurements and for the explored flux and fluence ranges. This is evident from the correlations between LY loss and induced absorption, which show similar behavior for proton and gamma irradiated crystals [51].

The studies published in [3] and [51] were all performed with 20 GeV/c protons, thus leaving open the question how they should be rescaled to the much softer spectrum of pions expected in CMS at the LHC. This issue was studied in [52], where the damage from protons and from 290 MeV/c pions is compared. There it is shown that the pion-to-proton ratio of induced absorption coefficients is in agreement with the corresponding ratio of the density of inelastic interactions (stars) obtained from simulations. Thus, the average star densities expected in CMS at various values of pseudorapidity η, as given in figure 3 of section 2 and in [3] can be used, together with the observed damage as a function of proton fluence in [3], to extract an expectation for the damage as shown in figure 12.

However it should be pointed out that the induced absorption values used to obtain figure 12 were measured 150 days after irradiating the crystals, allowing the recovery of a damage component observed to have a time constant of 17.2 days [3]. With the data available in [3], the remaining damage could be fitted as a combination of stable damage (which is cumulative with fluence) and a recovering component with a time constant of 650 days. Thus the expectation for charged-hadron induced damage of figure 12 could change slightly if the recovery of the slow component were taken into account.

6 Monitoring of LY degradation and recovery under irradiation

To avoid a degradation in the energy resolution, changes in the LY due to radiation induced absorption must be monitored during LHC operation. Variation of LY during irradiation exposure and spontaneous recovery cycles illustrated in figure 10 are caused only by color center formation and annihilation and can therefore be monitored by tracking the corresponding modification of the optical transmission of the crystal. The induced absorption coefficient follows the same evolution as can be seen in figure 13 where the time evolution of the induced absorption coefficient at 420
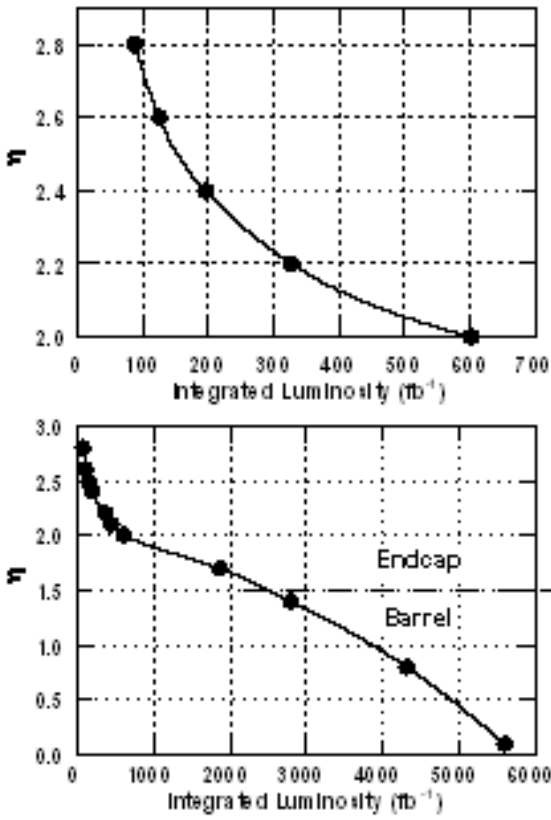
Figure 12. Values for η where an induced absorption coefficient $2\,\mathrm{m}^{-1}$ due to charged hadrons is anticipated at the scintillation emission peak wavelength, as a function of integrated luminosity. The lines through the data points are to guide the eye.

nm measured longitudinally for the same crystal for which the LY time evolution is reported in figure 10.

Figure 14 shows the correlation between the light yield and the longitudinal transmission at 420 nm for the data presented in figures 10 and 13. The strong correlation demonstrates that variations in light yield can be corrected for by monitoring the changes in longitudinal transmission in the region of the emission peak.

To take advantage of this correlation, a light monitoring system was designed and implemented [53]–[57]. This system was extensively used during high intensity tests in electron beams, showing that the energy resolution can be maintained by applying laser monitoring corrections under LHC-like conditions.

7   Crystal quality assurance during production

7.1   Crystal quality specification

It has been stressed throughout this paper that ensuring the radiation hardness of the crystals was of primary importance for CMS. Besides specifications related to dimension and optical properties needed for the required calorimeter performance, additional specifications for radiation hardness
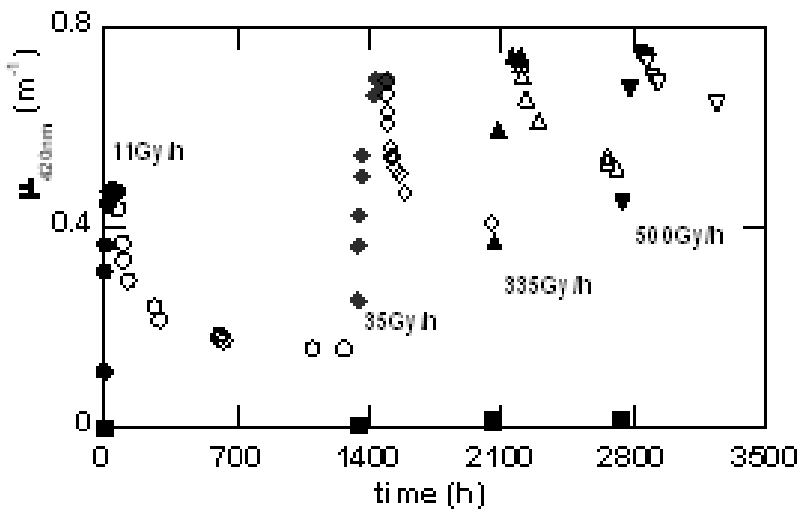
Figure 13. Time evolution of the induced absorption coefficient at 420 nm during gamma irradiation and successive room temperature recovery of a production crystal. Solid and open symbols correspond to irradiation and recovery respectively. Solid black squares are the values measured after thermal annealing.
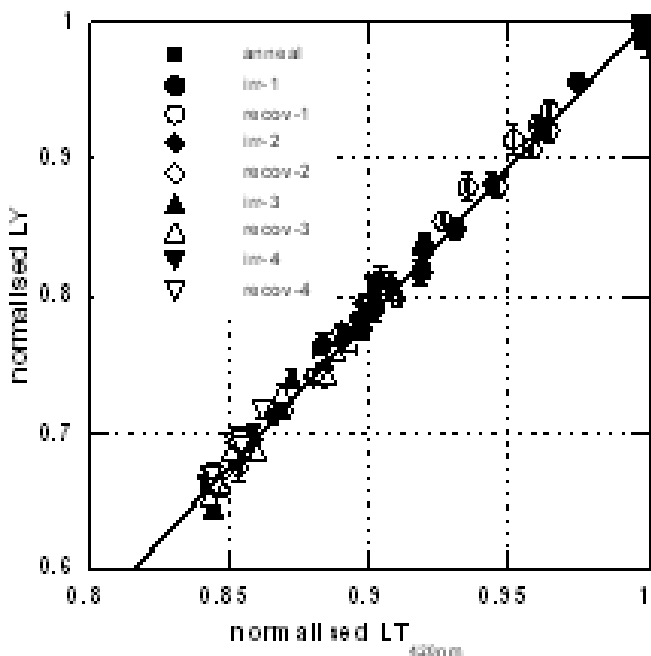
Figure 14. Correlation between normalised LY and normalized longitudinal transmission during several radiation exposure-recovery cycles, for a production crystal. The line is a linear fit.

were defined for crystals produced at both crystal suppliers. These specifications fixed the acceptable limit of optical transmission damage and related LY deterioration as follows.

1. induced absorption for full saturation of crystal: $\mu < 1.5$ m^{-1} at 420 nm; irradiation conditions: lateral ^{60}Co source exposure for a total dose > 500 Gy (> 100 Gy/h)
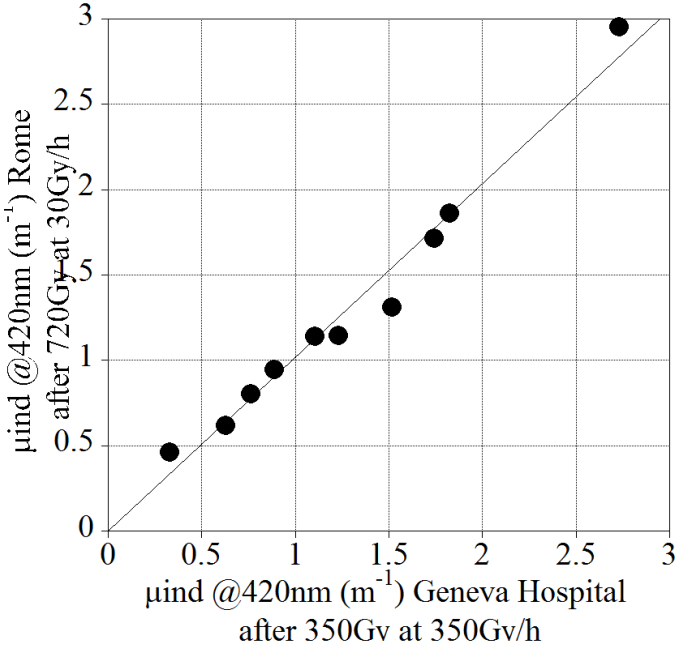
Figure 15. Correlation between irradiation tests results performed in CERN and Rome regional centers.

2. light yield loss: $LY_{loss} < 6\%$; irradiation conditions: front ^{60}Co source exposure for a total dose > 2 Gy $(> 0.15$ Gy/h$)$

The first specification was set up in order to prevent the total damage exceeding a certain level when the radiation damage in the crystal is fully saturated throughout its volume. This level corresponds to a defect density estimated to be $3 \cdot 10^{17}$ color centers per cm^3, corresponding to an induced absorption of 1.5 m^{-1} at the peak emission wavelength (420 nm) at full saturation. The limits imposed for irradiation conditions are the results of statistical studies made on production crystals showing that in general, the damage saturation is reached after a lateral gamma radiation exposure with a dose of at least 500 Gy at a rate above 10 Gy/h. The maximum value of 1.5 m^{-1} placed on the induced absorption at the emission wavelength also limits an associated variation in the longitudinal uniformity of light collection which could degrade the energy resolution of the calorimeter.

The second specification is related to LY loss due to gamma radiation exposure close to the LHC irradiation conditions (0.15 Gy/h at high luminosity at the region of shower maximum in the crystal, about 3 cm from the crystal front face). Statistical studies made on production crystals show that in the case of a front ^{60}Co source exposure at 0.15 Gy/h, the LY reaches a saturation level which is well above 94% of the initial value, i.e. a LY loss inferior to the 6% acceptance limit mentioned in section 5.1.

However, in the case of large scale production at BTCP it was not practical to check the radiation hardness of each crystal individually. Therefore studies were made during the R&D period to find correlations between radiation hardness behavior and optical parameters that can be measured easily for each crystal [42]. It was found that the presence of an initial absorption in the band edge region (350–360 nm) is correlated with poor radiation hardness [27]. Based on this correlation certification limits were defined for transmission spectra [42] which were systematically

measured for each crystal using the ACCOR and ACCOS machines. Transmission runs consisted in measuring the optical transmission along the crystal (beam direction from front face to rear face) and transversely at several points along the crystal length. Crystals having one of these optical certification parameters close to or above acceptance limits were subject to systematic irradiation tests. All other crystals were randomly irradiated in both regional centers either at high dose rate (350 Gy/h in Geneva hospital for the CERN regional centre or 30 Gy/h at the Calliope reactor for the Rome regional centre) or under conditions comparable to those in the LHC (0.15 Gy/h front irradiation with the low dose rate ^{60}Co source at the CERN regional centre). For high dose rates, the limiting value of 1.5 m^{-1} for the induced absorption at 420 nm was used as the qualification parameter. For low dose rates the light yield loss was measured directly and compared to the specification limit of 6% [42]. Crystals which did not fulfill these conditions were rejected. The reliability of these tests was checked on crystals subject to irradiation tests in both regional centers. Figure 15 shows the good correlation between the results of irradiation tests performed in the CERN and Rome regional centers.

The radiation hardness over the entire crystal production period (8 years for BTCP and 2 years for SICCAS crystals) was monitored through quality control procedures established for each of two suppliers as follows:

BTCP protocol: agreed between BTCP, INP-Minsk and CERN at the beginning of crystal production in 1998, was a three step radiation hardness certification protocol:

1. A sampling test of the radiation induced absorption performed at INP-Minsk on the top and bottom parts of ingots, aimed at controlling different technological aspects which influence the nature of crystal defects, the longitudinal distribution of the defects along the ingots, the damage recovery and the afterglow.

2. A sampling test performed at BTCP irradiation facilities on machined crystals. Crystals at BTCP were grown by Czochraski method. Several successive growths (crystallizations) were performed in a same crucible by adding new raw material at the end of each crystallization. Up to 13 qualified crystals could be grown by successive crystallizations from the same initial charge. Above this number the crystal quality started to deteriorate due to the increased concentration of impurities in the melt and the crucible was therefore emptied, cleaned and recharged for a new cycle. The selected crystals for radiation test were chosen among crystals coming from different crystallizations. Some crystals obtained from the first crystallization were selected to control the stoechiometry of the raw material, other crystals obtained from the 5th crystallization were chosen to control the doping concentration, and all crystals obtained from 9th to 13th crystallization were tested.

3. A sampling irradiation test under high or low irradiation rate performed at CERN. From each batch received, in addition to the crystals with optical certification parameters close or above acceptance limits mentioned above, a randomly chosen set of crystals was tested. Approximately 3% of the crystals produced at BTCP were subjected to this kind of test.

SICCAS Protocol: agreed between SICCAS and CERN was a two step radiation hardness certification protocol:

1. All crystals delivered by SICCAS were subject to an irradiation test at the producer consisting of 700 Gy irradiation exposure at a dose rate of 30 Gy/h. Crystals with a radiation induced absorption coefficient above 1.6 m^{-1} were rejected by the producer.

2. Crystals delivered to CERN were further subject to a sampling test performed in both regional centres (CERN and Rome) in order to check the coherence between induced absorption measured using CMS facilities and SICCAS facilities. In addition all crystals having an induced absorption value measured at SICCAS close to the specification limit were systematically irradiated at the Calliope irradiation plant in Rome.

The higher value of the limit of radiation induced absorption coefficient (1.6 m^{-1}) in the case of crystals produced at SICCAS is mainly due to their higher LY which makes the corresponding higher LY loss still acceptable for ECAL energy resolution constraints.

7.2 Certification of crystal mass production

Crystal production was completed in March 2007 for the Barrel and in March 2008 for the Endcaps. A total of 61335 Barrel crystals were produced in BTCP from September 1998 to March 2007 and 1825 at SICCAS from June 2005 to April 2007. Starting in March 2007, 12015 and 2668 Endcap crystals respectively were produced by the two suppliers.

7.2.1 Testing radiation damage at full saturation

Typical induced absorption spectra obtained for BTCP crystals and SICCAS crystals after high dose rate irradiation have already been shown in figure 5. Figure 16 shows the distribution of induced absorption measured at 420 nm after irradiation in a Geneva Cantonal Hospital (at a high dose rate of 350 Gy/h for an integrated dose of 350Gy) for a random sampling of BTCP Barrel and Endcap crystals in the frame of the point 3 of the "BTCP_Protocol". For all crystals subject to this test, the certification status (accepted or rejected) remained unchanged. The smaller dispersion in the case of the Endcap crystals is related to the learning curve in such a large production where the quality improves with time (Endcap crystals were produced after Barrel crystals). Furthermore, knowing that Endcap crystals will be more exposed to radiation, the production conditions were improved, particularly for what concerns the maximum number of crystallizations allowed from the same melt.

Figure 17 shows the correlation between the induced absorption obtained in the ECAL regional centers and at SICCAS for the Barrel and the Endcap crystals. For both producers, for all the crystals tested, an average value of about 1m^{-1} for the induced absorption at full saturation of the damage was obtained.

The spread of the correlation between the induced absorption measured at SICCAS and in ECAL regional centers (figure 17) is mainly due to the fact that irradiations at SICCAS were done at an industrial site where environmental conditions (and therefore recovery after irradiation) were difficult to control. This is also the reason for which all crystals having values μ_{LT} SICCAS > 1 m^{-1} were systematically subject to a supplementary irradiation test in ECAL regional centers (hence the larger statistics in the plot for large values of the induced absorption coefficient).
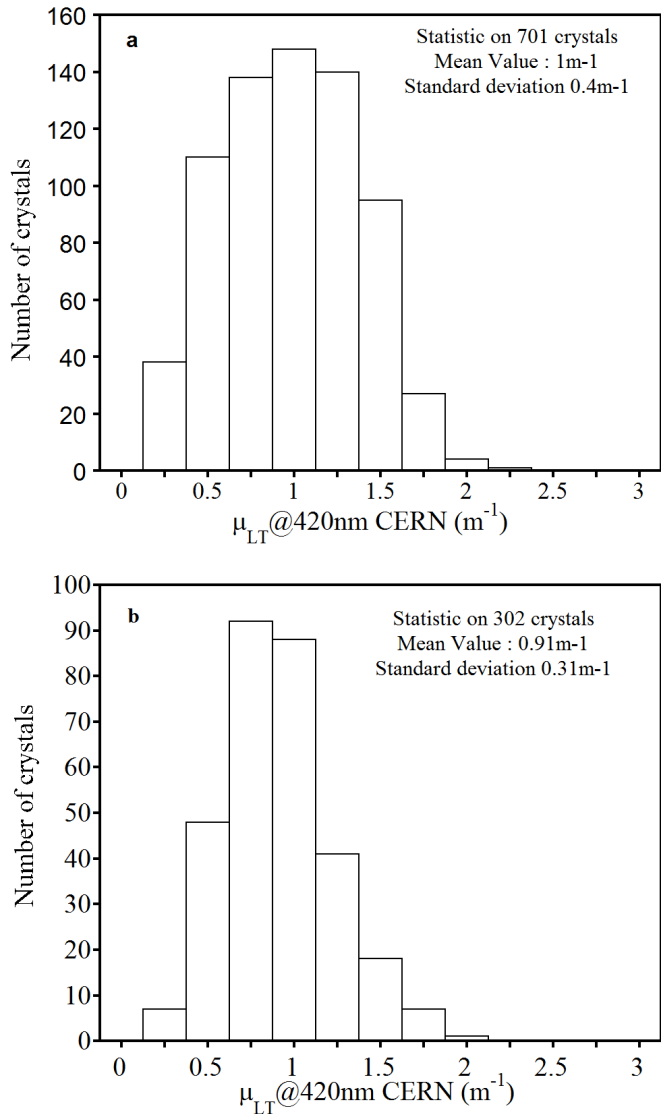
Figure 16. Distribution of induced absorption at 420 nm after 350 Gy at a dose rate of 350 Gy/h for: (a) BTCP Barrel crystals b) BTCP Endcaps crystals, randomly selected among those having optical parameters within ECAL certification limits.

7.2.2 Testing radiation damage in LHC-like conditions

Figure 18 shows the distribution of LY loss under front irradiation at LHC radiation levels (0.15Gy/h), for a random sampling of BTCP Barrel crystals. The average light yield loss is 2.4%. Figure 19 shows the same for a random sampling of SICCAS Barrel crystals. The average light yield loss is 1.6%.

The radiation damage level observed after irradiation in the LHC like conditions for the ECAL at both producers is below the specification limit of 6% and will guarantee the ability to monitor precisely the crystals transparency.
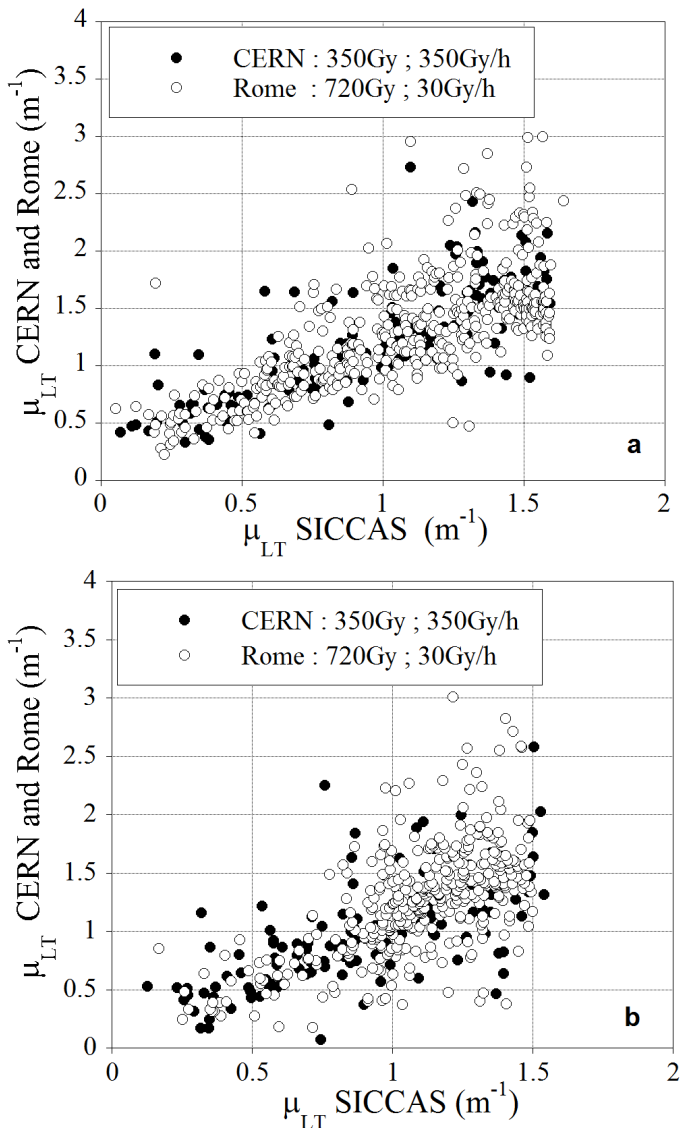
Figure 17. Correlation between induced absorption measured at SICCAS (700 Gy, 30 Gy/h) and in ECAL regional centres. (a) Barrel crystals, (b) Endcaps crystals.

8 Conclusions

This article has described the investigations that have led to a detailed understanding of $PbWO_4$ scintillation characteristics and radiation induced color centers. These activities were a fundamental contribution to enabling the production of $PbWO_4$ crystals with characteristics satisfying the CMS requirements. The certification of such production extended over several years and quality assurance results have been presented which demonstrate the reliability of the $PbWO_4$ used in CMS.

The excellent linear relationship between the variation of crystal light yield and longitudinal transmission in the wavelength region of 420–440 nm in repeated cycles of irradiation-recovery, allows a reliable monitoring of the light yield in LHC exploitation conditions.
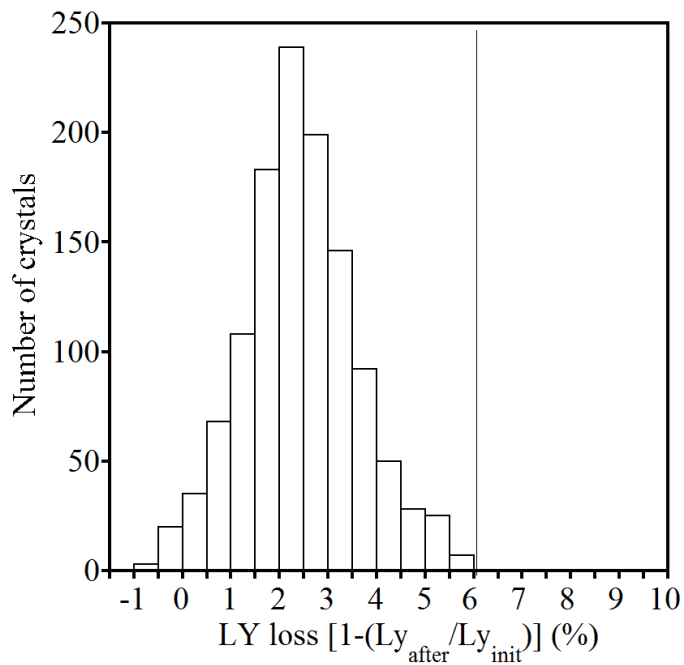
Figure 18. Distribution of relative LY loss after 1.5 Gy at a rate 0.15 Gy/h for 1203 BTCP crystals randomly selected among those having optical parameters within ECAL certification limits (vertical line defines the 6% certification limit for light yield loss).
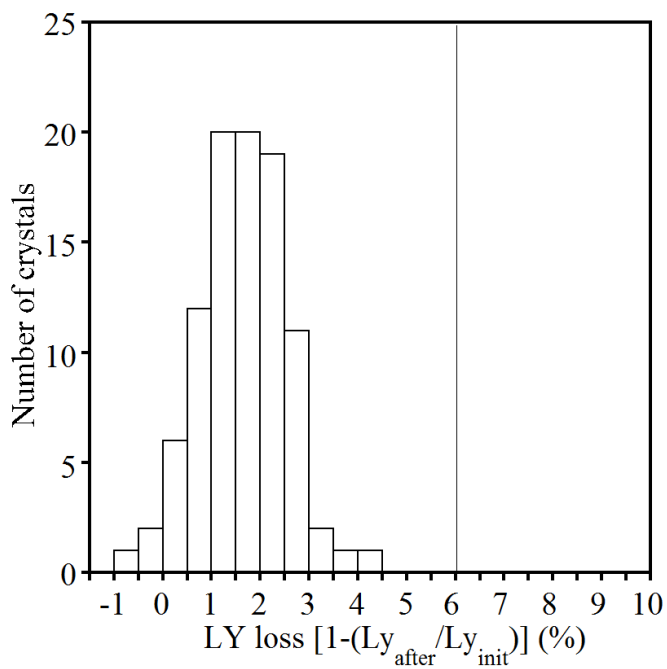

Figure 19. Distribution of relative LY loss after 1.5 Gy at a rate 0.15 Gy/h for a random sample of 96 SICCAS crystals.

A List of irradiation facilities used in this work

A.1 Gamma irradiations

Geneva Hospital ^{60}Co source. Crystals are irradiated from the side with a dose rate of 350 Gy/h. Variations of the crystal transversal and longitudinal transmission, light yield and scintillation kinetics are measured 40 min after the irradiation by a set of spectrometers located at CERN after transport in a thermally isolated box

CERN-TIS-B27 ^{60}Co source. This setup allows the front irradiation of 6 crystals (including one or 2 for reference) at a dose rate of 0.15Gy/h (CMS ECAL Barrel exposure under normal LHC conditions) and an integrated dose of up to 3Gy. The radiation induced light yield is recorded during the irradiation, allowing a direct monitoring of the light transmission loss.

CERN GIF-X5 beam facilities including a ^{137}Cs source (lateral irradiation at 0.15 Gy/h up to 2 Gy integrated dose) and the possibility to probe the crystal in parallel to the irradiation with a muon or an electron beam.

CERN H4 beam Crystals are used in the same configuration as in the CMS experiment, with the same photodetectors, readout electronics, thermal stabilization and monitoring systems. High energy electron beams are shot in the crystals with intensities allowing to mimic the LHC expected dose rate of about 0.15Gy/h.

COCASE Facility, at CEA/IRFU, Saclay. It consists of a ^{60}Co source (1.2 MeV, 14 Ci) with geometrical tuning of the dose rate in the region below 1 Gy/h. Relative change of the monitoring signals provided by a Xe pulse lamp and a fast tuning monochromator in the spectral region 380–800 nm is measured. Longitudinal transmission is also measured by a Perkin-Elmer spectrophotometer in the region 300-850 nm before and after the crystal irradiation.

Institute for Nuclear Problems (INP) ^{60}Co source facility, Minsk. It consists of a ^{60}Co well shaped source with fixed dose rate 2300 Gy/h. Variations of the crystal transmission are measured 60 min after irradiation by a Varian "Cary1E" spectrophotometer in the range 300-900 nm. Control of other scintillation parameters is also carried out.

Institute for Nuclear Research (INR) irradiation facility, Moscow. A microtron MK-25 and linear electron accelerator (both of 25 MeV electron energy) are used as electromagnetic radiation sources. Dose rates are tuned from 0.06 to 1800 Gy/h. Longitudinal transmission is measured in the region of 390 to 650 nm during the irradiation by a specially developed spectrophotometer based on a transparent grating.

ENEA-Casaccia, Rome *Calliope* ^{60}*Co* plant. This is a 24000Ci (July 2002) source in a water pool. The irradiation plant allows irradiation up to dose rates of 20 kGy/h. Different dosimetric positions are available for PbWO$_4$ radiation hardness study in the range from 10 to 400 Gy/h. Standard PbWO$_4$ tests are performed at irradiation points: 11.8Gy/h, 34.2Gy/h and 350Gy/h (values at October 2006) where PWO crystals are subject to irradiation cycles.

For a given dose rate the typical irradiation cycle consists in gamma radiation exposures at increasing doses until the saturation of the induced absorption coefficient is reached. Irradiation is followed by room temperature recovery until acquired data allow for a reliable estimation of the time component(s) of the recovery process. Transmission and LY measurements are performed at typically 15 min after the irradiation exposure is stopped. During the irradiation cycle(s) crystal are kept at room temperature, in the dark in order to avoid recovery processes induced by light.

CALTECH ^{60}Co 50Ci source. Crystals in a light tight package are irradiated from the side with a dose rate ranged from 0.1 to 10 Gy/h by placing samples at different distances to the source.

Imperial College/Brunel Univeristy ^{60}Co source.

Eichlabor, PSI-Villigen ^{60}Co source.

CALTECH ^{137}Cs 2000Ci source. Crystals in a light tight package are irradiated from the side with a dose rate of 90 Gy/h when placed at the center of the irradiation chamber with a uniformity of dose rate about 5%. Up to 360 Gy/h may be achieved in the closest position to the source. Variations of the crystal's optical transmission, photo-luminescence, light output and decay kinetics are measured about 5 minutes after the irradiation respectively by a PerkinElmer Lambda-950 spectrometer, Hitachi-F4500 fluorescence spectrophotometer and a Hamamatsu R2059 PMT and LeCroy 3001 QVT charge integrator based pulse height spectrometer. All measurements are carried out in the dark, or under a red light, at $18°C$.

In all irradiation facilities mentioned above, a common recovery protocol was defined for PWO crystals of ECAL-CMS. Recovery of radiation damage was obtained by a thermal bleaching process consisting in:

- ramp-up from room temperature to $200°C$ in not less than 3 hours
- plateau of 6 hours at $200°C$
- power stop and natural cooling

A.2 Neutron irradiations

Saclay Ulysse reactor: is a Uranium metal reactor with a fast neutron (about 1MeV) flux ranging from 10^6 to 10^{11} neutrons $cm^{-2}s^{-1}$. Irradiation tests with neutron fluences of 10^{12}, $2 \cdot 10^{13}$ and $2 \cdot 10^{14}$ neutrons cm^{-2} have been made on several crystals.

ENEA-Casaccia, Rome *TAPIRO* reactor: is a fast neutrons reactor particularly adapted for small size experiments due to its relatively low power (5 kW or $4.3 \cdot 10^{14}$ fission neutrons/s) and very small, highly enriched core (11cm height, 12cm diameter, 93.5% enriched Uranium).

A.3 Charged hadron irradiations

In order to test the possible role of charged hadrons induced lattice defects (stars) some crystals have been exposed to intense pion or proton beams at *PSI-Villigen* and *CERN-PS-IRRAD1* In this last case, crystals were exposed to 20 GeV proton beams with a flux ranging from 10^{12} to 10^{13} p $cm^{-2}h^{-1}$.

References

[1] CMS collaboration, *The Compact Muon Solenoid Technical Proposal*, CERN-LHCC-94-38 (1994).

[2] CMS collaboration, *ECAL Technical design report*, CERN-LHCC-97-033 (1997).

[3] M. Huhtinen, P. Lecomte, D. Luckey, F. Nessi-Tedaldi and F. Pauss, *High-energy proton induced damage in PbWO-4 calorimeter crystals*, *Nucl. Instrum. Meth.* **A 545** (2005) 63.

[4] A.N. Annenkov et al., *The influence of additional doping on the spectroscopic and scintillation parameters of PbWO4 crystals*, *Phys. Status Solidi (a)* **156** (1996) 493.

[5] M. Nikl et al., *Radiation induced formation of color centers in PbWO4 single crystals*, *J. Appl. Phys.* **82** (1997) 5758.

[6] E. Auffray et al., *Improvement of several properties of lead tungstate crystals with different doping ions*, *Nucl. Instrum. Meth.* **A 402** (1998) 75.

[7] M. Kobayashi et al., *Improvement in radiation hardness of PbWO-4 scintillating crystals by La doping*, *Nucl. Instrum. Meth.* **A 404** (1998) 149.

[8] A. Annenkov et al., *Suppression of the radiation damage in lead tungstate scintillation crystal*, *Nucl. Instrum. Meth.* **A 426** (1999) 486.

[9] M. Kobayashi et al., *Significant improvement of PbWO-4 scintillating crystals by doping with trivalent ions*, *Nucl. Instrum. Meth.* **A 434** (1999) 412.

[10] A.A. Annenkov, M.V. Korzhik and P. Lecoq, *Lead tungstate scintillation material*, *Nucl. Instrum. Meth.* **A 490** (2002) 30.

[11] I. Dafinei, E. Auffray, P. Lecoq and M. Schneegans, *Lead Tungstate for High Energy Calorimetry*, in *Scintillator and Phosphor Materials, M.J. Weber et al eds*, *Material Research Society Symposium Proceedings* **348** (1994) 99.

[12] S. Baccaro et al., *Ordinary and extraordinary complex refractive index of the lead tungstate (PbWO-4) crystal*, *Nucl. Instrum. Meth.* **A 385** (1997) 209.

[13] P. Yang, J. Liao, B. Shen, P. Shao, H. Ni and Z. Yin, *Growth of large-size crystal of PbWO$_4$ by vertical Bridgman method with multi-crucibles*, *J. Crystal Growth* **236** (2002) 589.

[14] J.M. Moreau, R.E. Gladyshevskii, Ph. Galez, J.P. Peigneux and M.V. Korzhik, *A new structural model for Pb-deficient PbWO$_4$*, *J. Alloys Compounds* **284** (1999) 104.

[15] R. Chipaux, G. André and A. Cousson, *Crystal structure of lead tungstate at 1.4 and 300 K*, *J. Alloys Compounds* **325** (2001) 91.

[16] P. Bohacek et al., *Stoechiometry and radiation damage of PWO crystals grown from melts of different composition*, in Tungstate Crystals, Proceedings of the International Workshop on Tungstate Crystals, S. Baccaro et al eds., Rome, October 12–14 (1998), ISBN 88-87242-10-0, pp 57–60.

[17] J. Sykora, M. Husák, O. Jarolímek, A. Strejc and D. Sedmidubsky, *The crystallographical study of compounds originating in the PbO-WO$_3$ system*, in *Tungstate Crystals, Proceedings of the International Workshop on Tungstate Crystals*, S. Baccaro et al eds., Rome, October 12–14 (1998), ISBN 88-87242-10-0, pp 95–97.

[18] K. Tanji et al., *Crystal growth of PbWO$_4$ by the vertical Bridgman method: Effect of crucible thickness and melt composition*, *J. Crystal Growth* **204** (1999) 505.

[19] B. Han, X. Feng, G. Hu, Y. Zhang and Z. Yin, *Annealing effects and radiation damage mechanisms of PbWO$_4$ single crystals*, *J. Appl. Phys.* **86** (1999) 3571.

[20] A. Annenkov et al., *Radiation damage kinetics in PWO crystals*, CMS-NOTE-1997-008 (1997).

[21] E. Auffray et al., *Performance of ACCOS, an Automatic Crystal quality Control System for the PWO crystals of the CMS calorimeter*, *Nucl. Instrum. Meth.* **A 456** (2001) 325.

[22] S. Baccaro et al., *An automatic device for the quality control of large-scale crystal's production*, *Nucl. Instrum. Meth.* **A 459** (2001) 278.

[23] M. Montecchi, S. Baccaro, I. Dafinei, M. Diemoz, R.M. Montereali and F. Somma, *Lumen: A highly versatile spectrophotometer for measuring the transmittance throughout very long samples as well as microstructures*, *Rev. Sci. Instrum.* **75** (2004) 4636.

[24] S. Baccaro et al., *Precise determination of the light yield of scintillating crystals*, *Nucl. Instrum. Meth.* **A 385** (1997) 69.

[25] I. Dafinei, *Optical and scintillation properties of lead tungstate crystals: a statistical approach*, in *Proc. 8th Int. Conference on Inorganic Scintillators, SCINT2005*, A. Getkin and B. Grinyov eds., Alushta, Crimea, Ukraine, September 19–23 (2005), pg. 327–330 [ISBN 9666-02-3884-3].

[26] M. Nikl et al., *Luminescence and scintillation of single PbWO$_4$ crystals*, in *Proc. Int. Conference on Inorganic Scintillators and their Applications, SCINT95*, P. Dorenbos and C.W.E. van Eijk eds., Delft, The Netherlands, August 28–September 1 (1995), pg. 257–259 [ISBN 90-407-1215-8].

[27] E. Auffray et al., *Scintillation characteristics and radiation hardness of PWO scintillators to be used at the CMS electromagnetic calorimeter at CERN*, in *Proc. Int. Conference on Inorganic Scintillators and their Applications, SCINT95*, P. Dorenbos and C.W.E. van Eijk eds., Delft, The Netherlands, August 28–September 1 (1995), pg. 282–285 [ISBN 90-407-1215-8].

[28] R.Y. Zhu et al., *A Study on the properties of lead tungstate crystals*, *Nucl. Instrum. Meth.* **A 376** (1996) 319.

[29] X. Qu et al., *A study on yttrium doping in lead tungstate crystals*, *Nucl. Instrum. Meth.* **A 480** (2002) 470.

[30] L.M. Bollinger and G.E. Thomas, *Measurement of the Time Dependence of Scintillation Intensity by a Delayed-Coincidence Method*, *Rev. Sci. Instrum.* **32** (1961) 1044.

[31] S. Baccaro et al., *Influence of La^{3+}-Doping on Radiation Hardness and Thermoluminescence Characteristics of PbWO$_4$*, *Phys. Status Solidi (a)* **160** (1997) R5.

[32] S. Baccaro et al., *Radiation Damage and Thermoluminescence of Gd-Doped PbWO$_4$*, *Phys. Status Solidi (a)* **164** (1997) R9.

[33] M. Kobayashi et al., *Improvement in transmittance and decay time of PbWO-4 scintillating crystals by La-doping*, *Nucl. Instrum. Meth.* **A 399** (1997) 261.

[34] A.N. Annenkov et al., *Systematic study of the short-term instability of PBWO-4 scintillator parameters under irradiation*, *Radiat. Meas.* **29** (1998) 27.

[35] A. Annekov, E. Auffray, M. Korzhik, P. Lecoq and J.P. Peigneux, *On the Origin of the Transmission Damage in Lead Tungstate Crystals under Irradiation*, *Phys. Status Solidi (a)* **170** (1998) 47.

[36] M.V. Korzhik et al., *Spectroscopy and Origin of Radiation Centers and Scintillation in PbWO$_4$ Single Crystals*, *Phys. Status Solidi (a)* **154** (1996) 779.

[37] A.N. Annenkov et al., *On the Mechanism of Radiation Damage of Optical Transmission in Lead Tungstate Crystal*, *Phys. Status Solidi (a)* **191** (2002) 277.

[38] Q. Deng, Z. Yin and R.Y. Zhu, *Radiation-induced color centers in La-doped PbWO₄ crystals*, *Nucl. Instrum. Meth.* **A 438** (1999) 415.

[39] K. Hara et al., *La-doped PbWO-4 scintillating crystals grown in large ingots*, *Nucl. Instrum. Meth.* **A 414** (1998) 325.

[40] I. Dafinei et al., *Colour centres production in PbWO₄ crystals by UV light exposure*, in *Proc. Int. Conf. on Inorganic Scintillators and Their Applications, SCINT97*, Y. Zhiwen et al. eds., September 22–25 (1997), Shanghai, China, pg. 219–222.

[41] E. Auffray, E. Baguer Battalla, P. Lecoq, S. Paoletti and M. Schneegans, *Progress in the radiation hardness of PWO scintillators for CMS calorimeter*, in *Proc. Int. Conf. on Inorganic Scintillators and Their Applications, SCINT97*, Y. Zhiwen et al. eds., September 22–25 (1997), Shanghai, China, pg. 199–202.

[42] E. Auffray, M. Lebeau and P. Lecoq, *Specifications for Lead Tungstate Crystals Preproduction*, CMS-NOTE-1998-038 (1998).

[43] E. Auffray, *Overview of the 63000 PWO barrel crystals for CMS₋ECAL production*, *IEEE Trans. Nucl. Sci.* **55** (2008) 1314.

[44] J. Chen, R. Mao, L. Zhang and R.-Y. Zhu, *A damage and recovery study for lead tungstate crystal samples from BTCP and SIC*, *IEEE Nucl. Sci. Symp. Conf. Rec.* **1** (2005) 249.

[45] P. Lecoq, A. Annenkov, A. Gektin, M. Korzhik and C. Pedrini, *Inorganic Scintillators for Detector Systems: Physical Principles and Crystal Engineering*, Springer, Berlin Germany (2006).

[46] C. D'Ambrosio, C. Ercoli, S. Jaaskelainen, E. Rosso and P. Wicht, *Low dose-rate irradiation set-up for scintillating crystals*, *Nucl. Instrum. Meth.* **A 388** (1997) 119.

[47] R. Chipaux et al., *Study of neutron damage resistance of some scintillating crystals and associated photodetectors with the nuclear reactor ULYSSE*, in *Scintillator and Phosphor Materials*, M.J. Weber et al. eds., *Material Research Society Symposium Proceedings* **348** (1994) 481.

[48] R. Chipaux and O. Toson, *Resistance of lead tungstate and cerium fluoride to low rate gamma irradiation or fast neutrons exposure*, in *Proc. Int. Conference on Inorganic Scintillators and their Applications, SCINT95*, P. Dorenbos and C.W.E. van Eijk eds., Delft, The Netherlands, August 28–September 1 (1995), pg. 274–277, also CMS-TN-95-126 [ISBN 90-407-1215-8].

[49] M.Kh. Ashurov, Sh.Kh. Ismoilov, K. Khatamov, É.M. Gasanov, I.R. Rustamov and V.A. Kozlov, *Radiation-Induced Optical Absorption in PbWO₄:La Scintillation Crystals*, *Atom. Energy* **91** (2001) 560.

[50] R. Chipaux, M.V. Korzhik, A. Borisevich, P. Lecoq and C. Dujardin, *Behaviour of PWO scintillators after high fluence neutron irradiation*, in *Proc. 8th Int. Conference on Inorganic Scintillators, SCINT2005*, A. Getkin and B. Grinyov eds, Alushta, Crimea, Ukraine, September 19–23 (2005), pg. 369–371 [ISBN 9666-02-3884-3].

[51] P. Lecomte, D. Luckey, F. Nessi-Tedaldi and F. Pauss, *High-energy proton induced damage study of scintillation light output from PbWO-4 calorimeter crystals*, *Nucl. Instrum. Meth.* **A 564** (2006) 164.

[52] P. Lecomte, D. Luckey, F. Nessi-Tedaldi, F. Pauss and D. Renker, *Comparison between high-energy proton and charged pion induced damage in PbWO₄ calorimeter crystals*, *Nucl. Instrum. Meth.* **A 587** (2008) 266.

[53] The CMS Electromagnetic Calorimeter Group, P. Adzic et al., *Results of the first performance tests* ∗ *of the CMS electromagnetic calorimeter*, *Eur. Phys. J.* **C 44S2** (2006) 1.

[54] M. Anfreville et al., *Laser monitoring system for the CMS lead tungstate crystal calorimeter*, *Nucl. Instrum. Meth.* **A 594** (2008) 292.

[55] L. Zhang, K. Zhu, D. Bailleux, A. Bornheim and R.-y. Zhu, *Implementation of a software feedback control for the CMS monitoring lasers*, *IEEE Trans. Nucl. Sci.* **55** (2008) 637.

[56] L.Y. Zhang, K.J. Zhu, R.Y. Zhu and D.T. Liu, *Monitoring light source for CMS lead tungstate crystal calorimeter at LHC*, *IEEE Trans. Nucl. Sci.* **48** (2001) 372.

[57] L.-Y. Zhang, D. Bailleux, A. Bornheim, K.-J. Zhu and R.-Y. Zhu, *Performance of the monitoring light source for the CMS lead tungstate crystal calorimeter*, *IEEE Trans. Nucl. Sci.* **52** (2005) 1123.

Transparency Variations and Calibration in CMS Electromagnetic Calorimeter Crystals: Monte Carlo Studies

Rémi Chipaux and François-Xavier Gentit

Abstract—The aging of CMS electronic calorimeter scintillating crystals under radiation leads to a deterioration of their transparency, and thus of their effective light yield and their calibration. The correlation between transparency variation, as measured by the fiber-optic monitoring system, and the calibration variation depends on the optical properties of the scintillating material itself and of its environment. In previous studies, the possibility of light scattering within the bulk of the crystals was not taken into account.

We present here the results of the simulation of this correlation for different types of CMS electronic calorimeter crystals using the program Litrani improved to allow light scattering in bulk. They show that scattering could explain the variation of correlation coefficients observed between CMS/ECAL endcap and barrel crystals.

Index Terms—Calibration, electromagnetic calorimetry, Monte Carlo simulation, scintillation detectors.

I. INTRODUCTION

THE lead tungstate scintillating crystals of the CMS electromagnetic calorimeter (ECAL) will be exposed to an intense radiation throughout the accelerator operation, interrupted by quiet periods. The optical transmission of crystals, and consequently their light-collection efficiency and calibration coefficients, will fluctuate. In order to preserve the calibration precision of the instrument, both calibration with physical events, at a time scale of a few weeks, and continuous monitoring of the optical characteristics of the crystals are required. This last technique is the purpose of the ECAL laser monitoring system [1].

Previous papers [2]–[4] have shown that, in general, the correlation between variations of collection efficiencies for scintillation light (directly related to the calibration parameters) and monitoring light is dominated, for crystals of good optical quality, by the quality of light containment in crystals, defined by the properties of their surfaces and coating. The properties of the readout device are also important: surface, optical coupling, quantum efficiency versus wavelength, etc.

In CMS/ECAL, the situation is complicated by the fact that numerous cases are encountered: different crystal shapes, crystal origin, readout devices etc.

In ECAL barrel, the crystals have 17 different truncated pyramidal shapes. One of their lateral faces is slightly depolished to correct for the nonuniformity of the light collection induced by the pyramidal shape. They are placed in alveolas covered by a diffusive white coating and read by two avalanche photodiodes (APDs) of surface 5 x 5 mm^2 each, glued on the rear (outer) face of the crystal. The monitoring light is injected by an optical fiber through the front (inner) face. All crystals have been grown in Russia by the Bogoroditsk Techno Chemical Plant (BTCP).

In the ECAL endcaps, all the crystal have an identical truncated shape, 22 cm long by 3 x 3 cm^2 at rear face, with all faces polished. They are read by vacuum phototriodes (VPTs), diameter 26.5 mm glued on the rear face, but during the research and development phase, some of them have been read by APDs. The monitoring light is injected on the photodetector end face. Part of the endcap crystals have been grown in China by the Shanghai Institute of Ceramics (SIC); the remainder are from BTCP.

If one defines:

— R_0: signal of a crystal under laser light injection, before any radiation damage;

— R: signal of a crystal under laser light injection, after radiation damage;

— S_0: signal of a crystal from an electromagnetic shower, before any radiation damage;

— S: signal of crystal from an electromagnetic shower, after radiation damage;

it has been shown [5] that, to a good approximation, one has

$$\frac{S}{S_0} = \left(\frac{R}{R_0}\right)^{\alpha}. \tag{1}$$

The correlation coefficient α is constant for a given crystal in a given optical environment—or, in other words, the S/S_0 versus R/R_0 plot is a straight line with a slope α in log/log scale. This will be the case for all CMS-ECAL crystals, designed to have an induced absorption of less than 1.5 m^{-1} and a light yield loss below 6% at LHC conditions [6].

Measurements of this coefficient have given sometimes puzzling results: Variations of α observed for crystals of the same shape and optical environment seem to indicate that internal parameters previously not taken into account could also play an important role. In particular, the occurrence of light scattering

in the bulk of the material has been proposed to explain some of the measurements.

We report here new simulation results obtained with the Litrani [7] program of simulation of optical photons, in which the possibility of light scattering into materials has been added for the first time.

II. MEASUREMENTS

To our knowledge, no summary paper presently exists on the measurements of the α parameter for the CMS/ECAL. The content of this section is the result of a compilation of notes and presentations posted on CMS/ECAL Web site and may not be complete. We refer the interested reader to the references for additional information on the way these measurements were taken. The mean values and standard deviations given hereafter are computed from the data indicated in the references, weighted by data errors when available.

A. Barrel BTCP Crystals With APDs

Twenty BTCP crystals of the barrel were measured in a dedicated test beam during summer 2002 [8]. The result was $\alpha = 1.532 \pm 0.021$ (20 crystals).

B. Barrel SIC Crystals With APDs

No measurements exist for these crystals.

C. Endcap BTCP Crystals With APDs

Two sets of measurements on SC04 exist, coming from the H4 test beam of 2004. The first measurement [9] gives $\alpha = 1.25 \pm 0.11$ (four crystals) and the second [10] $\alpha = 1.21 \pm 0.07$ (five crystals).

D. Endcap BTCP Crystals With VPTs

Two sets of measurements on SC03 exist, coming from the H4 test beams of 2004 [11] $\alpha = 1.565 \pm 0.021$ (two crystals) and 2007 [12] $\alpha = 1.525 \pm 0.305$ (29 crystals).

E. Endcap SIC Crystals With APDs

Ten measurements exist, coming from the H4 2004 test beam [10]: $\alpha = 0.79 \pm 0.08$ (ten crystals).

F. Endcap SIC Crystals With VPTs

Two sets of measurements on SC03 exist, coming from the H4 test beams of 2004 [11] $\alpha = 0.986 \pm 0.065$ (nine crystals) and 2007 [12] $\alpha = 1.07 \pm 0.32$ (12 crystals).

G. Comments

The barrel crystals, all grown at the same place, present a correlation coefficient α with little variation around 1.53, despite their differences in geometrical shape. In contrast, the endcap crystals, identical in shape but of different origin and readout, show large variations. It is understandable that the different VPT and APD readouts lead to different α parameters, the surface covered by photodetectors and their refractive indexes and quantum efficiencies being different, but the dispersion of

parameters and the differences of their mean between Russian and Chinese crystals could only be due to variations in the optical properties of the crystals themselves. Among the possible causes of α variation, the presence of light-scattering centers in the crystal bulk has often been supposed.

III. SIMULATIONS

A. Generalities

1) The Model: The characteristics of the generation were the following.

— The geometry was simulated exactly, without any approximation: shape of crystals, of APDs, or of VPTs.
— The characteristics of all wrappings or alveola used were also simulated very precisely using measurement results: the presence or not of a slice of air, proportion of scattering versus reflection, albedo. In particular, for the endcaps, the alveola was described as a totally black wrapping, but with a slice of air, so that total reflection remains possible, whereas for the barrel, the alveola was described as partly reflective and diffusive.
— The characteristics of the glue were also simulated exactly using data from the producer.
— Precise description of the characteristics of the APDs including the description of the optical thin slice of the front window.
— Precise description of the characteristics of the VPTs: quantum efficiency versus wavelength of photon, index of reflection versus wavelength of entrance window, and so on.
— The light injection was modelled precisely: there is a gap of air between fiber and crystal, and the angular distribution of light from the fiber is the one measured at Saclay. The monitoring light wavelength was assumed to be 450 nm, unfortunately slightly above the actual monitoring wavelength, set at 440 nm.
— The emission spectrum of lead tungstate was approximated by two Gaussians, centered at 420 and 500 nm, respectively, 94 and 118 nm full-width at half-maximum, relative intensity 3/4 and 1/4, respectively. These parameters well fit the photoluminescence spectrum measured in our lab (shown in Fig. 1) and are also similar to the one shown in [13].
— With (1) implying a logarithmic dependence, it was necessary to generate a very high number of photons in order to get statistically significant results (some 45×10^9 photons for the second simulation quoted in this paper). In order to speed up the calculations (by a factor of about four), $PbWO_4$ was treated as isotropic, not birefringent. A comparative run made with anisotropic material did not show any significant difference.

2) Absorption Data: The absorption length of the $PbWO_4$ crystal is simulated exactly, with a wavelength dependence corresponding to the measurement done on a real crystal, number
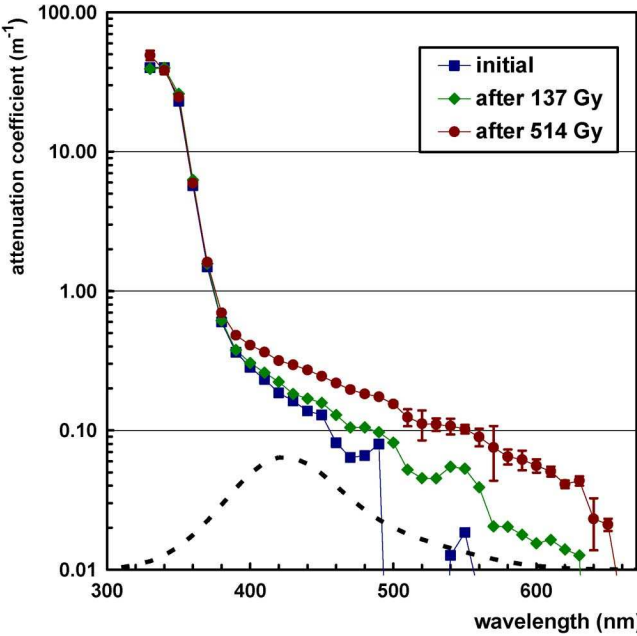
Fig. 1. Attenuation coefficient versus wavelength for crystal 8981 before irradiation and after the two last steps of irradiation. Dotted line: emission spectrum used for the calculations, in linear arbitrary scale.

Fig. 2. Correlation coefficient α simulated by Litrani as a function of the shape of CMS/ECAL barrel crystals.

TABLE I
PARAMETERS OF THE IRRADIATION OF CRYSTAL CMS 8981

step	duration	dose rate (Gy/h)	cumulated dose (Gy)
1	30h 40mn	0.092	6.8
2	117h 41mn	0.143	44.0
3	146h 25mn	0.25	90.7
4	45h 31mn	1.0	137
5	184h 43mn	2.0	514

8981 in the CMS database, which is a BTCP crystal. The variation of this absorption length with irradiation has also been simulated exactly, using measurements done under five various irradiations for this crystal. The crystal has been irradiated by ^{60}Co gamma rays in the installation Cocase [14] up to the equivalent of 514 Gy in air. The crystal was placed transversal to the direction of the source. The parameters of irradiation are reported in Table I.

The longitudinal optical absorption of the crystal was measured using the apparatus and method previously described in [15], initially and after each irradiation step. Due to the length of this peculiar time interval, two measurements were taken between the two last steps. The attenuation coefficient was calculated after applying correction for the surface refraction, using the optical indexes given in [16]. Fig. 1 shows the values of the mean absorption coefficient versus wavelength of this crystal, before irradiation and after the two last steps of irradiation. Seven absorption data sets have thus been obtained.

3) Simulations: Using these seven sets of data, 14 runs of simulation, for each value of scattering length, were done: seven runs for laser pulses ("laser") and seven runs for 120 GeV electromagnetic showers ("beam"). To simulate electromagnetic showers, Litrani uses the simplified formulas proposed in

the "Review of Particle Physics" [17].[1] α is then determined by the slope of the linear fit of normalized data "beam" versus "laser."

4) Scattering Length: In the second simulation described in this paper, we investigated the role that a scattering length might play in the measured results. The possibility of the presence of optical scattering in addition to absorption has been added in Litrani, where the scattering length was defined as the mean distance after which a photon is stopped and reemitted with the same wavelength in any direction, chosen isotropically on 4π. In this first stage, no dependence of scattering length upon wavelength of photon was included.

B. Dependence of α on the Shape of the Barrel Crystals

This first simulation with Litrani was done in 2003/2004 to study the possible effect of the 17 different shapes of the barrel crystals on the α parameter. No scattering length was included in the simulation. Data were fitted to (1) for the 17 different shapes.

The calculated correlation coefficients and their distribution are shown in Figs. 2 and 3. The mean value of the α parameter is 1.542 ± 0.020, to be compared to the measurements quoted in Section II-A. Within statistical errors, no obvious variation with the crystal shape is observed.

C. α Parameter for the Endcap Crystals; Influence of Readout and Light Scattering

Figs. 4 and 5 show the variation of α versus scattering length, as explained in Section III-A4, for VPTs and APDs readout, respectively.

---

[1]More details are available in http://gentit.home.cern.ch/gentit/litrani/AllModules/LitraniCode/TelecCascade.html.
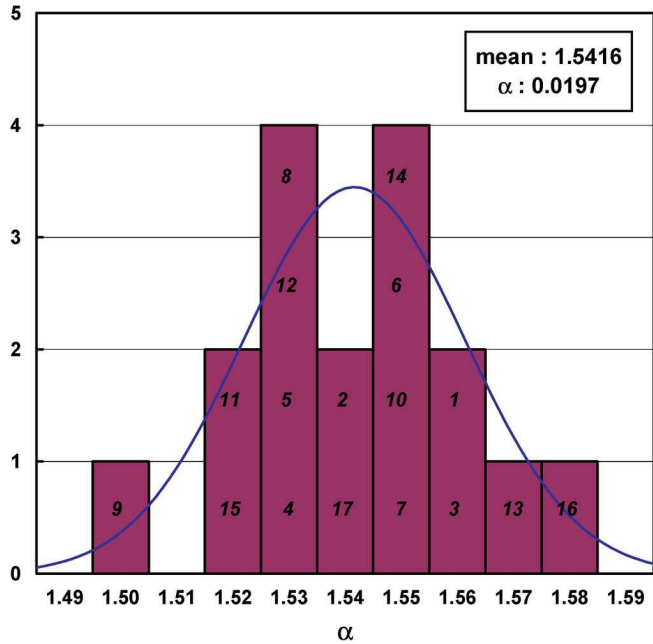
Fig. 3. Distribution of the α parameter simulated by Litrani for CMS/ECAL barrel crystals (the numbers in the histogram refer to the crystal shapes).

Fig. 4. α parameters calculated with Litrani for an endcap crystal with VPTs readout in function of the light scattering length in crystal and fit.

TABLE II
VALUES AND ERRORS OF THE PARAMETERS OF THE FIT OF $\alpha(l_{\text{scat}})$ BY THE
FUNCTION $\alpha(x) = (a_0 - a_1 + a_3 x) \exp(-a_2^2 x) + a_1$

parameter	VPT		APD	
	value	error	value	error
a_0	1.749	0.085	1.312	0.060
a_1	4.27	1.09	2.58	0.61
a_2^2 (cm^{-1})	0.0767	0.0124	0.0790	0.0196
a_3 (cm^{-1})	-0.296	0.0997	-0.133	0.0558

To allow a more quantitative analysis, the data have been fitted to a function of the form

$$\alpha(l_{\text{scat}}) = \left(a_0 - a_1 + \frac{a_3}{l_{\text{scat}}}\right) \exp\left(\frac{-a_2^2}{l_{\text{scat}}}\right) + a_1 \quad (2)$$

where the fitted parameters a_0, a_1, a_2, and a_3 are:

a_0 asymptotic value of α without light scattering ($l_{\text{scat}} \to \infty$);

a_1 asymptotic value of α for large light scattering ($l_{\text{scat}} \to 0$);

$-a_2^2$ factor of l_{scat}^{-1} in exponential;

a_3 factor of l_{scat}^{-1} in polynomial.

The values of the fitted parameter are reported in Table II.

The increase of α for small scattering length observed in simulations (fit parameter a_1) could be explained by the geometry of the laser monitoring in endcap crystals, for which light is injected through the same face as the photodetector. Thus, for long scattering lengths, the monitoring light crosses the crystal length twice, whereas for strong scattering, it is rapidly back-scattered toward the photodetectors. This is obviously only a theoretical


Fig. 5. α parameters calculated with Litrani for an endcap crystal with APDs readout in function of the light scattering length in crystal and fit.

case; a crystal with such huge light scattering would have been rejected for CMS-ECAL.

Litrani correctly reproduces the increase of the α parameters when switching from APD to VPT readouts for Russian endcap crystals for which simulations are in good agreement with the experimental data. Without light scattering: we calculate $\alpha = 1.749 \pm 0.085$ for VPTs readout and 1.312 ± 0.060 for APDs, to be compared with, respectively, $\sim$1.53 and $\sim$1.23 (see Section II-C and II-D). The best agreement is found for a scattering length of about 60 cm (more exactly, 55 cm for APDs and 61 cm for VPTs, statistically compatible).

A strong light scattering (about 20 to 30 cm for l_{scat}) lowers α values down to approximately one. However, even lower α values are measured in SIC crystals in which $\alpha \approx 0.8$ for VPTs and ≈ 1.0 for APDs (see Section II-E and II-F).

It is important to note that the present simulations have been done using spectral, transparency, and irradiation data measured on a BTCP crystal, and it is known that crystals from the two origins do not have exactly the same optical properties. Also, they do not have the same cristallographic orientation: the Chinese crystals are oriented along the c axis, which is the optical axis, and the Russian ones along the a axis, so perpendicularly to the optical axis.

Secondly, the approximations taken for the light-scattering model—no wavelength dependence, isotropic re-emission of photons, etc.—are certainly too crude to represent in detail the real behavior of photons in crystals. Thus these simulations are only an indication that light scattering, as suggested many times, can explain the low values of α observed in Chinese crystals. The lack of experimental data on the light scattering does not allow us for the moment to give more precise and quantitative predictions. It would be extremely interesting to measure the proportion of scattering versus absorption for BTCP and SIC crystals, using, for example, the new "Monte Carlo refractive index matching technique" method proposed by Wahl [18].

IV. CONCLUSION

It is shown here that the correlation between scintillation light and laser monitoring light signals variations—or, in other words, the correction parameter of the calibration coefficients, the so-called α or S/R parameter—is well reproduced by our simulation with the program Litrani for CMS/ECAL barrel crystals. The influence of the crystal's shape remains below the statistical and experimental dispersions.

For endcap crystals, the Litrani simulation, completed by the introduction of a crude model of light scattering in bulk material, agreed less precisely with measurements but suggests strongly that light scattering within Chinese crystals could be at least part of the reason for the low values of the measured correlation coefficients and for their dispersion. More experimental data, on optical and irradiation parameters of these crystals, are needed to make more quantitative conclusions.

REFERENCES

[1] M. Anfreville *et al.*, "Laser monitoring system for the CMS lead tungstate crystal calorimeter," *Nucl. Instrum. Methods A*, vol. 594, pp. 292–320, 2008.

[2] R. Chipaux and M. Géléoc, "Modelisation and simulation of the light collection in the CMS lead tungstate crystals," *Nucl. Instrum. Methods A*, vol. 451, pp. 610–622, 2000.

[3] R. Chipaux, V. V. Mikhailin, Ed., "Light collection in the CMS lead tungstate crystals : relation between monitoring and calibration variations," in *Proc. 5th Int. Conf. Inorgan. Scint. Applicat. SCINT 99*, 2000, pp. 639–642.

[4] R. Chipaux and X.-F. Gentit, "Simulation of light collection in the CMS lead tungstate crystals with the program Litrani: coating and surface effects," *Nucl. Instrum. Methods A*, vol. 486, pp. 48–54, 2002.

[5] P. Bonamy *et al.*, The ECAL calibration: Use of the light monitoring system, version 2.0 CMS Note 1998/013, Feb. 1998.

[6] E. Auffray, "Overview of the 63000 PWO barrel crystals for CMS_ECAL production," *IEEE Trans. Nucl. Sci.*, vol. 55, pp. 1314–1320, 2008.

[7] F. X. Gentit, "Litrani: a general purpose Monte-Carlo program simulating light propagation in isotropic or anisotropic media," *Nucl. Instrum. Methods A* vol. 486, pp. 35–39, 2002 [Online]. Available: http://gentit.home.cern.ch/gentit/litrani/

[8] A. van Lysebetten and P. Verrecchia, Performance and measurements of the light monitoring system for CMS-ECAL from 2002 test beam data CMS RN-2004/001, Feb. 2004.

[9] P. Verrecchia, Monitoring and R measurement results from SC03/04 Jul. 2004 [Online]. Available: http://indico.cern.ch/conferenceDisplay.py?confId=a043075

[10] ——, Latest results from «online monitoring» Jul. 2004 [Online]. Available: http://indico.cern.ch/conferenceDisplay.py?confId=a043327

[11] ——, Monitoring and R Measurement From SC03 Jun. 2004 [Online]. Available: http://indico.cern.ch/conferenceDisplay.py?confId=a042794

[12] C. Rogan, Update on 2007 EE testbeam alpha measurements Dec. 2007 [Online]. Available: http://indico.cern.ch/conferenceDisplay.py?confId=24835

[13] R. Mao, L. Zhang, and R-Y. Zhu, "Quality of mass-produced lead tungstate crystals," *IEEE Trans. Nucl. Sci.*, vol. 51, pp. 1777–1783, 2004.

[14] A. N. Annenkov *et al.*, "Systematic study of the PbWO$_4$ crystal short term instability under irradiation," *Rad. Meas.*, vol. 29, pp. 27–38, 1998.

[15] R. Chipaux and M. Géléoc, V. Mikhailin, Ed., "Optical anisotropy effects in lead tungstate crystals," in *Proc. 5th Int. Conf. Inorgan. Scint. Applicat. (SCINT 99)*, Moscow, Russia, 2000, pp. 629–635.

[16] S. Baccaro *et al.*, "Ordinary and extraordinary complex refractive index of the lead tungstate (PbWO$_4$) crystal," *Nucl. Instrum. Methods A*, vol. 385, pp. 209–214, 1997.

[17] C. Amsler *et al.*, "Review of particle physics," *Phys. Lett. B*, vol. 667, p. 276, 2008.

[18] D. Wahl, "The Monte-Carlo refractive index matching technique for determining the input parameters for simulation of the light collection in scintillating crystals," *Nucl. Instrum. Methods A*, vol. 570, pp. 529–535, 2007.